Cover Page

Universiteit Leiden

Leiden University Repository

The following handle holds various files of this Leiden University dissertation:
http://hdl.handle.net/1887/61131

Author: Elsland, D.M. van
Title: A bioorthogonal chemistry approach to the study of biomolecules in their ultrastructural cellular context
Issue Date: 2018-01-11

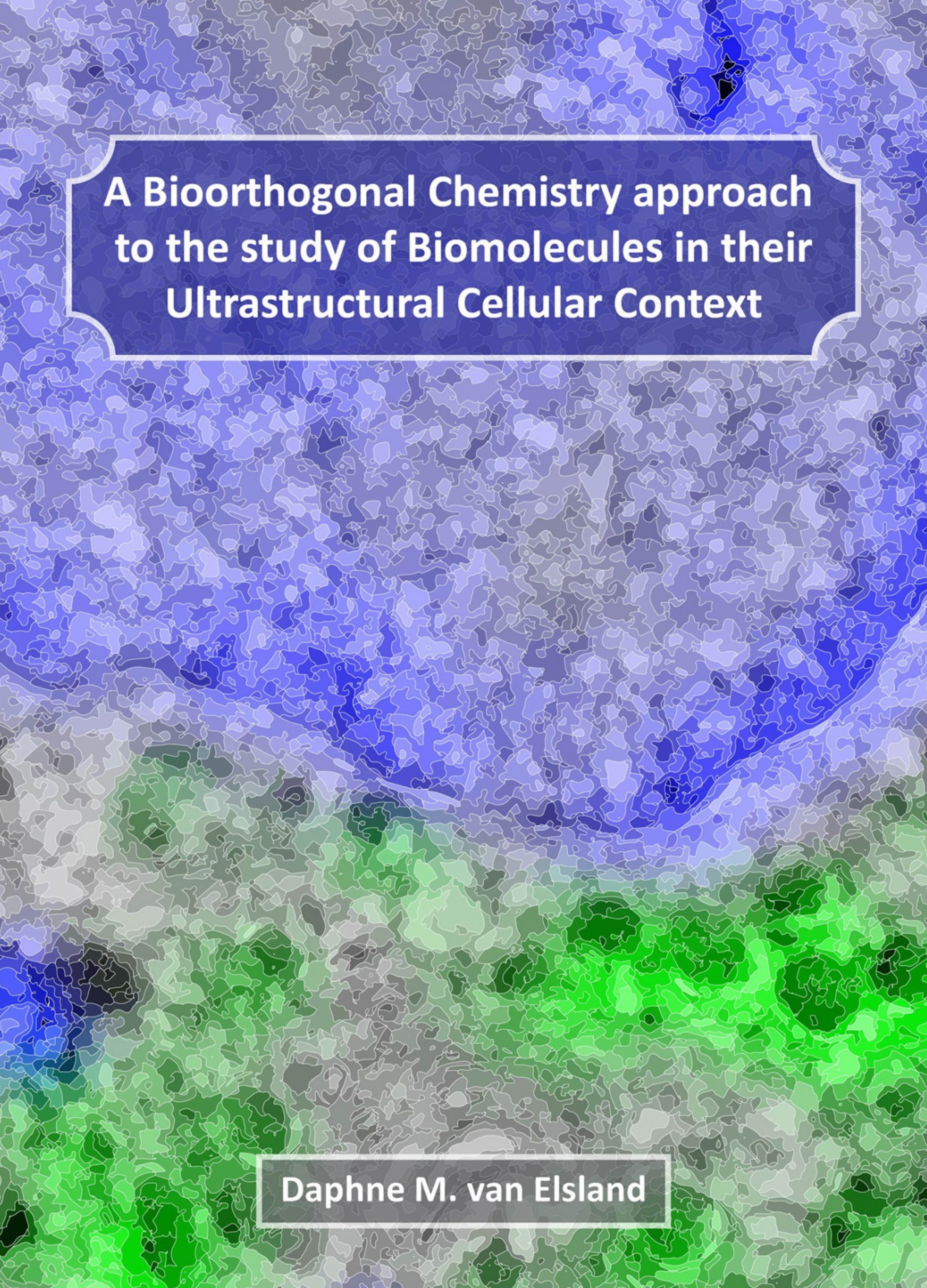

A Bioorthogonal Chemistry approach to the study of Biomolecules in their Ultrastructural Cellular Context

Daphne M. van Elsland

A Bioorthogonal Chemistry approach to the study of Biomolecules in their Ultrastructural Cellular Context

PROEFSCHRIFT

ter verkrijging van

de graad van Doctor aan de Universiteit Leiden,

op gezag van Rector Magnificus prof. mr. C.J.J. Stolker,

volgens het besluit van het College voor Promoties

te verdedigen op donderdag 11 Januari 2018

klokke 13.45

door

Daphne Marjoleine van Elsland

geboren te Zaandam in 1989

Promotiecommissie

Promotor	Prof.dr. H. S. Overkleeft
Co-promotor	Dr. S. I. van Kasteren
Overige leden	Dr. I. Berlin (LUMC)
	Prof.dr. A. Briegel (LU)
	Prof.dr.ir. A.J. Koster (LUMC)
	Prof.dr. J. Klumperman (UMC Utrecht)
	Prof.dr. M.H.M. Noteborn (LU)
	Dr. M. van der Stelt (LU)

ISBN: 978-94-6299-806-3
Printed by: Ridderprint BV, Ridderkerk
Cover design: D. M. van Elsland
All rights reserved. No part of this book may be reproduced in any manner or by any means without permission.

> “The important thing is not to stop questioning.
> Curiosity has its own reason for existing.”
>
> - Albert Einstein

Table of contents

Scope of the Thesis **7**

Chapter 1 **13**
Electron Microscopy for Biochemical Research

Chapter 2 **27**
The Potential of Bioorthogonal Chemistry for Correlative Light and Electron Microscopy

Chapter 3 **37**
Electron Microscopy of Bioorthogonally-Labelled Biomolecules

Chapter 4 **57**
Correlative Light and Electron Microscopy reveals Discrepancy between Gold and Fluorescence Labelling

Chapter 5 **75**
Detection of Bioorthogonal Groups by Correlative Light and Electron Microscopy allows Imaging of Degraded Bacteria in Phagocytes

Chapter 6 **91**
Towards Ultrastructural Imaging of *Salmonella*-Host Interactions using Bioorthogonal Labelling and Super-Resolution CLEM

Chapter 7 **111**
Towards Ultrastructural Imaging of Enzyme Activity with Correlative Light and Electron Microscopy

Chapter 8 **133**
Summary and Future Prospects

Nederlandse Samenvatting **139**

List of publications **143**

Curriculum Vitae *English* **145**

Curriculum Vitae *Nederlands* **147**

Scope of the Thesis

Cells are composed of billions of biomolecules, all of which have defined properties that enable them to coordinate cellular activities in both health and disease. To dissect these molecular properties, tools are required to enable researchers to track biomolecules within their native environments. It is for this purpose that numerous methods have been developed to equip biomolecules with reporter tags for visualisation within, and isolation from, biological samples. Most renowned among these are genetic protein tagging and antibody labelling approaches that have provided profound insights into protein function within cellular processes. However, these strategies are predominantly amenable to protein labelling and can not be applied to the study of other biomolecular classes, such as glycans, lipids, or metabolites.

To allow the analysis of biomolecules beyond the scope of the aforementioned labelling techniques, bioorthogonal chemistry was developed at the turn of the millennium.[1] Bioorthogonal chemistry is a chemical labelling strategy applicable to the study of a multitude of biomolecules, including nucleic acids, proteins, glycans and lipids. Its mechanism relies on a two-step labelling sequence, where a small chemical reporter is installed onto a biomolecule of interest, which is subsequently ligated to a detection group upon a chemical ligation reaction (Figure 1).[2, 3] Chemical reporters can be installed upon the introduction of functionalised metabolites into the growth medium, such as nucleotides or amino acids, which are then incorporated by the cell's own metabolic machinery (reviewed in[4]). Subsequently, functionalised metabolites are chemically conjugated to a fluorescent or affinity group for detection purposes. This conjugation reaction can take place in a physiological setting and does not interfere with biological functionalities.[3]

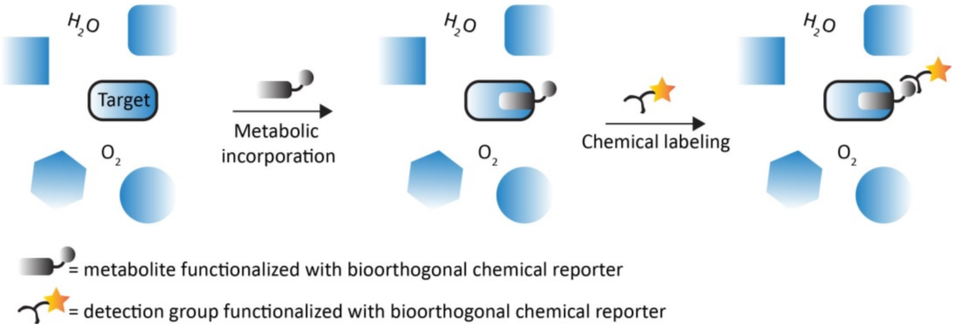
H_2O
Target
O_2
Metabolic incorporation
H_2O
O_2
Chemical labeling
H_2O
O_2
= metabolite functionalized with bioorthogonal chemical reporter
= detection group functionalized with bioorthogonal chemical reporter

Figure 1: A chemical reporter (grey circle) linked to a metabolite (grey box) is introduced into a target biomolecule by the cell's own biosynthetic machinery. In the second step, the reporter is covalently ligated to an exogenously added detection group, also functionalised with a chemical reporter (yellow star). Chemical reporters must be solely reactive towards each other, avoiding side reactions with non-target biomolecules (blue shapes).

Imaging of bioorthogonally functionalised biomolecules

Due to the wide range of functionalised metabolites, the broad spectrum of ligation reactions and the diversity of available detection groups, bioorthogonal chemistry has been of great value to the field of imaging. One of the first imaging studies that explored bioorthogonal chemistry was a study by Chang et al., in which the labelling and imaging of glycans was reported for various mammalian cell lines.[5] Since this inception, applications for the use of bioorthogonal chemistry have been ever expanding, especially through diversification of available detection groups, such as fluorogenic[6, 7] and near infra-red[8] probes for fluorescence imaging purposes. However, thus far, no studies have been reported that allow visualisation of bioorthogonal groups with electron microscopy (EM) approaches. With EM, cellular ultrastructures can be revealed at nanometer resolution, making it the method of choice for analysis of the cell's ultrastructural environment wherein biomolecules of interest reside.[9] Since this information can be of great value to the study of cellular biomolecules, *it is the aim of this thesis to explore combinatorial use of bioorthogonal labelling and EM-based imaging techniques to enable observation of specific molecular targets in their ultrastructural context within the cell.*

Aim and outline of this thesis

In **chapter 1** the principles of EM-imaging for biochemical research are discussed, including two different types of electron microscopes and various techniques to prepare specimens for transmission electron microscopy. **Chapter 1** additionally describes several labelling strategies that can be employed to identify the molecular identity of EM-revealed structures. One of these approaches; correlative light and electron microscopy (CLEM) imaging, is explained by means of two generally used CLEM strategies; live-cell CLEM and on-section CLEM.

In **chapter 2** the importance and potential of bioorthogonal chemistry for CLEM is emphasised. In this review an overview is given of frequently used bioorthogonal ligation strategies for imaging, including the copper-catalysed Huisgen cycloaddition, the strain-promoted cycloaddition, the inverse electron-demand Diels-Alder cycloaddition and the photoclick reaction. In addition, inroads that have been made towards the CLEM-imaging of bioorthogonal functionality are reviewed, including azide-modified gold particles, bioorthogonally functionalised selenide/zinc sulphide core-shell quantum dots and bioorthogonally functionalised fluorophores that are capable of photooxidizing diaminobenzidine.

Chapter 3 describes the development of two methods for the EM-detection of bioorthogonal labels in cryo-sectioned biological samples. The first method is a gold labelling strategy that allows for the direct detection of bioorthogonal tags in the electron microscope. The second method is a CLEM-based imaging method in which bioorthogonal tags are detected with fluorescence microscopy (FM) after which EM imaging is performed and images of both FM and EM are correlated.

Chapter 4 describes an in-depth analysis of gold and fluorescence labelling for EM-imaging. Upon comparison of these labelling strategies it is shown that there exist inherent discrepancies between the fluorescence signals and the distribution of gold particles. This was demonstrated by several examples and is characterised upon use of the techniques developed in **chapter 3**; the on-section gold and fluorescence labelling of bioorthogonal tags for EM imaging.

In **chapter 5** the CLEM technique described in **chapter 3** is applied to the imaging of bacterial processing in the phagolysosomal system of phagocytic cells. The *in situ* study of bacteria in the phagocytic pathway is very difficult, as genetic modification is often complicated and, if successful, only allows the tracking of pathogen phagocytosis up until the degradation of the genetically encoded protein reporters. In **chapter 5** it is shown that detection of bioorthogonal groups by CLEM allows acquisition of high resolution information on the subcellular location of the bioorthogonally-labelled bacteria, even after the proteolytic degradation of genetically encoded protein reporters.

Many bacterial pathogens have evolved clever strategies to subvert and exploit the immune response in order to enter and replicate in eukaryotic cells. A prime example of such a bacterial pathogen is *Salmonella enterica*. Upon the injection of effector proteins *Salmonella* modulates the host cell environment and as such ensures its own replication. In **chapter 6** the CLEM strategy previously reported in **chapter 5** is applied to the imaging of bioorthogonally-labelled *Salmonella* upon implementation of stochastic optical reconstruction (STORM)-super resolution imaging in the CLEM imaging sequence. This strategy has great potential to elucidate the temporal and spatial injection of *Salmonella* virulence factors and their interactions with host cells organelles.

In **chapter 7**, the potential of CLEM-based imaging of bioorthogonal functionalities, is explored for the imaging of active enzyme populations using activity-based probes (ABPs). The CLEM imaging of active cysteine protease populations is demonstrated upon use of both two-step and direct ABP labelling approaches. It is shown that with both strategies active populations of cysteine proteases can be labelled in a similar fashion with high selectivity and efficiency. In addition it is shown that with direct ABPs multiple enzyme populations can be simultaneously CLEM imaged and their relative ultrastructural location can be determined.

In the concluding **chapter 8**, all findings are summarised and alternative and future applications of the developed technique are suggested. These include bioorthogonal diaminobenzidine labelling; 3D-CLEM imaging of bioorthogonally-labelled bacteria in phagocytic cells; incorporation of bioorthogonal amino acids in *Salmonella* mutant strains and improvements for CLEM-ABP imaging.

References

1. E. Saxon and C. R. Bertozzi, *Science*, 2000, **287**, 2007-2010.
2. J. A. Prescher and C. R. Bertozzi, *Nat Chem Biol*, 2005, **1**, 13-21.
3. Craig S. McKay and M. G. Finn, *Chem Biol*, 2014, **21**, 1075-1101.
4. M. Grammel and H. C. Hang, *Nat Chem Biol*, 2013, **9**, 475-484.
5. P. V. Chang, J. A. Prescher, M. J. Hangauer and C. R. Bertozzi, *J Am Chem Soc*, 2007, **129**, 8400-8401.
6. P. Shieh, V. T. Dien, B. J. Beahm, J. M. Castellano, T. Wyss-Coray and C. R. Bertozzi, *J Am Chem Soc*, 2015, **137**, 7145-7151.
7. P. Agarwal, B. J. Beahm, P. Shieh and C. R. Bertozzi, *Angew Chem Int Ed Engl*, 2015, **54**, 11504-11510.
8. R. S. Erdmann, H. Takakura, A. D. Thompson, F. Rivera-Molina, E. S. Allgeyer, J. Bewersdorf, D. Toomre and A. Schepartz, *Angew Chem Int Ed Engl*, 2014, **53**, 10242-10246.
9. J. J. Bozzola, and Russell, L. D. , *Jones & Bartlett, Boston*, 1992.

1

Electron Microscopy for Biochemical Research

The magnification power of an electron microscope (EM) can reach over a thousand times beyond that of a conventional light microscope and allows scientists to study specimens with nanometer scale resolution.[1] The EM is therefore the main tool for the imaging of cellular ultrastructures and has given rise to many observations that form the foundation of modern cell biology. Virtually all organelles and cell inclusions were either discovered or resolved in finer detail using the EM. These descriptions have laid the foundation for experimental manipulations directed at unravelling cell function and understanding how cellular structures vary in normal, experimental, and diseased states.

Electron microscopes

Generally two different types of electron microscopes are used for biological research; the scanning electron microscope (SEM) and the transmission electron microscope (TEM) (Figure 1). The SEM is commonly used to obtain three-dimensional ultrastructural information on the surface of individual cells or small specimens and makes use of a low-energy electron beam (~0.2 keV to 40 keV) that scans the surface of a specimen. When this beam strikes the specimen, low energy secondary electrons are produced from the uppermost layers of the specimen, that are collected, processed, and eventually translated into an image.[2, 3]

The transmission electron microscope (TEM) transmits a high-energy electron beam (120-300 keV) through a specimen. The TEM can be used to study (the interior of) bacterial, mammalian and plant cells as well as viruses and proteins, and provides a two-dimensional image of the substructures that these specimens consist of.[2, 4]

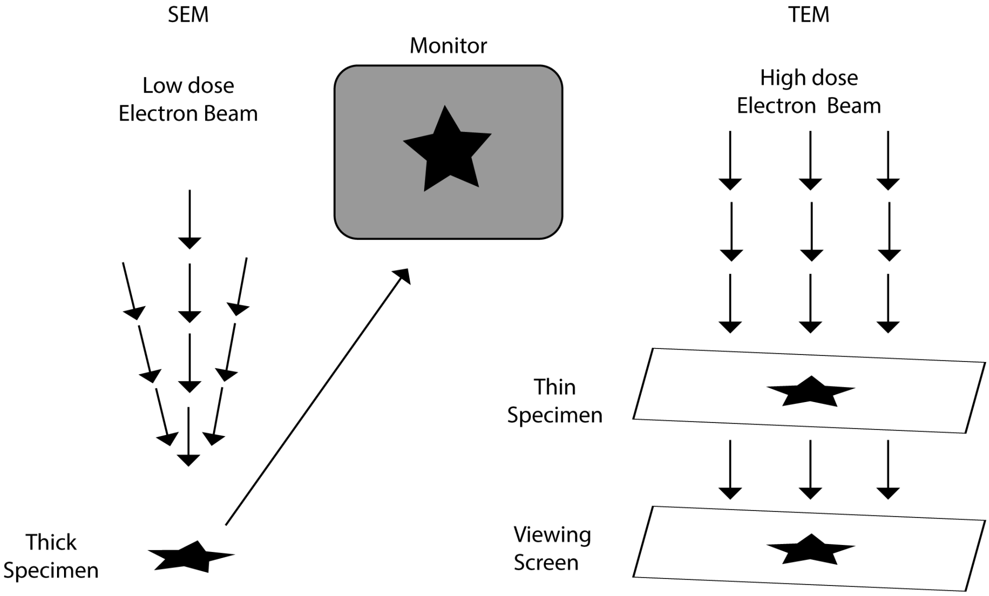

Figure 1: Basic principles of the transmission electron microscope (TEM) and the scanning electron microscope (SEM) (adapted from [2]).

TEM sample preparation; fixation, dehydration, embedding, sectioning and staining

Biological samples cannot be imaged with the electron microscope whilst alive. The vacuum in the column of the EM -necessary for the coherent targeting of the electron beam- evaporates water in (living) biological samples and this causes damage to both the sample and the EM. Moreover, at the location where the (high-)energy electron beam hits the sample temperatures are elevated. Biological samples must therefore be dehydrated prior to EM analysis. For small samples, such as purified proteins or virus particles, this can be done by air-drying or rapid freezing. However, larger biological samples need additional sample preparations, such as fixation and dehydration. Moreover, since with TEM the electron beam is transmitted through the sample, biological specimens such as mammalian cells need to be sectioned into ultrathin sections (30 to 150 nm), which requires hardening of the sample. Throughout the years many protocols have been developed to ensure the TEM analysis of biological samples and can be broadly grouped into; cryo-fixation strategies for cryo-EM analysis, whereby chemical fixation dehydration, plastic embedding and staining are obsolete; freeze-substitution strategies, whereby samples are first cryo-fixed after which frozen water is dissolved by organic solvents that contain chemical fixatives and chemical fixation strategies whereby samples are chemically fixed after which freezing or resin embedding can be performed. In the next part of this chapter the main used chemical fixation strategies will be discussed that can be used for the TEM analysis of mammalian cells.

Aldehyde fixation

Fixation is usually the first step of TEM sample preparation and protects the sample against disruption during embedding, sectioning and electron beam exposure. Generally the aldehydes glutaraldehyde and (para)formaldehyde are used for the (primary) fixation of a biological EM sample. Glutaraldehyde is a five-carbon compound that contains terminal aldehyde groups that primarily react with the amino groups of lysines (amino acids), and -to a lower extent- with lipids, carbohydrates, and nucleic acids (Figure 2A).[2] Formaldehyde forms methylene hydrate in aqueous solutions that primarily reacts with the side chains of amino acids and forms reactive hydroxymethyl side groups that can react with eachother (Figure 2B).[5] Methylene hydrate has the highest affinity for cysteine, lysine, histidine and tyrosine, but also reacts with nucleic acids and lipids.[6]

Aldehydes cross-link molecules adjacent to each other. For example, soluble proteins can cross-link to each other or to cytoskeletal or membrane-associated proteins, eventually resulting in a meshwork held together by a multitude of aldehyde molecules.[2] Glutaraldehyde cross-linking is irreversible and withstands acids, urea and heat, while paraformaldehyde cross-linking is reversible.[2] In case bridging of the hydroxymethylene groups has not yet occurred they can be rapidly returned to their original groups if the paraformaldehyde is washed away. It is therefore that the cross-linking capacities of glutaraldehyde are stronger than those of paraformaldehyde.[2] Besides differences in their cross-linking capacities, the penetration rates of glutaraldehyde and paraformaldehyde also differ. Glutaraldehyde penetrates generally very poorly in compacts tissues that have multiple membrane layers.[7] Paraformaldehyde on the other hand penetrates about five times faster than glutaraldehyde.[7] It is therefore that fixation protocols have been designed that combine both aldehyde fixatives. An example of such a protocol is the Karnovsky fixative.[8] This fixation protocol utilises a relatively low percentage of formaldehyde that in theory penetrates fast and temporarily cross-links structures that are later more permanently stabilised by glutaraldehyde.[2, 8]

Osmium tetroxide fixation

Osmium tetroxide contains four double-bonded oxygen molecules and works as a secondary fixative by reacting with lipid moieties (Figure 2C). Glutaraldehyde followed by osmium tetroxide is considered as a fixation protocol that is capable of stabilizing the maximum number of different cell components.[2] In addition to its fixation capacities, it is widely believed that the unsaturated bonds of fatty acids are oxidised by osmium tetroxide, which adds additional density and contrast to the biological sample when imaged with the TEM.[9]

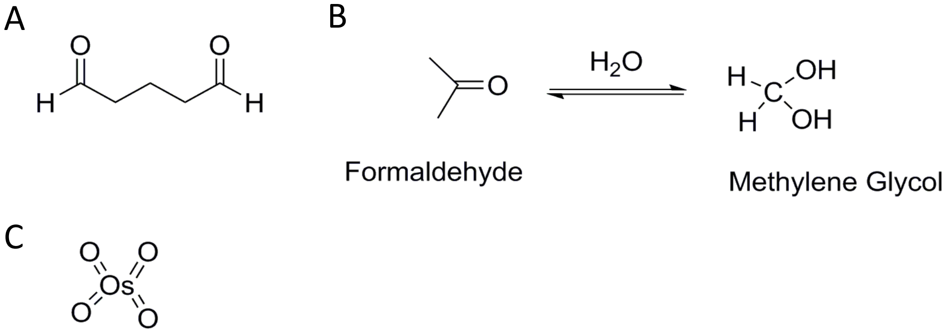

Figure 2: A) chemical structure of glutaraldehyde, B) chemical structures of formaldehyde and methylene glycol, C) chemical structure of Osmium tetroxide.

Dehydration and resin embedding

To cut ultrathin sections from relatively soft biological specimens, specimens need to be hardened. Conventionally this is done by infiltrating fixed and dehydrated specimens with a liquid plastic monomer that is subsequently polymerised *in situ*.

Dehydration is generally performed upon the gradual replacement of water by graded series of dehydrating agents such as ethanol or acetone. After dehydration the dehydrants are gradually replaced by resin monomers. These resin monomers are in the majority of instances epoxy resins, such as Epon[10] and Araldite.[11, 12] Epoxy resins are polyaryl ethers of glycerol bearing terminal epoxy groups (Figure 3A). To ensure resin polymerisation, three components must be included in the resin: (1) the epoxy resin monomer, (2) a hardening agent (for example; dodecenyl succinic anhydride (DDSA) (Figure 3B) or nadic methyl anhydride (NMA) (Figure 3C)), and (3) an accelerator (for example benzyldimethylamine (BDMA)) (Figure 3D). After resin infiltration, resins get cured at 60 ˚C. As an alternative to epoxy resins, acrylic embedding media such as Lowicryl can be used, which get cured at lower temperatures.[2, 13]

Hardening the sample without resin; the Tokuyasu technique

TEM samples can also be hardened with rapid freezing. However, this has to occur fast and samples need to be cryo-protected in order to prevent ice-crystal formation. The most renowned method for freezing samples for TEM analysis is the Tokuyasu technique.[14] With this strategy biological samples are first aldehyde fixed and embedded in gelatine, after which small sample blocks are cut and subjected to a sucrose infiltration step that functions as a cryo-protectant. Sample blocks are then placed on a metal specimen holder and are rapidly frozen and stored in liquid nitrogen.

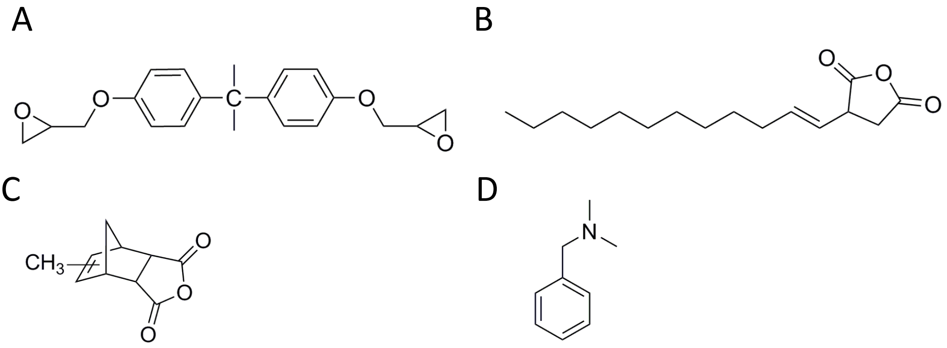

Figure 3: A) Idealised chemical structure of a typical epoxy, B) chemical structure of dodecenyl succinic anhydride (DDSA), C) chemical structure of nadic methyl anhydride (NMA), D) chemical structure of benzyldimethylamine (BDMA).

Sectioning

Once a sample is hardened by one of the above methods, ultrathin sections can be obtained. Sectioning of resin embedded samples is performed using a diamond knife and an ultramicrotome, and generally involves the following steps; trimming or shaping of the specimen block with a glass or diamond knife, cutting of sample sections in an ultramicrotome with a diamond knife, retrieving sections and placing sections onto a specimen grid holder.[2] Sections can vary in size from 30 to 150 nm. However, the general rule is the thinner the section, the higher the resolution.[2] Sectioning of frozen samples is known as cryo-ultramicrotomy and works along the same principle, with the exception that sectioning is performed at -80°C to -140°C and frozen sections are retrieved with a sucrose droplet.[14]

Staining

EM images consist of various shades of grey that represent the density differences in a specimen; darker shades are areas of the specimen that have greater density, whereas brighter areas of the specimen have less density. Since unstained biological samples have little density differences it is important to increase the image contrast by reacting cellular components with heavy metals.[2] Contrast enhancement can be established with the secondary fixative osmium tetroxide (Figure 2C)[15], and with the heavy metal stains lead citrate and uranyl acetate (Figure 4A/B). Osmium reacts with the lipid moieties of a specimen and the lead ions of lead citrate bind to negatively charged components such as carboxylate groups and osmium-reacted areas. Lead citrate staining is therefore commonly performed on sample sections that have been osmium-fixed and resin-embedded. Uranyl ions react with phosphate and amino groups, thereby staining nucleic acids and certain proteins, and are generally used to stain rehydrated cryo-sections.[16, 17]

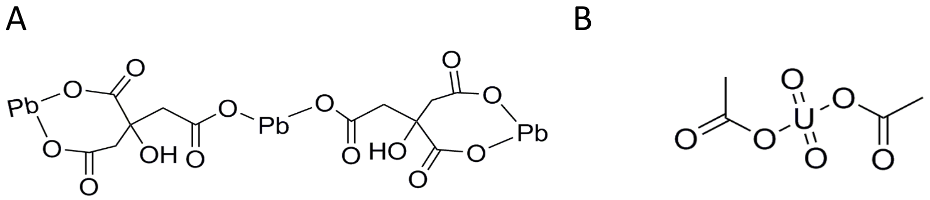

Figure 4: A) chemical structure of lead citrate, B) chemical structure of uranyl acetate.

Biomolecule detection with electron microscopy

Although TEM enables observations at nanometer-scale resolution, the revealed ultrastructures remain uncharacterised. It is therefore that several techniques have been developed to label the biomolecules that are present in the EM-revealed structures. Most commonly colloidal gold particles are used for this purpose.[18-21] These particles can be functionalised with macromolecules used in immunocytochemistry, such as antibodies and protein A,[18] and give a punctate and precise labelling pattern of the biomolecule of interest (Figure 5).[18, 19] Gold labelling is generally performed on Tokuyasu cryo-sections as with this technique epitopes remain preserved and accessible to the functionalised gold particles.[14, 22, 23]

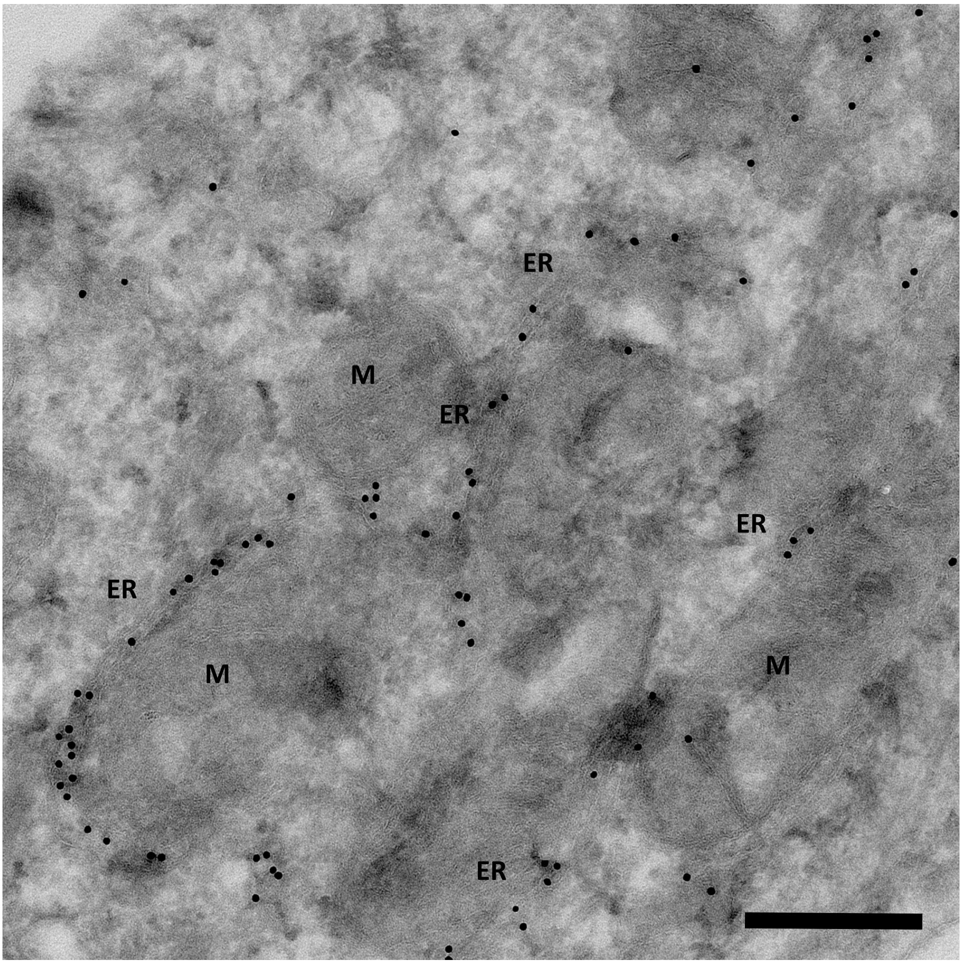

Figure 5: Example of 15 nm immunogold labelling of the endoplasmic reticulum, Endoplasmic Reticulum (ER), Mitochondria (M) (*Figure example from author's own data collection*).

Besides gold markers oxidizing substrates, such as diamino-benzidine (DAB), are also often used to generate localised osmiophilic precipitates which can serve as electron dense markers.[24] These reporter precipitates can be formed using photosensitizing dyes[25, 26], peroxidases such as horseradish peroxidase (HRP)[24] and engineered peroxidase enzymes, such as APEX/APEX2.[27] By conjugating the photosensitizing dyes/enzymes to specific antibodies or ligands, this approach can be used to visualise specific proteins.[28, 29] Due to the high penetrability of DAB it can be performed prior to sectioning. Moreover, since DAB precipitates are not affected by resin embedding, the DAB-labelling approach is commonly applied to resin-embedded samples which are generally not susceptible to any on-section labelling strategies.[2]

Correlative Light and Electron Microscopy approaches

Fluorescent markers can also be used for biomolecule detection in case fluorescent microscopy (FM) is combined with EM.[30] Specific biomolecules and cellular structures can be identified -upon use of a fluorescent marker- with FM, after which ultrastructural information about their subcellular location and context can be obtained with the EM.[30] As a result, one can interpret the fluorescent labelling on a complete cell, whereas electron dense markers are too small for detection at a low magnification. Over the years many of these correlative light and electron microscopy (CLEM) strategies have been reported,[30] which can generally be divided into these two: the ones that combine live-cell FM imaging with EM imaging, and those that combine FM and EM imaging of the same sample sections.

Correlating live-cell dynamics with EM ultrastructures

When combining live-cell FM imaging with EM imaging, dynamic processes observed with FM can be analysed with ultrastructural detail using the EM.[30] Live-cell CLEM imaging methods basically consist of six steps: 1) the incorporation of a fluorescent marker in live cells, 2) live-cell FM imaging, 3) sample preparation for EM analysis, 4) ultramicrotomy, 5) EM imaging, 6) correlation of FM and EM images.[31] An example of this workflow is illustrated in Figure 6. One of the first attempts of combining live-cell FM with EM, has been reported by Nakata et al.[32] In this study the subsequent EM imaging of *in vivo* imaged GFP-tagged plasma membrane proteins was demonstrated. Although this strategy attempted to image the same cell with both imaging modalities, it did not allow for the identification of the very same cell or region of interest (ROI).[32] This problem relies in the fact that EM imaging is in need of extra sample preparations and ultrathin sectioning; it is therefore very difficult to retrace the originally live-cell FM-imaged location with the EM. To this end various methods have been reported that focus on the EM retrieval of a ROI that has been imaged with live-cell microscopy. For example Van Rijnsoever et al. reported the retrieval of a ROI by using gridded coverslips.[33]

Correlating LM and EM from the same sections

Although strategies have been reported that improve the retrieval of the ROI in live cells with EM, it remains problematic to retrieve the exact ROI. It is therefore that strategies have been developed to correlate FM and EM images of the same sample section, a strategy referred to as on-section CLEM. This strategy does not allow for live-cell imaging, but does ensure that the exact same ROI is imaged with both imaging modalities. The on-section CLEM workflows generally consist of the following six steps: 1) the labelling with of a fluorescent marker in live, fixed or sectioned cells, 2) sample preparation for EM analysis, 3) cryo-ultramicrotomy, 4) FM imaging, 5) EM imaging, 6) correlation of FM and EM images. An example of this workflow is illustrated in Figure 7. The main difference between live-cell CLEM and on-section CLEM is that the fluorescence labelling can occur at different stages. For example, live or fixed cells can be labelled with a fluorescent reporter that remains fluorescent after EM sample preparation and ultrathin sectioning.[34] Another approach is to label the specimen after embedding and ultrathin sectioning.[35] This can also be applied in sequence to specimens that already contain fluorescence labelling, and thus allows for additional labelling steps after sample preparation. In general the on-section CLEM strategy is very useful to use FM as a map to guide through the sectioned sample, to identify transiently transfected cells, and to identify rare structures of interest. Moreover ultrathin sections (typically 50-80 nm) yield very sharp fluorescence images that lack the z-axis blur.[36] Correlation of LM and FM in case of on-section CLEM is facilitated by the use of fluorescent/electron-dense fiducials. These fiducials can be imaged with both imaging strategies and are used as a reference during correlation.[35]

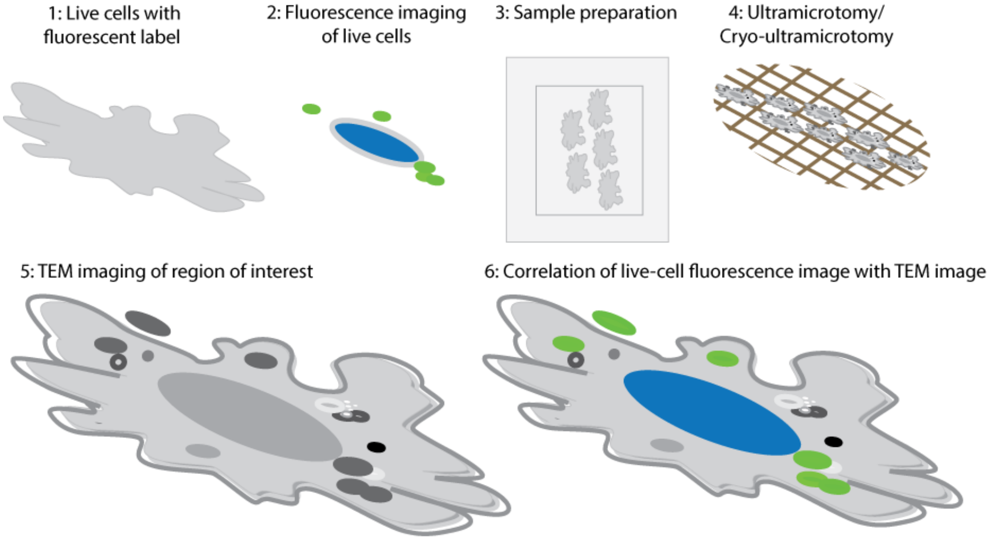
1: Live cells with fluorescent label
2: Fluorescence imaging of live cells
3: Sample preparation
4: Ultramicrotomy/ Cryo-ultramicrotomy
5: TEM imaging of region of interest
6: Correlation of live-cell fluorescence image with TEM image

Figure 6: Schematic representation of a CLEM workflow that combines live-cell imaging with EM.

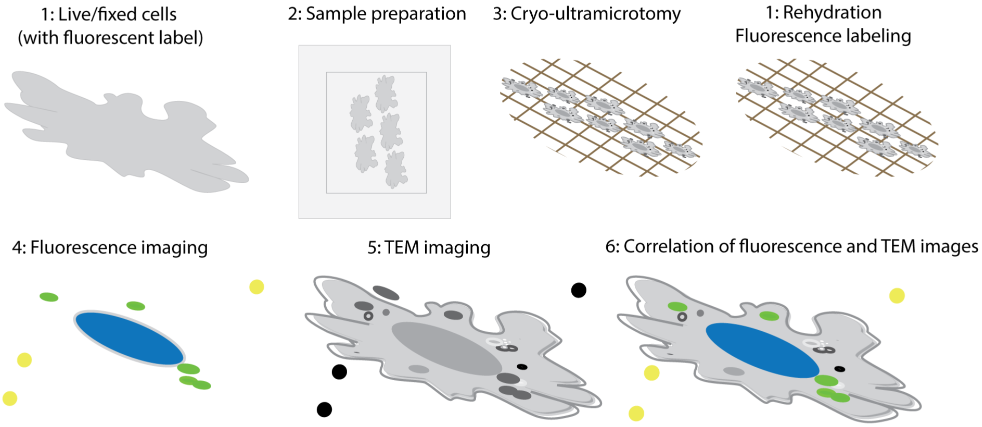
1: Live/fixed cells (with fluorescent label)
2: Sample preparation
3: Cryo-ultramicrotomy
1: Rehydration Fluorescence labeling
4: Fluorescence imaging
5: TEM imaging
6: Correlation of fluorescence and TEM images

Figure 7: Schematic representation of an on-section CLEM workflow.

Conclusion

To ensure the TEM analysis of large biological samples, samples need to be fixed, dehydrated, hardened, sectioned and stained. These procedures can be varied upon the research questions to be answered, and as a result many protocols have been developed. For example, research questions in need of the best possible ultrastructural preservation usually involve vigorous cross-linking with glutaraldehyde and resin embedding, whereas mild aldehyde fixation and cryosectioning is performed when (immuno-)labelling of the EM-revealed structures is desired.

Labelling of biological samples for TEM analysis is traditionally performed with electron-dense markers such as colloidal gold or DAB. Alternatively, specimens are imaged with both FM and the EM, followed by correlation of the acquired data sets. This strategy referred to as CLEM is especially useful for the localisation of rare events, and can be applied in combination with a wide variety of fluorescent labelling techniques.

References

1. K. R. Porter, A. Claude and E. F. Fullam, *J Exp Med*, 1945, **81**, 233-246.
2. J. J. Bozzola, and Russell, L. D. , *Jones & Bartlett, Boston*, 1992.
3. K. Tanaka, *Biol Cell*, 1989, **65**, 89-98.
4. D. B. Williams and C. B. Carter, in *Transmission Electron Microscopy: A Textbook for Materials Science*, Springer US, Boston, MA, 1996, 3-17.
5. R. Thavarajah, V. K. Mudimbaimannar, J. Elizabeth, U. K. Rao and K. Ranganathan, *J Oral Maxillofac Pathol: JOMFP*, 2012, **16**, 400-405.
6. I. Eltoum, J. Fredenburgh, R. B. Myers and W. E. Grizzle, *J Histotechnol*, 2001, **24**, 173-190.
7. M. A. Hayat, in *Fixation for Electron Microscopy*, Academic Press, 1981, 64-147.
8. M. J. Karnovsky, *J Cell Biol* , 1965, **11**, 137-140.
9. M. A. Hayat, in *Fixation for Electron Microscopy*, Academic Press, 1981, 148-182.
10. L. J. H., *J Biophys Biochem Cytol*, 1961, **9**, 409-414.
11. A. M. Glauert and R. H. Glauert, *J Biophys Biochem Cytol*, 1958, **4**, 191-194.
12. M. A. Hayat and R. Giaquinta, *Tissue Cell*, 1970, **2**, 191-195.
13. E. Carlemalm, *J Struct Biol*, 1990, **104**, 189-191.
14. K. T. Tokuyasu, *J Cell Biol*, 1973, **57**, 551-565.
15. L. Russel and S. Burguet, *Tissue Cell*, 1977, **9**, 751-766.
16. J. M. Frasca and V. R. Parks, *J Cell Biol*, 1965, **25**, 157-161.
17. J. G. Stempak and R. T. Ward, *J Cell Biol*, 1964, **22**, 697-701.
18. G. Griffiths, in *Fine Structure Immunocytochemistry*, Springer Berlin Heidelberg, 1993, 9-25.
19. T. M. Mayhew and J. M. Lucocq, *Histochem Cell Biol*, 2008, **130**, 299-313.
20. W. P. Faulk and G. M. Taylor, *Immunochemistry*, 1971, **8**, 1081-1083.
21. M. S. Sirerol-Piquer, A. Cebrian-Silla, C. Alfaro-Cervello, U. Gomez-Pinedo, M. Soriano-Navarro and J. M. Verdugo, *Micron*, 2012, **43**, 589-599.
22. J. W. Slot and H. J. Geuze, *Nature Protoc*, 2007, **2**, 2480-2491.
23. P. Webster, H. Schwarz and G. Griffiths, *Methods Cell Biol*, 2008, **88**, 45-58.
24. R. C. Graham, Jr. and M. J. Karnovsky, *J Histochem Cytochem*, 1965, **13**, 448-453.
25. G. Gaietta, T. J. Deerinck, S. R. Adams, J. Bouwer, O. Tour, D. W. Laird, G. E. Sosinsky, R. Y. Tsien and M. H. Ellisman, *Science,* 2002, **296**, 503-507.
26. X. Shu, V. Lev-Ram, T. J. Deerinck, Y. Qi, E. B. Ramko, M. W. Davidson, Y. Jin, M. H. Ellisman and R. Y. Tsien, *PLoS biology*, 2011, **9**, e1001041.
27. J. D. Martell, T. J. Deerinck, Y. Sancak, T. L. Poulos, V. K. Mootha, G. E. Sosinsky, M. H. Ellisman and A. Y. Ting, *Nat Biotechnol*, 2012, **30**, 1143-1148.

28. T. J. Deerinck, M. E. Martone, V. Lev-Ram, D. P. Green, R. Y. Tsien, D. L. Spector, S. Huang and M. H. Ellisman, *J Cell Biol*, 1994, **126**, 901-910.
29. A. R. Maranto, *Science*, 1982, **217**, 953-955.
30. P. de Boer, J. P. Hoogenboom and B. N. G. Giepmans, *Nat Meth*, 2015, **12**, 503-513.
31. S. Kobayashi, M. Iwamoto and T. Haraguchi, *Microscopy*, 2016, **65**, 296-308.
32. T. Nakata, S. Terada and N. Hirokawa, *J Cell Biol*, 1998, **140**, 659-674.
33. C. van Rijnsoever, V. Oorschot and J. Klumperman, *Nat Meth*, 2008, **5**, 973-980.
34. V. M. Oorschot, T. E. Sztal, R. J. Bryson-Richardson and G. Ramm, *Methods Cell Biol*, 2014, **124**, 241-258.
35. G. Vicidomini, M. C. Gagliani, K. Cortese, J. Krieger, P. Buescher, P. Bianchini, P. Boccacci, C. Tacchetti and A. Diaspro, *Microsc Res Tech*, 2010, **73**, 215-224.
36. M. Mori, G. Ishikawa, T. Takeshita, T. Goto, J. M. Robinson and T. Takizawa, *J Electron Microsc*, 2006, **55**, 107-112.

2

The Potential of Bioorthogonal Chemistry for Correlative Light and Electron Microscopy[*]

Introduction

Correlative light and electron microscopy (CLEM) is an imaging technique that combines the virtues of light microscopy (LM) with those of electron microscopy (EM). With this technique specific molecular and cellular structures in a cell can be identified with LM, after which ultrastructural information about their subcellular location and context can be obtained. CLEM studies that involve fluorescence microscopy may benefit from fluorescent markers that can be attached to molecules of interest to allow their identification and localisation. To date, this has most readily been done by fluorescent fusion proteins, by fluorescent antibody labelling or by the chemical modification of a protein with a fluorescent detection group.[1-3] As well as these fluorescent detection moieties, structures must be present in the CLEM sample that are both EM- and LM- detectable in order to correlate (overlay) the LM image with the EM image. Examples of such

---

[*] Published as part of; Daphne M. van Elsland, Erik Bos, Herman S. Overkleeft, Abraham J. Koster and Sander I. van Kasteren. *J. Chem. Biol*, **8**, 153–157 (2015).

EM/LM detectable structures are fluorescently-labelled cellular structures that are suitable to be identified by EM through their distinct morphology (e.g. stained nuclei), or fluorescently-labelled electron-dense particles (e.g. fluorescent microspheres).[1-4]

The above-mentioned labelling approaches have been very successfully applied to CLEM imaging of specific proteins in their cellular context. However, they carry some limitations. First, the use of fluorescent fusion proteins requires genetic manipulation of the cell, which can be difficult and can affect the function of the protein of interest.[5] An alternative to genetic manipulation is antibody labelling. However, for specimens prepared for CLEM, antibody labelling is an elaborate procedure, of which the success rate is notoriously low due to lack of functional antibodies.[6] Finally, all these labelling approaches do not readily allow imaging of non-templated biomolecules, such as glycans and lipids.

Bioorthogonal chemistry is a powerful new labelling tool that circumvents the disadvantages mentioned above and allows for the imaging of a wide range of biomolecules. Its mechanism[7] relies on the introduction of a small abiotic chemical group (one that is non-reactive with other chemical functionalities found in the cell) into a biomolecule of interest which can be specifically reacted with a detection moiety using a so-called ‘bioorthogonal’ chemical reaction: a reaction of the tag with a detectable group that is essentially background free in biological systems (Fig. 1A).[8] As this labelling strategy makes use of a small chemical group to tag a biomolecule of interest it minimally interferes with the structure of the labelled biomolecule and as such minimally affects cellular biochemistry.[9] Since the initial development of the Keto-oxime and Staudinger-Bertozzi-ligations, bioorthogonal labelling chemistry has evolved rapidly. Currently, a wide-ranging chemical toolkit is available of both tags for incorporation into biomolecules and reactions for subsequent labelling of these tags.[10] The choice of tag and modification chemistry can therefore be optimised and tailored for the specific biological hypothesis.[7]

The introduction of a bioorthogonal tag into a biomolecule of interest occurs most readily by the metabolic incorporation of a tagged biomolecule building block. One of the approaches that exemplifies the metabolic incorporation strategy was reported by Saxon et al.[11] They synthesised a cell-permeable azide-tagged N-acetylmannosamine analogue ($Ac_4ManNAz$) which was administered to mammalian cells during cell culture.[12] Inside these cells the acetyl groups were removed from $Ac_4ManNAz$, after which it was passed on to the steps of the sialic acid biosynthetic pathway where it was converted to N-azidoacetyl sialic acid (SiaNAz). After conversion to the nucleotide sugar CMP-SiaNAz, SiaNAz is incorporated into various glycoconjugates by sialyltransferase enzymes. With this approach Saxon et al. produced cells containing azide-tagged sialoglycans and visualised these using the Staudinger-Bertozzi reaction (Fig. 1B).

Since this first inception, the applications and classes of biomolecules that can be labelled with this approach have expanded rapidly. For instance, Salic & Mitchinson nicely demonstrated that bioorthogonal tags can be incorporated into newly synthesised DNA of both cultured cells and mouse tissues after metabolic incorporation of the tagged nucleic acid 5-ethynyl-2'-deoxyuridine.[13] An additional example is the metabolic incorporation of bioorthogonal tags into lipids in order to study protein lipidation and lipid trafficking (thoroughly reviewed in [14]). Likewise, metabolic incorporation of bioorthogonal chemical tags has been reported for proteins.[15] Kiick et al. showed the incorporation of bioorthogonal tags in the proteome of *Escherichia coli* (*E. coli*) cells upon addition of the tagged amino acid azidohomoalanine. They showed that azidohomoalanine could be incorporated at sites where the amino acid methionine naturally resides. Hatzenpichler et al. showed that tagging of proteins using this abiotic amino acid is a successful approach to study newly synthesised proteins in individual microorganisms within environmental samples.[9] In addition to the proteome-wide metabolic incorporation of bioorthogonal tags, single proteins can also be modified by using amber codon suppression (reviewed in [16]). Although genetic modification is needed for this approach –with the same downsides as other genetic techniques– it is a great addition to the bioorthogonal toolkit. Attachment of abiotic tags to covalent enzyme inhibitors even allows to selective visualise active populations of enzymes in a complex mixture.[17-19] Moreover, it can be applied to the tagging of biomolecules in living multicellular organisms, such as C. elegans[20], zebrafish (*Danio rerio)*[21, 22] and mice (*Mus musculus*)[23].

There are now also numerous bioorthogonal reactions available for labelling these tags (thoroughly reviewed in [24] and [10]). Examples of the most often used labelling strategies are illustrated in Fig. 1C-F. The copper-catalysed Huisgen cycloaddition (ccHc) is well-known for its high reaction rate and selectivity and is often used on fixed sample material, as copper is toxic to cells (Fig. 1C).[25] The strain-promoted cycloaddition reaction is a faster alternative of the Staudinger ligation and allows in vivo labelling as there is no need of copper catalysis during this reaction (Fig. 1D).[26] The inverse electron-demand Diels-Alder cycloaddition is a fast bioorthogonal reaction that does not require catalysis. An example of such a reaction is the cycloaddition of s-tetrazine and trans-cyclooctene derivatives (Fig. 1E).[27] It is also possible to use photo-activatable chemical groups for so-called 'photoclick'-reactions. Nitrile imine mediated [1,3]-dipolar cycloaddition reaction and has been employed to selectively functionalise an alkene genetically encoded in a protein inside *E. coli* cells.[28] The reaction procedure was reported to be simple, straightforward, and nontoxic to *E. coli* cells (Fig. 1F). This variety in labelling strategies and chemical reactions highlights the versatility of the approach as it can be altered upon experimental settings. It is even possible to 'multiplex' different bioorthogonal reactions;[29] i.e. to first label one class of biomolecules (in this case a proteasome subunit) using one bioorthogonal reaction, then perform an additional bioorthogonal reaction on a second class and a third reaction on a third class of bioorthogonal groups. This approach shows that the reactions are not just bioorthogonal, but also mutually orthogonal to one another.

Bioorthogonal chemistry is anticipated to become a powerful and useful addition to the CLEM labelling toolkit. It would allow the imaging of non-protein biomolecules and it precludes the need for genetic tagging and antibody labelling. Furthermore, the fate of biomolecules labelled by these approaches can even be monitored during the degradation process. For example, a protein labelled with bioorthogonal amino acids can be imaged, even when it is proteolytically degraded, as - unlike reporter proteins – the tags survive this catabolic pathway.[30] At the start of this project, bioorthogonal reactions had not been combined with CLEM-imaging. This is surprising, since fluorescent imaging of bioorthogonal tags has become commonplace over the last decade and a half.[7] In this review, some of the inroads that have been made towards the CLEM-imaging of bioorthogonal reactions will be highlighted.

Bioorthogonal labelling for CLEM imaging

To allow EM imaging of bioorthogonal tags an electron-dense group is required that can be introduced using a bioorthogonal reaction. The most commonly used EM-detectable groups are gold nano-particles (GNPs).[31] However, GNPs in combination with bioorthogonal labelling have not been explored for this purpose. This is remarkable, since the inverse use of bioorthogonal chemistry – to synthesise protein/DNA-modified gold particles - has been reported.[32, 33] In these studies, no change in GNP size was observed and hydrophobic, organometallic and hydrophilic moieties could be introduced onto the particles. Brennan et al.[34] used a similar biochemical approach to produce biomolecule-modified gold particles. They first produced azide-modified gold particles and 4-pentynoic acid modified lipase and reacted the two using a copper (II) catalyst with ascorbate reducing agent to generate the active Cu(I) species in situ. Under reducing conditions the thiol-gold linkage appeared stable and gold particles modified with lipase were observed. These examples indicate that GNPs have the potential to be used in combination with bioorthogonal chemistry as a labelling strategy for EM samples.

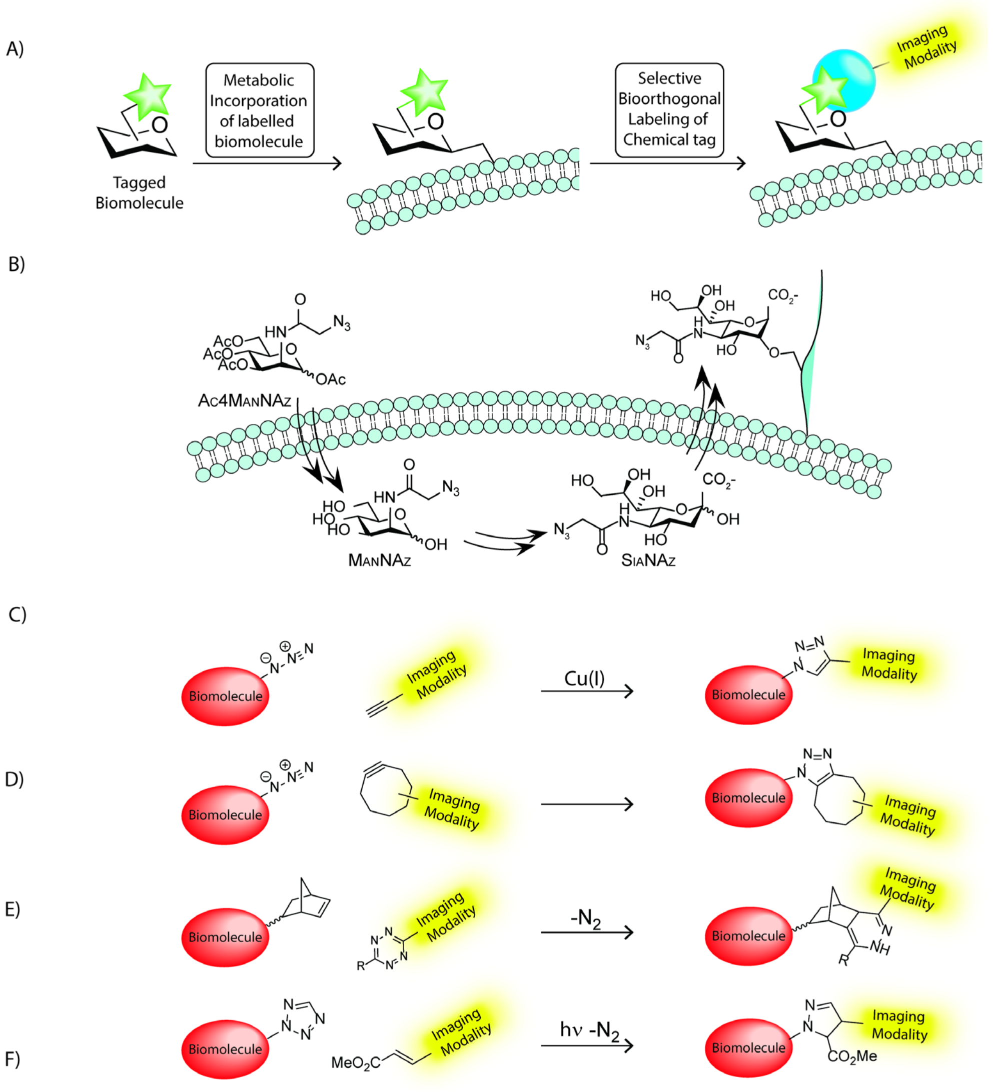
A)
Tagged Biomolecule
Metabolic Incorporation of labelled biomolecule
Selective Bioorthogonal Labeling of Chemical tag
Imaging Modality
B)
Ac4ManNAz
AcO
AcO
AcO
HN
O
N_3
OAc
ManNAz
HO
HO
HO
OH
SiaNAz
CO_2^-
HO
OH
OH
C)
Biomolecule
Imaging Modality
Cu(I)
D)
E)
$-N_2$
R
F)
MeO_2C
hν $-N_2$
CO_2Me

Figure 1: Bioorthogonal chemistry for imaging. A) General approach: a biologically inert group is incorporated into a biomolecule class in a living cell and selectively visualised using chemistry specific for this bioorthogonal group; B) An azide-labelled N-acetylmannosamine analogue is converted to CMP-sialic acid in vivo. Azido-sialic is then incorporated into the nascent glycoproteins. C-F) Recently applied bioorthogonal reactions for imaging; C) the copper-catalysed Huisgen cycloaddition [25], D) the strain-promoted cycloaddition [26], E) the inverse electron-demand Diels-Alder cycloaddition [27], F) or the photoclick reaction [28].

Instead of electron-dense EM-detectable particles, bioorthogonal fluorophore introduction could also be used for EM-imaging; namely in combination with

CLEM, especially considering that fluorescent bioorthogonal labelling strategies are very well established in the field. Additionally, to perform CLEM with this particular strategy, detectable moieties are required that are visible in both imaging modalities (e.g. fluorescent electron-dense nano- or micro-particles).

One approach to circumvent this would be to directly react the bioorthogonal tags with such electron-dense fluorophores. Quantum dots (Qdots) are suitable candidates for this purpose.[35] As with GNP modification, significant development has gone into the modification of Qdots with biomolecules using bioorthogonal strategies. Again, they have not yet been used for introducing these fluorophores for CLEM. In the case of CLEM labelling, one difficulty with the modification of Qdots using 'classic' copper-catalysed Huisgen reaction (Fig. 1C) is fluorescence quenching.[36] Fluorescence quenching was circumvented by using either the strain-promoted [3+2]-cycloaddition reaction (Fig. 1D)[36], or the tetrazine-norbornene inverse electron demand Diels-Alder reaction (Fig. 1E).[37] In the former reaction, cyclooctyne-modified cadmium selenide/zinc sulphide (CdSe/ZnS) core-shell Qdots were modified with cyclooctyne groups and as such used to image the presence of azide-containing sugars on the surface of cultured CHO cells, analogous to the work performed by the Bertozzi group. However, in these experiments no CLEM was performed. Zhang et al.[38] recently used a similar approach to image the intracellular presence of viruses. CdSe/ZnS-Qdots were modified with an azide-containing outer coating. These particles were then reacted with dibenzocyclooctyne-modified viruses that had been used to infect GFP-expressing A549 cells. This approach allowed the imaging of viral infection in these cells with good selectively. Recently, the same group published the in vivo imaging of virus infection using a near-infrared Qdot variant[39], highlighting the power of this approach.

A second alternative approach by which the subcellular location of fluorophores can be made EM-visible is by photoconversion of diaminobenzidine (DAB).[40] This approach uses fluorophores to photooxidise DAB, which results in precipitates after reaction with osmium. These precipitate are electron-dense and therefore EM-detectable. Such fluorophores are readily available as detecting agents for bioorthogonal reactions and numerous examples exist of the use of these to label biomolecules. However, again no examples have been reported of the approach where first the fluorophore is used to image a bioorthogonal label followed by photoconversion of DAB to allow for EM-imaging.

A final example of an approach that has great potential for CLEM imaging of enzyme activities is the use of an aggregating probe. Ye et al.[41] reported the use of a probe that upon cleavage by the apoptosis-related caspases 3 or 7 cyclises and precipitates to form insoluble fluorescent nano-aggregates. Rather than imaging these aggregates by CLEM, the authors imaged them by super-resolution microscopy and conventional confocal microscopy. They also showed that these probes could be applied to the in vivo imaging of tumour apoptosis after treatment with doxorubicin.

Conclusion

The examples and strategies discussed here highlight the power of bioorthogonal chemistry for the labelling of biomolecules in a cellular context. Bioorthogonal chemistry has not been explored for CLEM imaging, although many inroads have been made. It is anticipated that bioorthogonal chemistry will enable CLEM imaging of molecules for which the current toolkit is not amenable, such as non-genetically templated biomolecules, temporal subpopulations of proteins (those expressed in a given time window), or the imaging of enzymatically active subpopulation of a protein class.

References

1. C. van Rijnsoever, V. Oorschot and J. Klumperman, *Nat Meth*, 2008, **5**, 973-980.
2. M. H. Ellisman, T. J. Deerinck, X. Shu and G. E. Sosinsky, *Methods Cell Biol*, 2012, **111**, 139-155.
3. E. Bos, L. Hussaarts, J. R. van Weering, M. H. Ellisman, H. de Wit and A. J. Koster, *J Struct Biol*, 2014, **186**, 273-282.
4. E. Brown and P. Verkade, *Protoplasma*, 2010, **244**, 91-97.
5. C. L. Thomas and A. J. Maule, *J Gen Virol*, 2000, **81**, 1851-1855.
6. G. Griffiths and J. M. Lucocq, *Histochem Cell Biol*, 2014, **142**, 347-360.
7. D. M. Patterson, L. A. Nazarova and J. A. Prescher, *ACS Chem Biol*, 2014, **9**, 592-605.
8. H. C. Kolb, M. G. Finn and K. B. Sharpless, *Angew Chem Int Ed Engl*, 2001, **40**, 2004-2021.
9. R. Hatzenpichler, S. Scheller, P. L. Tavormina, B. M. Babin, D. A. Tirrell and V. J. Orphan, *Environ Microbiol*, 2014, **16**, 2568-2590.
10. K. Lang and J. W. Chin, *ACS Chem Biol*, 2014, **9**, 16-20.
11. E. Saxon and C. R. Bertozzi, *Science*, 2000, **287**, 2007-2010.
12. O. T. Keppler, R. Horstkorte, M. Pawlita, C. Schmidt and W. Reutter, *Glycobiology*, 2001, **11**, 11R-18R.
13. A. Salic and T. J. Mitchison, *Proc Natl Acad Sci U S A*, 2008, **105**, 2415-2420.
14. S. Ito, L. Shen, Q. Dai, S. C. Wu, L. B. Collins, J. A. Swenberg, C. He and Y. Zhang, *Science*, 2011, **333**, 1300-1303.
15. K. L. Kiick, E. Saxon, D. A. Tirrell and C. R. Bertozzi, *Proc Natl Acad Sci U S A*, 2002, **99**, 19-24.
16. J. Xie and P. G. Schultz, *Nat Rev Mol Cell Biol*, 2006, **7**, 775-782.
17. A. E. Speers, G. C. Adam and B. F. Cravatt, *J Am Chem Soc*, 2003, **125**, 4686-4687.
18. H. Ovaa, P. F. van Swieten, B. M. Kessler, M. A. Leeuwenburgh, E. Fiebiger, A. M. van den Nieuwendijk, P. J. Galardy, G. A. van der Marel, H. L. Ploegh and H. S. Overkleeft, *Angew Chem Int Ed Engl*, 2003, **42**, 3626-3629.
19. L. I. Willems, H. S. Overkleeft and S. I. van Kasteren, *Bioconjug Chem*, 2014, **25**, 1181-1191.
20. M. Ullrich, V. Liang, Y. L. Chew, S. Banister, X. Song, T. Zaw, H. Lam, S. Berber, M. Kassiou, H. R. Nicholas and J. Gotz, *Nat Protoc*, 2014, **9**, 2237-2255.
21. S. T. Laughlin, J. M. Baskin, S. L. Amacher and C. R. Bertozzi, *Science*, 2008, **320**, 664-667.
22. J. A. Prescher, D. H. Dube and C. R. Bertozzi, *Nature*, 2004, **430**, 873-877.

23. P. V. Chang, J. A. Prescher, E. M. Sletten, J. M. Baskin, I. A. Miller, N. J. Agard, A. Lo and C. R. Bertozzi, *Proc Natl Acad Sci U S A*, 2010, **107**, 1821-1826.
24. C. P. Ramil and Q. Lin, *Chem Commun (Camb)*, 2013, **49**, 11007-11022.
25. C. W. Tornoe, C. Christensen and M. Meldal, *J Org Chem*, 2002, **67**, 3057-3064.
26. N. J. Agard, J. A. Prescher and C. R. Bertozzi, *J Am Chem Soc*, 2004, **126**, 15046-15047.
27. M. L. Blackman, M. Royzen and J. M. Fox, *J Am Chem Soc*, 2008, **130**, 13518-13519.
28. W. Song, Y. Wang, J. Qu and Q. Lin, *J Am Chem Soc*, 2008, **130**, 9654-9655.
29. L. I. Willems, N. Li, B. I. Florea, M. Ruben, G. A. van der Marel and H. S. Overkleeft, *Angew Chem Int Ed Engl*, 2012, **51**, 4431-4434.
30. S. P. Ouellette, F. C. Dorsey, S. Moshiach, J. L. Cleveland and R. A. Carabeo, *PLoS One*, 2011, **6**, e16783.
31. J. Roth, *Histochem Cell Biol*, 1996, **106**, 1-8.
32. M. K. Rahim, R. Kota, S. Lee and J. B. Haun, *Nanotechnology Reviews*, 2013, **2**, 215-227.
33. W. R. Algar, D. E. Prasuhn, M. H. Stewart, T. L. Jennings, J. B. Blanco-Canosa, P. E. Dawson and I. L. Medintz, *Bioconjug Chem*, 2011, **22**, 825-858.
34. J. L. Brennan, N. S. Hatzakis, T. R. Tshikhudo, N. Dirvianskyte, V. Razumas, S. Patkar, J. Vind, A. Svendsen, R. J. Nolte, A. E. Rowan and M. Brust, *Bioconjug Chem*, 2006, **17**, 1373-1375.
35. B. N. Giepmans, T. J. Deerinck, B. L. Smarr, Y. Z. Jones and M. H. Ellisman, *Nat Meth*, 2005, **2**, 743-749.
36. A. Bernardin, A. Cazet, L. Guyon, P. Delannoy, F. Vinet, D. Bonnaffe and I. Texier, *Bioconjug Chem*, 2010, **21**, 583-588.
37. H. S. Han, N. K. Devaraj, J. Lee, S. A. Hilderbrand, R. Weissleder and M. G. Bawendi, *J Am Chem Soc*, 2010, **132**, 7838-7839.
38. P. Zhang, S. Liu, D. Gao, D. Hu, P. Gong, Z. Sheng, J. Deng, Y. Ma and L. Cai, *J Am Chem Soc*, 2012, **134**, 8388-8391.
39. H. Pan, P. Zhang, D. Gao, Y. Zhang, P. Li, L. Liu, C. Wang, H. Wang, Y. Ma and L. Cai, *ACS Nano*, 2014, **8**, 5468-5477.
40. K. Cortese, A. Diaspro and C. Tacchetti, *J Histochem Cytochem*, 2009, **57**, 1103-1112.
41. D. Ye, A. J. Shuhendler, L. Cui, L. Tong, S. S. Tee, G. Tikhomirov, D. W. Felsher and J. Rao, *Nat Chem*, 2014, **6**, 519-526.

3

Electron Microscopy of Bioorthogonally-Labelled Biomolecules*

Introduction

Bioorthogonal chemistry is a powerful tool to image (sub)-populations of biomolecules in complex biological systems. Its mechanism relies on the introduction of a physiologically-inert tag into a biomolecule of interest that can be reacted with a detection moiety using a chemical reaction selective solely for this chemical moiety.[1] The small size of the chemical tag, which minimally interferes with cellular biochemistry and the broad scope of the labelling strategies make this method a valuable part of the biochemist's toolkit.[2, 3] It has proven especially powerful for the labelling of nongenetically-templated biomolecules such as glycans[4], lipids[5, 6], peptidoglycans[7, 8] and even active sub-populations of proteins using activity-based probes.[9, 10] Moreover, the approach is amenable to labelling biomolecules in a wide range of cell types and species spanning the prokaryotes, eukaryotes and metazoans.[11]

---

* Published as part of: Daphne M. van Elsland, Erik Bos, Wouter de Boer, Herman S. Overkleeft, Abraham J. Koster and Sander I. van Kasteren. *Chem. Sci*, **7**, 752-758 (2016). W.S. Jong and J. Luirink are kindly acknowledged for providing the HbpΔβ-cleav plasmid.

The most commonly used detection techniques for the imaging of bioorthogonal handles are the reaction of these moieties with biotin, FLAG tags, or with a fluorophore for direct visualisation using confocal fluorescence microcopy.[2] However, the main limitations of all these imaging approaches is the lack of resolution and the lack of information regarding the cellular environment in which these bioorthogonally-labelled molecules reside. Attempts to address this with super resolution microscopy have been reported[12], but this technique only provides the localisation information of the labelled molecule to very high accuracy but does not provide ultrastructural information of the cellular context of the handle.

Electron microscopy (EM) on the other hand, allows to map cellular ultrastructures at nanometer-scale resolution,[13] but the identification of specific biomolecules using conventional EM-approaches can be cumbersome.[14] Most readily the identification of biomolecules within EM imaged specimens is established upon colloidal gold labelling. Colloidal gold can be functionalised with macromolecules used in immunocytochemistry, such as protein A, antibodies, lectins or even polysaccharides.[15] It can be easily visualised with the electron microscope due to its electron-dense character and gives a punctate and precise labelling pattern. These features make them favourable for the localisation of biomolecules within structures studied at nanometer-scale resolution. Additionally, their particulate nature allows the labelling to be quantified with the possibility of estimating the amount of a particular protein molecule in a given structure.[15, 16]

Besides colloidal gold markers, which are directly visible in the EM, one can also decide to use fluorescent markers;[17] an approach known as CLEM (correlative light and electron microscopy). It combines the strengths of both light microscopy (LM) and EM imaging. For example, an image acquired with fluorescence microscopy (whereby fluorescently labelled biomolecules are identified) is overlaid on an EM image, which provides ultrastructural context to the fluorescent signal.[18] To date, CLEM has been used successfully to image GFP-fusion proteins, biomolecules labelled with immunofluorescence,[19, 20] or for the detection of small molecule fluorophores.[19-22]

These labelling techniques have, however, not been exploited to localise bioorthogonal groups in biological samples. One problem may be partial loss of the bioorthogonal functional groups during the (often harsh) conditions required for resin embedding of the samples (e.g. heating in presence of epoxide during Epon-embedding or exposure to radical polymerisation during Lowicryl-embedding).[23] This, combined with the fact that the yield of the bioorthogonal detection reaction must be very high and essentially background-free to allow detection of the label in ultrathin sections, may have prevented the application of this imaging modality to the detection of bioorthogonal functionalities in biological samples to date.

In this chapter the method development of EM compatible bioorthogonal labelling approaches are presented. These approaches build further on the Tokuyasu technique commonly used for on-section immuno-labelling[21, 24] which uses vitrification of cryoprotected, aldehyde-fixed samples and subsequent cryosectioning. The first method presented makes use of gold labelling, allowing the direct EM-visualisation of bioorthogonal groups in a biological sample. The second approach is a CLEM-based approach. This approach uses bioorthogonal fluorophore labelling and fluorescence microscopy prior to EM contrast enhancement and EM imaging of the same section. These methods were developed using the model bacterium *Escherichia coli* (*E. coli*). In this bacterium bioorthogonal azide handles[25, 26] can be readily incorporated by replacement of the methionine (Met) with azidohomoalanine (Aha) in the Met auxotrophic strain B834(DE3).[27, 28]

Results

Aha-incorporation in *E.coli* B834(DE3) was optimised with respect to cell viability and amount of incorporation. Culturing *E. coli* B834(DE3) for > 1 hour in the presence of 4 mM Aha (azido-*E. coli*) resulted in reduced outgrowth in comparison to cultures grown in the presence of Met (Figure 1). As well as showing reduced outgrowth, inclusion bodies were found to be formed at these time points (Figure 2), suggesting negative effects on protein folding upon prolonged exposure to Aha.[29] Labelling for 1 h in the presence of 4 mM Aha gave a robust signal throughout the *E. coli* proteome and showed minimal inhibition of viability (supported by[30]; Figure 3). These conditions (1 h, 4 mM Aha) were used for all further imaging studies.

Next it was tested whether the azido-*E. coli* B834(DE3) cells could be labelled with gold particles. Initial attempts aiming to directly conjugate gold particles to the bioorthogonal groups proved unsuccessful. But a labelling method based on a two-step strategy did prove fruitful: bioorthogonal copper-catalysed Huisgen cycloaddition (ccHc) was performed with a fluorophore,[31-33] followed by immunogold labelling against the fluorophore (Figure 4A). This two-step gold labelling strategy was tested on the surface of whole mount *E. coli* cells.

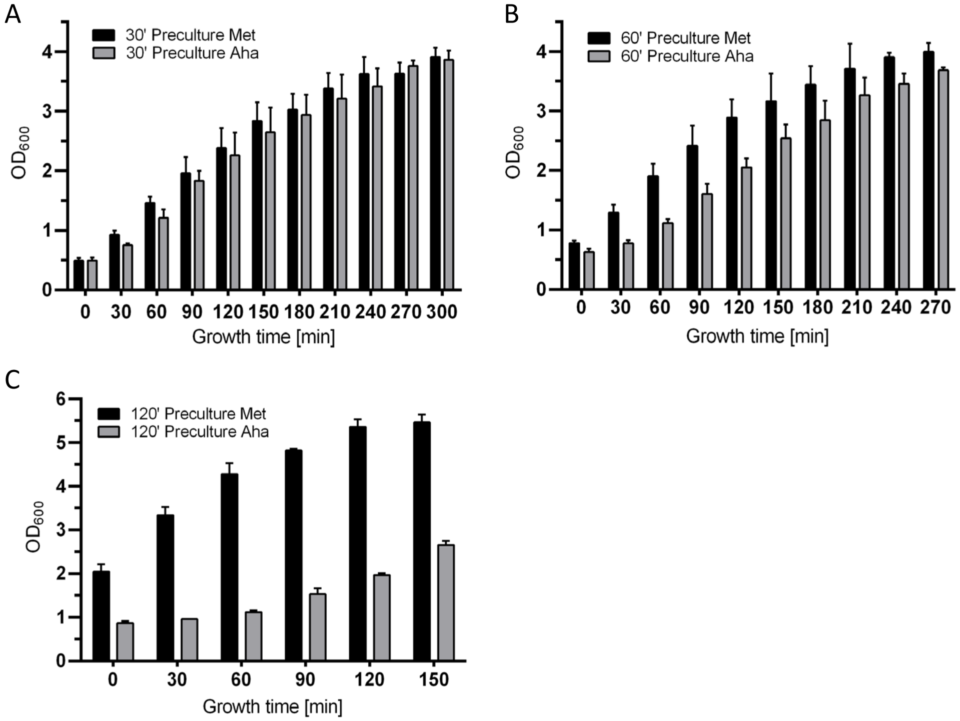

Figure 1: Outgrowth of *E. coli* B834(DE3) that were cultured in the presence of Aha (n=2): *E. coli* B834(DE3) cells were grown to an OD_{600} of 0.3-0.5. Cultures were then incubated with 4 mM Aha for either 30(A), 60(B) or 120 minutes (C). Cells were then collected and left to grow in LB medium. OD_{600} was measured at indicated time points. Cultures grown in the presence of Aha for t > 60 minutes showed severe effects on the outgrowth.

To ensure a high density of bioorthogonally labelled proteins on the surface of *E. coli*, *E. coli* B834(DE3) was transformed with the uncleavable autotransporter protein hemoglobin protease (Hbp).[34, 35] Upon incorporation of Aha in both the Hbp(Δβ-cleav) expressing and the Wild type (Wt) bacteria, the bioorthogonal gold labelling strategy resulted in a robust labelling of the *E. coli* surface. Surface labelling of the Hbp(Δβ-cleav)-transformed *E. coli* was more pronounced compared to Wt *E. coli*, demonstrating the presence of bioorthogonally labelled Hbp(Δβ-cleav) (Figure 4B). Expression of the Hbp(Δβ-cleav) in the presence of 4 mM Aha was additionally confirmed with SDS-PAGE (Figure 5).

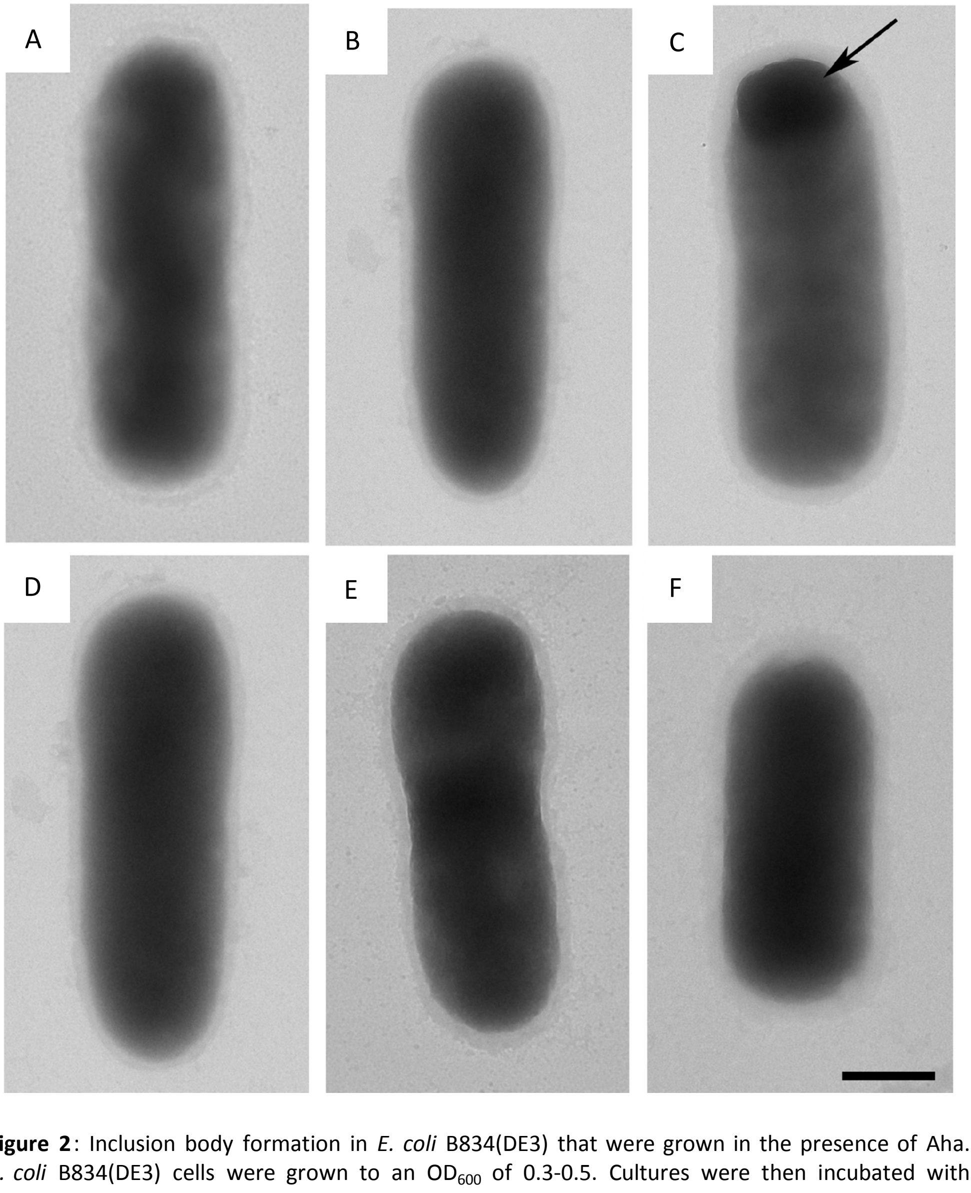

Figure 2: Inclusion body formation in *E. coli* B834(DE3) that were grown in the presence of Aha. *E. coli* B834(DE3) cells were grown to an OD_{600} of 0.3-0.5. Cultures were then incubated with 4 mM Aha (A-C) or 4 mM Met (D-F). After 30 (A, D), 60 (B, E) and 120 minutes (C, F) cells were harvested, fixed with 2% PFA and imaged with the electron microscope. Inclusion bodies were present in *E. coli* cells cultured for 120 minutes in the presence of 4 mM Aha (C). Inclusion body is indicated with an arrow. Scale bar 500 nm.

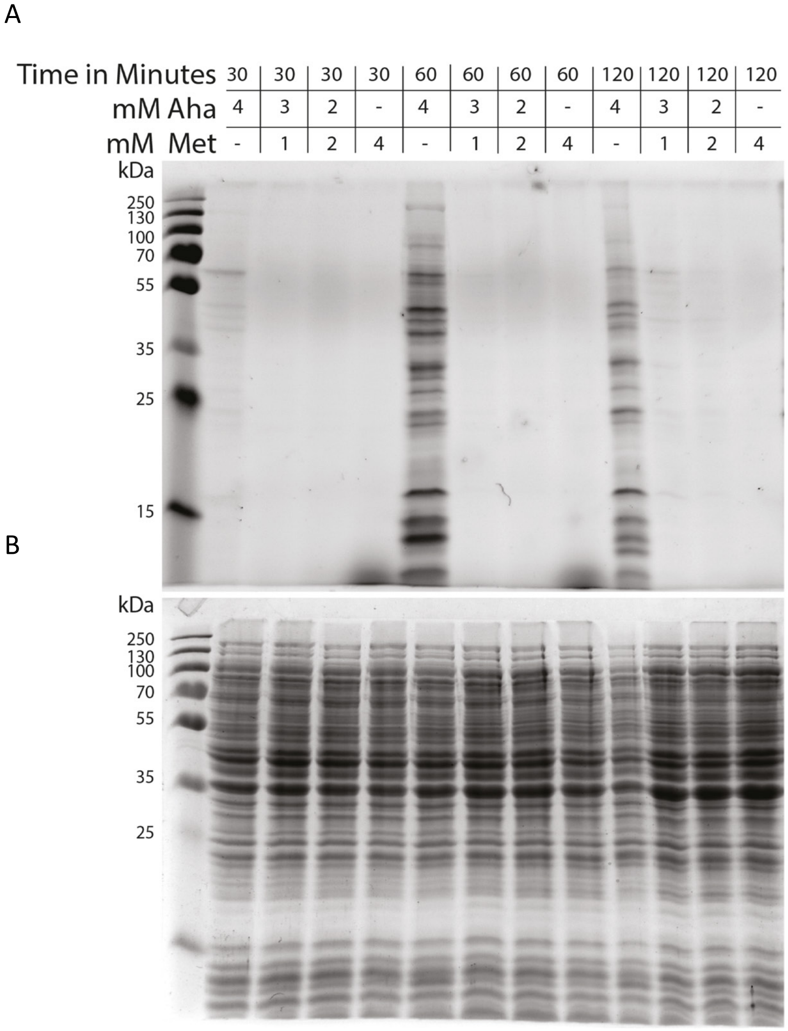
A
Time in Minutes 30 30 30 30 60 60 60 60 120 120 120 120
mM Aha 4 3 2 - 4 3 2 - 4 3 2 -
mM Met - 1 2 4 - 1 2 4 - 1 2 4
kDa
250
130
100
70
55
35
25
15
B
kDa
250
130
100
70
55
35
25

Figure 3: Aha incorporation in *E. coli* B834(DE3): (A) Fluorescence gel of AlexaFluor-488 alkyne-labelled *E. coli* cells grown in the presence of the indicated concentrations of Aha and Met. Maximal label incorporation was seen after 60 minutes in absence of Met and in presence of 4 mM Aha. (B) Coomassie-staining loading control shows relative amounts of total proteins per sample.

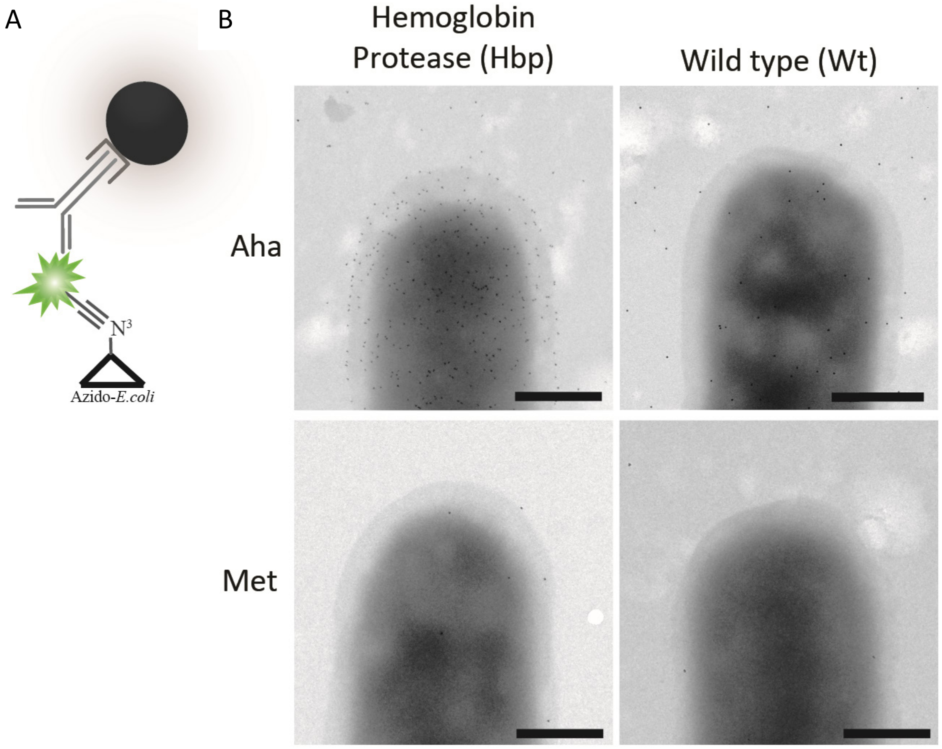
A
B
Hemoglobin Protease (Hbp)
Wild type (Wt)
Aha
Met
N3
Azido-E.coli

Figure 4: A) Schematic overview of bioorthogonal gold labelling strategy. Azido-*E. coli* B834(DE3) cells are surface-labelled with AlexaFluor-488 alkyne (green), after which gold particle labelling is performed using a rabbit anti-AlexaFluor-488 binding step. B) Bioorthogonal gold surface-labelling of Hbp (Δβ-cleav)-expressing and Wild type (Wt) *E. coli* B834(DE3) bacteria cultured in the presence of either 4 mM Aha or 4 mM Met. Scale bars 500 nm.

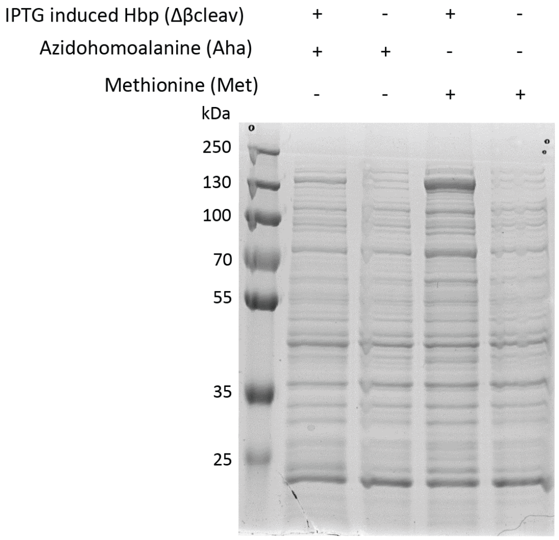
IPTG induced Hbp (Δβcleav) + - + -
Azidohomoalanine (Aha) + + - -
Methionine (Met) - - + +
kDa
250
130
100
70
55
35
25

Figure 5: Coomassie-stained SDS-PAGE gel of *E. coli* B834(DE3) cells with/without Hbp(Δβ-cleav) expression and grown in the presence of either 4 mM Aha or 4 mM Met.

To ensure the analysis of bioorthogonal labelling on ultrastructures, it was next tested whether the bioorthogonal tagged *E. coli* B834(DE3) cells could be specifically gold-labelled after Tokuyasu sample preparation and cryosectioning.[36] To this end a mixture of the bioorthogonal tagged azido-*E. coli* cells and *E. coli* control cells (grown in the presence of Met) was subjected to Tokuyasu sample preparation. *E. coli* cells (Aha and Met treated) were fixed for 24h in 0.1 M phosphate buffer containing 2% paraformaldehyde (PFA). Labelling with the bioorthogonal gold labelling method shows that the azido-*E. coli* bacteria could be labelled and detected within a mixture with Met control cells (Figure 6). The ccHc reaction has sufficient signal-to-noise ratio for detection of azides even in ultrathin sections. Fixation of the bacteria with 2% PFA supplemented with 0.2% glutaraldehyde (GA) gave undesired background labelling, which is clearly visible on the Met treated control cells (Figure 7). This background was also present on whole mount *E. coli* cells upon fixation with 0.2% GA (Figure 7). All following fixations were therefore performed without GA.

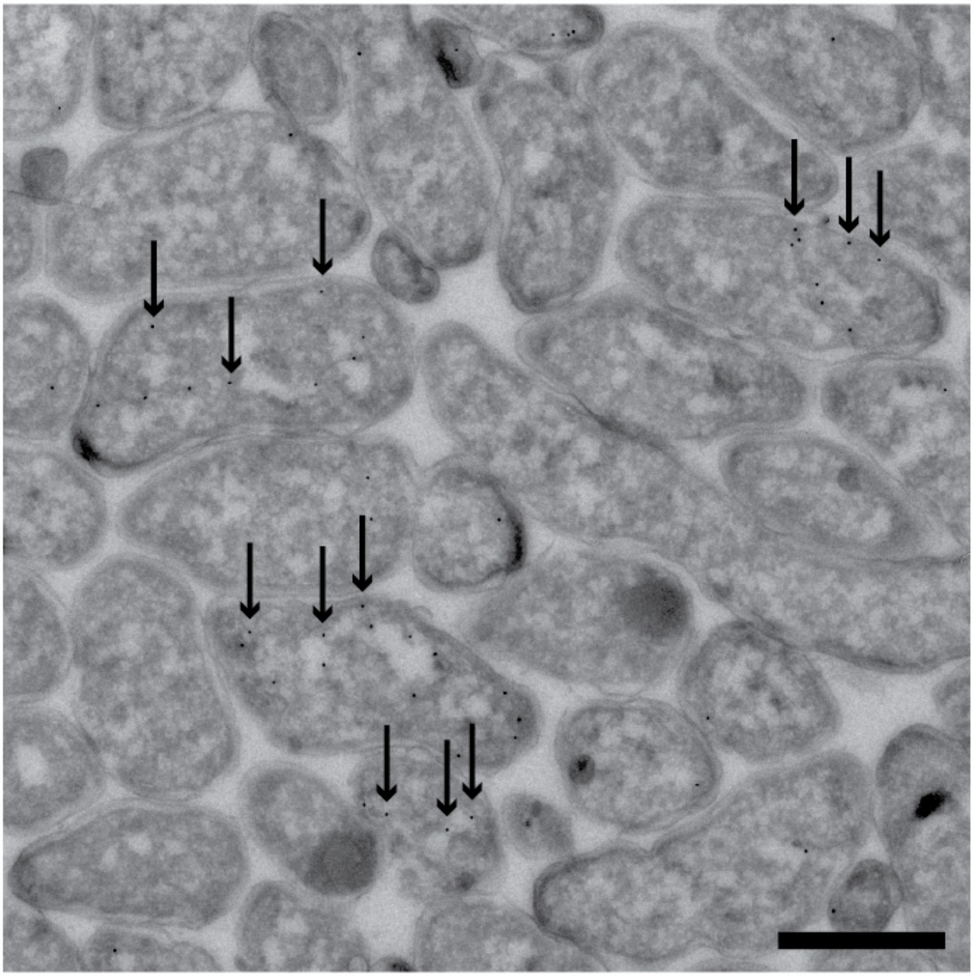

Figure 6: EM image of azido-*E. coli* mixed 1:25 with Met-treated *E. coli*. After mixing, cells were fixed with 2% PFA and subjected to Tokuyasu sample preparation (including gelatin embedding and sucrose infiltration) prior to cryosectioning into 75 nm sections. An on-section ccHc reaction was performed to react azido-*E. coli* cells with AlexaFluor-488 alkyne. AlexaFluor-488 was then labelled with 15 nm protein A coated gold particles using an anti-AlexaFluor-488 antibody. Arrows indicate gold particles. Scale bar 1 µm.

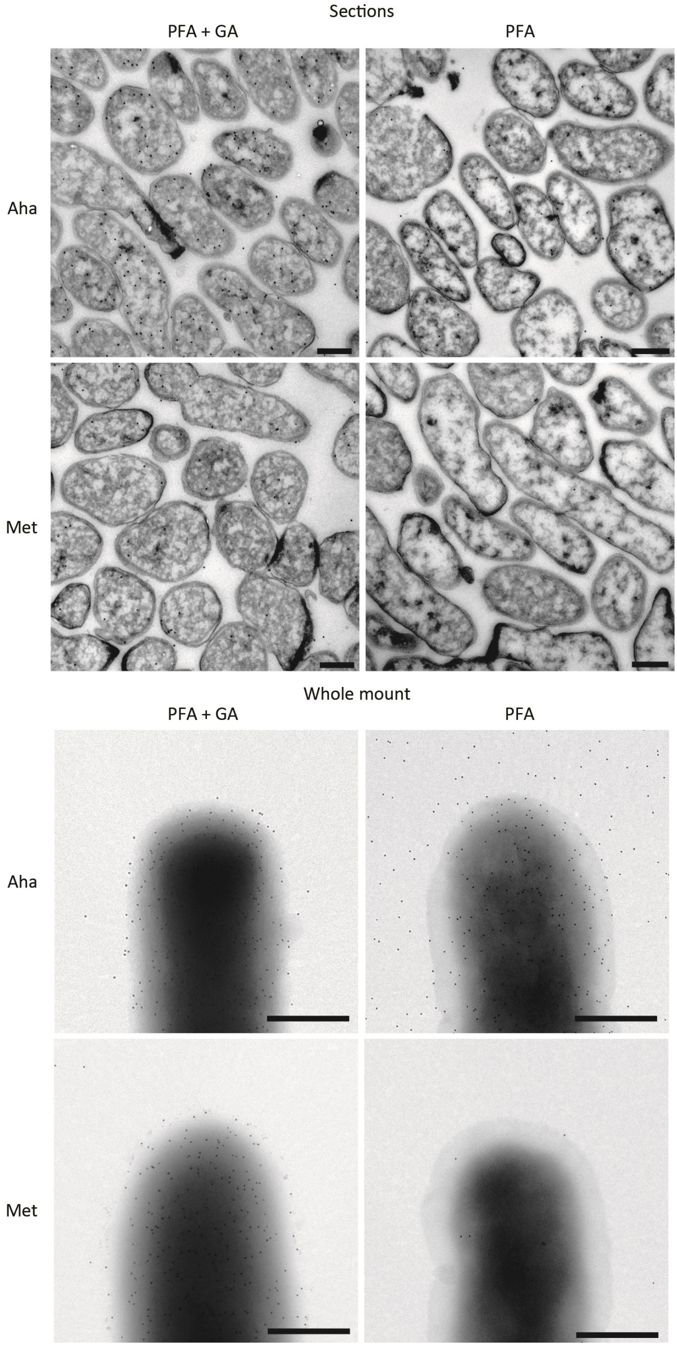
Sections
PFA + GA
PFA
Aha
Met
Whole mount
PFA + GA
PFA
Aha
Met

Figure 7: Upper panel; Azido-*E. coli* and Met-treated *E. coli* fixed with either 2% PFA or 2% PFA supplemented with 0.2% GA and labelled with bioorthogonal gold labelling strategy. Scale bar 1 µm. Lower panel; bioorthogonal gold surface-labelling of Hbp(Δβ-cleav) expressing *E. coli* B834(DE3) bacteria cultured in the presence of either 4 mM Aha or 4 mM Met and fixed with either 2% PFA or 2% PFA supplemented with 0.2% GA. Scale bars 500 nm.

It was then verified whether bioorthogonal labels could be additionally detected in an EM setting using a CLEM approach. To this end a strategy was developed that is outlined in Figure 8A. Mixed azido-*E. coli* and Met-incubated *E. coli* were cryosectioned and transferred to a TetraSpeck bead-containing EM grid and were labelled with AlexaFluor-488-alkyne using a ccHc-reaction. These sections were then imaged with the confocal microscope and were embedded in methyl cellulose with uranyl acetate and subjected to EM imaging. Correlation of the confocal- and EM-images was performed using TetraSpeck beads[37] as fiducials (Figure 8A and 9). Results show that CLEM imaging of azides using bioorthogonal labelling is selective and that the ccHc reaction has sufficient signal-to-noise ratio for the detection of fluorescently-labelled azides in ultrathin sections (Figure 8B).

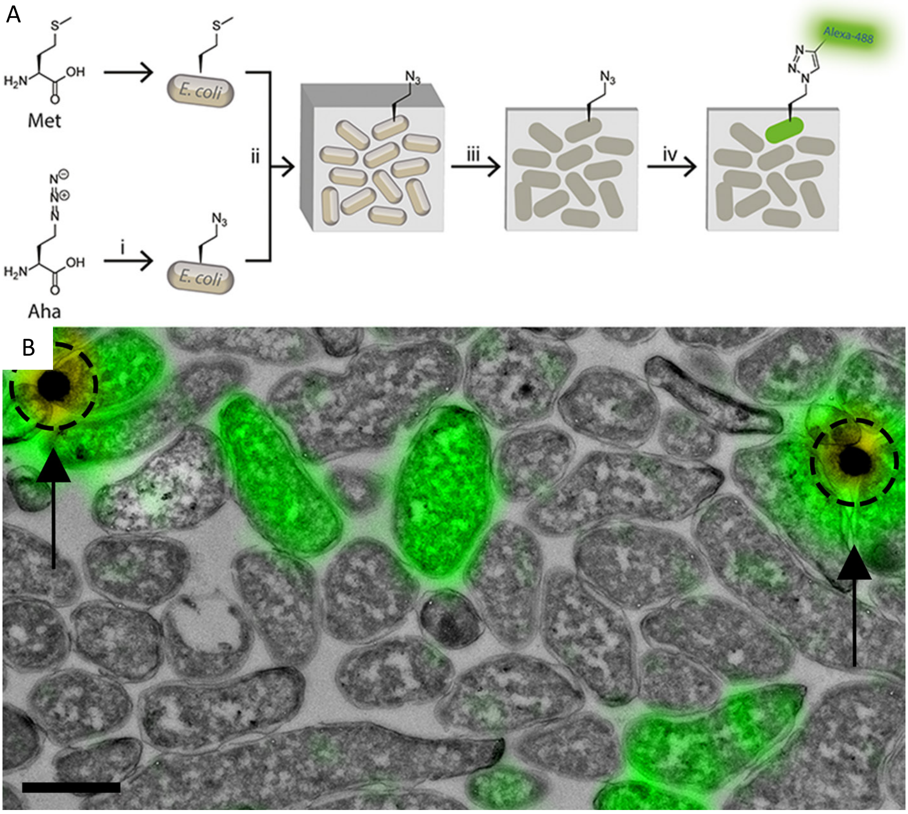

Figure 8: A) Schematic overview of bioorthogonal labelling strategy for CLEM-imaging. Azido and unlabelled *E. coli* were mixed in non-equal ratio (1:25). After Tokuyasu sample preparation and cryosectioning into 75 nm sections, a ccHc-reaction with AlexaFluor-488 was performed. B) CLEM-image of the above experiment. Green: AlexaFluor-488 label. Dotted circles: signal from the 100 nm TetraSpeck beads. Scale bar 1 µM.

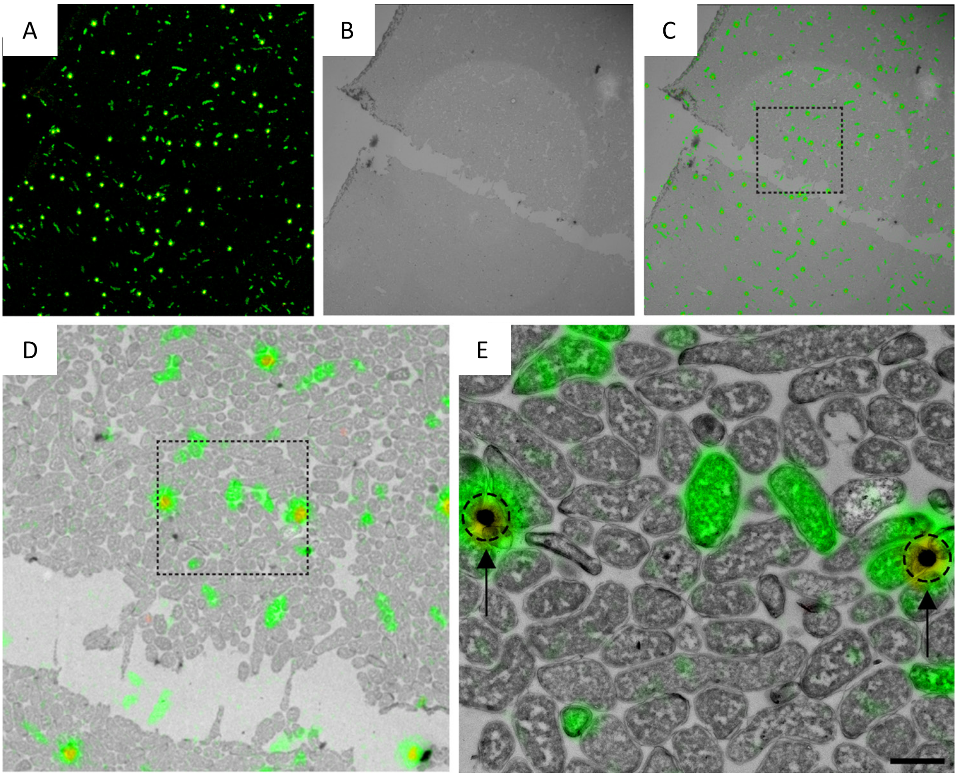

Figure 9: CLEM image of azido-*E. coli* B834(DE3) in a mixture with unlabelled *E. coli* B834(DE3) (A) Confocal microscopy image of azido-*E. coli* B834(DE3) in a mixture with unlabelled *E. coli* B834(DE3). Green: AlexaFluor-488 and 100 nm TetraSpeck beads, Yellow = 100 nm Tetraspeck bead. (B) EM image of azido-*E. coli* B834(DE3) in a mixture with unlabelled *E. coli* B834(DE3). (C) CLEM image obtained from figure A and B using section shape for correlation. (D) Detail from C. Green: AlexaFluor-488 alkyne and 100 nm TetraSpeck beads, Yellow 100 nm Tetraspeck beads. Tetraspeck beads were used for correlation. (E) Detail from D. Green: AlexaFluor-488 alkyne and 100 nm TetraSpeck beads, Yellow 100 nm Tetraspeck beads (indicated with circles and arrows). Tetraspeck beads were used for correlation. Scale bar 1 µM.

Conclusion

Two methods were developed for the EM detection of intracellular bioorthogonal groups on ultrathin cryosections. The first method is a bioorthogonal gold labelling strategy that allows for the direct detection of gold-labelled bioorthogonal tags in the EM. The second method uses CLEM for the detection of bioorthogonal labels in cryosectioned biological samples. This approach provides facile detection of bioorthogonal tags with fluorescence microscopy and gives ultrastructural information on the cellular location of these tags using EM. Both methods show that bioorthogonal labelling can be used to selectively label and localise the presence of bioorthogonal tags with EM in a non-homogenous sample of tagged and untagged *E. coli*.

Since a wide variety of both templated and non-templated biomolecules can be modified by this method, it is foreseen that these labelling stratagies can be applied to address a wide range of research questions, which would benefit from the combination of these bioorthogonal labels and the ultrastructural context provided by EM. A final advantage and challenge would be to image biomolecules in organisms for which genetic modification is not an option, such as many bacterial and viral pathogens, which could lead to new insights regarding infectivity and clearance of these organisms by host cells. Furthermore, the stability of azides[38] to intracellular conditions would allow imaging of events long after the degradation of reporter proteins.

Experimental

E. coli culturing conditions and growth measurements

E. coli B834(DE3) bacteria were grown overnight at 37°C in Lysogeny Broth (LB) medium. The following day cultures were diluted 1:50 in LB medium and grown at 37°C untill an OD_{600} between 0.3-0.5 was reached. Subsequently cells were collected and resuspended in Selenomet medium (Molecular Dimensions) and supplemented with different concentrations of either Aha (Bachem) or Met (Sigma-Aldrich). After 30 minutes, 1 h, 2 h and 3 h OD_{600} were measured and cells were collected by centrifugation (13,000 x g for 1 minute) for further analysis. To monitor the outgrowth of *E. coli* cells that were cultured in the presence of Aha/Met, cells were collected by centrifugation (13,000 x g for 1 minute) at the indicated time points, after which Aha/Met-containing medium was replaced for LB medium and OD_{600} measurements were performed.

E. coli B834(DE3)Hbp(Δβ-cleav) bacteria were grown overnight at 37°C in LB medium supplemented with chloramphenicol (cam) (f.c. 30 µg/ml). The following day cultures were diluted 1:50 in LB medium with cam (f.c. 30 µg/ml) and grown at 37°C untill an OD_{600} between 0.3-0.5 was reached. Subsequently cells were collected and resuspended in Selenomet medium (Molecular Dimensions) and supplemented with either 4 mM Aha (Bachem) or 4 mM Met (Sigma-Aldrich). Expression of HbpΔβ-cleav was induced by addition of 1 mM Isopropyl β-D-1-thiogalactopyranoside (IPTG, Sigma-Aldrich). After 2 h of induction cells were collected by centrifugation (13,000 x g for 1 minute) for further analysis.

Inclusion body analysis

At the indicated time points *E. coli* cells were fixed for 2 h with 2% PFA in 0.1 M phosphate buffer. The fixed cells were harvested by centrifugation (13,000 x g for 1 minute) and resuspended in PBS. Formvar carbon-coated copper grids were floated on small drops of fixed *E. coli* cells for 5 minutes at room temperature. Grids were then washed on 3 drops of PBS and 10 drops of aquadest. Cells were imaged with a Tecnai 12 transmission electron microscope (FEI) at 120 kV acceleration voltage.

SDS-PAGE Analysis

At the indicated time points *E. coli* B834(DE3) cells were collected and lysed with lysis buffer (50 mM HEPES pH 7.3, 150 mM NaCl and 1% NP-40) and incubated on ice for 1 h. Subsequently protein concentrations were determined with a Quibit 2.0 fluorimeter (Life Technologies), after which 20 µg of the protein was incubated for 1 h with ccHc-cocktail (0.1 M HEPES pH 7.3, 1 mM $CuSO_4$, 10 mM sodium ascorbate, 1 mM THPTA ligand, 10 mM amino-guanidine, 5 µM AlexaFluor-488 alkyne (Invitrogen)). Samples were then resuspended in 4x SDS Sample buffer (250 mM Tris.HCl pH 6.8, 8% w/v SDS, 40% glycerol, 0.04% w/v bromophenol blue, 5% 2-mercaptoethanol) and incubated at 100°C for 5 minutes. After the samples were run through a Hamilton syringe multiple times to shear genomic DNA, samples were subjected to SDS-PAGE. Gels were then directly imaged with a Biorad Universal Hood III for in-gel visualisation of fluorescent labelling. As a loading control gels were stained with Coomassie Brilliant Blue. PageRuler Plus Prestained Protein Ladder (Thermo Scientific) was used as a protein standard.

At the indicated time points *E. coli* B834(DE3)Hbp(Δβ-cleav) cells were collected and lysed with lysis buffer (50 mM HEPES pH 7.3, 150 mM NaCL and 1% NP-40) and incubated on ice for 1 h. Subsequently protein concentrations were determined with a Quibit 2.0 fluorimeter (Life Technologies). Samples were then resuspended in 4x SDS Sample buffer (250 mM Tris.HCl pH 6.8, 8% w/v SDS, 40% glycerol, 0.04% w/v bromophenol blue, 5% 2-mercaptoethanol) and incubated at 100°C for 5 minutes. After the samples were run through a Hamilton syringe multiple times to shear genomic DNA, samples were subjected to SDS-PAGE. Approximately 20 µg protein was loaded per lane. Gels were then stained with Coomassie Brilliant Blue. PageRuler Plus Prestained Protein Ladder (Thermo Scientific) was used as a protein standard.

Bioorthogonal gold labelling on whole mount E. coli B834(DE3)

At the indicated time points *E. coli* B834(DE3)wt and *E. coli* B834(DE3)HbpΔβ-cleav cells were collected and resuspended in either 4% PFA in 0.1 M phosphate buffer or 4% PFA, 0.2% GA in 0.1 M phosphate buffer for 1 h at room temperature. The fixed cells were harvested by centrifugation (13,000 x g for 1 minute), resuspended in storage solution (0.5% PFA in 0.1 M phosphate buffer) and kept at 4°C until further analysis.

Fixed *E. coli* cell pellets, containing ~1 OD_{600} were resuspended in blocking buffer (1% Bovine Serum Albumin (BSA), 1% Gelatin from Cold Water Fish (GCWSF) in 0.1

M HEPES pH 7.3) and blocked for 15 minutes. Subsequently cells were collected by centrifugation (13,000 x g for 1 minute) and resuspended in click cocktail (0.1 M HEPES pH 7.3, 1 mM $CuSO_4$, 10 mM sodium ascorbate, 1 mM THPTA ligand, 10 mM amino-guanidine, 5 µM AlexaFluor-488 alkyne (Invitrogen)). The cells were incubated for 1 h with the click cocktail, then washed 3 times with HEPES 0.1 M pH 7.3. Subsequently Formvar carbon-coated copper grids were floated on small drops of the fluorescently-click-labelled *E. coli* cells for 5 minutes at room temperature. Grids were then washed on 3 drops of PBS and blocked with 1% BSA in PBS for 15 minutes. Next, the grids were incubated for 1 h with an AlexaFluor-488 antibody diluted in PBS supplemented with 1% BSA. After 5 washes with PBS, the antibodies were probed with protein A conjugated to 15 nm gold (PAG; CMC, Utrecht University). Labellings were imaged with an Tecnai 12 transmission electron microscope (FEI) at 120 kV acceleration voltage.

Preparation of cryosections

Samples were prepared for cryosectioning as described elsewhere.[39] Briefly, *E. coli* cells were fixed for 24 h in freshly prepared 2% PFA in 0.1 M phosphate buffer with or without 0.2% GA. Fixed cells were embedded in 12% gelatin (type A, bloom 300, Sigma Aldrich) and cut with a razor blade into 0.5 mm^3 cubes. The sample blocks were infiltrated in phosphate buffer containing 2.3 M sucrose for 3 h. Sucrose-infiltrated sample blocks were mounted on aluminium pins and plunged in liquid nitrogen. The frozen samples were stored under liquid nitrogen.

Ultrathin *E.coli* cell sections of 75 nm were obtained as described elsewhere.[39] Briefly, the frozen sample was mounted in a cryo-ultramicrotome (Leica). The sample was trimmed to yield a squared block with a front face of about 300 x 250 µm (Diatome trimming tool). Using a diamond knife (Diatome) and antistatic devise (Leica) a ribbon of 75 nm thick sections was produced that was retrieved from the cryo-chamber with a droplet of 1.15 M sucrose containing 1% methylcellulose. Obtained sections were transferred to a specimen grid previously coated with formvar and carbon. In case of CLEM imaging, grids were additionally coated as indicated with 100 nm TetraSpeck beads (Life Technologies).

Bioorthogonal gold labelling on cryosections

Sections were labelled as follows: thawed cryosections on an EM grid were left for 30 minutes on the surface of 2% gelatin in phosphate buffer at 37°C. Subsequently, grids were incubated on drops of PBS/glycine and PBS/glycine containing 1% BSA. Grids were then incubated on top of the ccHc- cocktail (0.1 M HEPES pH 7.3, 1 mM $CuSO_4$, 10 mM sodium ascorbate, 1 mM THPTA ligand, 10 mM amino-guanidine, 5 µM AlexaFluor-488 alkyne (Invitrogen) for 1 h and washed 6 times with PBS. Then the grids were blocked again with PBS/glycine containing 1% BSA after which the grids were incubated for 1 h with PBS/glycine 1% BSA supplemented with an AlexaFluor-488 antibody (Invitrogen). After washing with PBS/glycine and blocking with PBS/glycine 0.1% BSA, grids were incubated for 20 minutes on PBS/glycine 1% BSA supplemented with 15 nm PAG (CMC, Utrecht University). Grids were then washed with PBS, and washed 10 times with aquadest, after which they were incubated for 5 minutes on droplets of uranylacetate/methylcellulose. Excessive uranylacetate/methylcellulose was blotted away and grids were dried to air. Labellings were imaged with a Tecnai 12 Biotwin transmission electron microscope (FEI) at 120 kV acceleration voltage.

Bioorthogonal fluorophore labelling on cryosections

Sections were labelled as follows: thawed cryosections on an EM grid were left for 30 minutes on the surface of 2% gelatin in phosphate buffer at 37°C. Subsequently grids were incubated on drops of PBS/glycine and PBS/glycine containing 1% BSA. Grids were then incubated on top of the ccHc-cocktail (0.1 M HEPES pH 7.3, 1 mM $CuSO_4$, 10 mM sodium ascorbate, 1 mM THPTA ligand, 10 mM amino-guanidine, 5 µM AlexaFluor-488 alkyne (Invitrogen) for 1 h and washed 6 times with PBS and 10 times with aquadest.

Microscopy and correlation

The CLEM approach used was adapted from Vicidomini et al.[21] Grids containing the sample sections were washed with 50% glycerol and placed on glass slides (pre- cleaned with 100% ethanol). Grids were then covered with a small drop of 50% glycerol after which a coverslip was mounted over the grid. Coverslips were fixed using Scotch Pressure Sensitive Tape. Samples were imaged with a Leica TCS SP8 confocal microscope (63x oil lens, N.A.=1.4). Confocal microscopy was used as it allowed to make image stacks from the sections at different focus planes; this was convenient as the sections were found to be in different focus planes whilst placed between the glass slides and coverslip. After fluorescence microscopy the EM grid with the sections was remove from the glass slide, rinsed in distilled water and incubated for 5 minutes on droplets of uranylacetate/methylcellulose.

Excess of uranylacetate/methylcellulose was blotted away and grids were air-dried. EM imaging was performed with a Tecnai 12 Biotwin transmission electron microscope (FEI) at 120 kV acceleration voltage.

Correlation of confocal and EM images was performed in Photoshop CS6. In Adobe Photoshop, the LM image was copied as a layer into the EM image and made 50% transparent. Transformation of the LM image was necessary to match it to the larger scale of the EM image. This was performed via isotropic scaling and rotation. Interpolation settings; bicubic smoother. Alignment at high magnification was carried out using fiducial beads.[40]

References

1. H. C. Kolb, M. G. Finn and K. B. Sharpless, *Angew Chem Int Ed Engl*, 2001, **40**, 2004-2021.
2. E. M. Sletten and C. R. Bertozzi, *Angew Chem Int Ed Engl*, 2009, **48**, 6974-6998.
3. C. P. Ramil and Q. Lin, *Chem Commun (Camb)*, 2013, **49**, 11007-11022.
4. E. Saxon and C. R. Bertozzi, *Science*, 2000, **287**, 2007-2010.
5. S. Ito, L. Shen, Q. Dai, S. C. Wu, L. B. Collins, J. A. Swenberg, C. He and Y. Zhang, *Science*, 2011, **333**, 1300-1303.
6. A. J. Perez and H. B. Bode, *J Lipid Res*, 2014, **55**, 1897-1901.
7. M. S. Siegrist, S. Whiteside, J. C. Jewett, A. Aditham, F. Cava and C. R. Bertozzi, *ACS Chem Biol*, 2013, **8**, 500-505.
8. G. W. Liechti, E. Kuru, E. Hall, A. Kalinda, Y. V. Brun, M. VanNieuwenhze and A. T. Maurelli, *Nature*, 2014, **506**, 507-510.
9. A. E. Speers, G. C. Adam and B. F. Cravatt, *J Am Chem Soc*, 2003, **125**, 4686-4687.
10. H. Ovaa, P. F. van Swieten, B. M. Kessler, M. A. Leeuwenburgh, E. Fiebiger, A. M. van den Nieuwendijk, P. J. Galardy, G. A. van der Marel, H. L. Ploegh and H. S. Overkleeft, *Angew Chem Int Ed Engl*, 2003, **42**, 3626-3629.
11. E. M. Sletten and C. R. Bertozzi, *Acc Chem Res*, 2011, **44**, 666-676.
12. R. S. Erdmann, H. Takakura, A. D. Thompson, F. Rivera-Molina, E. S. Allgeyer, J. Bewersdorf, D. Toomre and A. Schepartz, *Angew Chem Int Ed Engl*, 2014, **53**, 10242-10246.
13. D. W. Dorward, *Methods Mol Biol*, 2008, **431**, 173-187.
14. J. Roth, *Histochem Cell Biol*, 1996, **106**, 1-8.
15. G. Griffiths, in *Fine Structure Immunocytochemistry*, Springer Berlin Heidelberg, Berlin, Heidelberg, 1993, DOI: 10.1007/978-3-642-77095-1_2, pp. 9-25.
16. T. M. Mayhew and J. M. Lucocq, *Histochem Cell Biol*, 2008, **130**, 299-313.
17. K. A. Sjollema, U. Schnell, J. Kuipers, R. Kalicharan and B. N. Giepmans, *Methods Cell Biol*, 2012, **111**, 157-173.
18. B. N. Giepmans, *Histochem Cell Biol*, 2008, **130**, 211-217.
19. E. Bos, L. Hussaarts, J. R. van Weering, M. H. Ellisman, H. de Wit and A. J. Koster, *J Struct Biol*, 2014, **186**, 273-282.
20. G. Vicidomini, M. C. Gagliani, M. Canfora, K. Cortese, F. Frosi, C. Santangelo, P. P. Di Fiore, P. Boccacci, A. Diaspro and C. Tacchetti, *Traffic*, 2008, **9**, 1828-1838.
21. G. Vicidomini, M. C. Gagliani, K. Cortese, J. Krieger, P. Buescher, P. Bianchini, P. Boccacci, C. Tacchetti and A. Diaspro, *Microsc Res Tech*, 2010, **73**, 215-224.

22. M. Grabenbauer, *Methods Cell Biol*, 2012, **111**, 117-138.
23. J. H. Luft, *J Biophys Biochem Cytol*, 1961, **9**, 409-414.
24. J. W. Slot and H. J. Geuze, *Nat Protoc*, 2007, **2**, 2480-2491.
25. K. L. Kiick, E. Saxon, D. A. Tirrell and C. R. Bertozzi, *Proc Natl Acad Sci U S A*, 2002, **99**, 19-24.
26. K. L. Kiick, J. C. M. van Hest and D. A. Tirrell, *Angew Chem Int Ed Engl*, 2000, **39**, 2148-2152.
27. D. J. Leahy, W. A. Hendrickson, I. Aukhil and H. P. Erickson, *Science*, 1992, **258**, 987-991.
28. W. B. Wood, *J Mol Biol*, 1966, **16**, 118-133.
29. A. K. Upadhyay, A. Murmu, A. Singh and A. K. Panda, *PLoS One*, 2012, **7**, e33951.
30. R. Hatzenpichler, S. Scheller, P. L. Tavormina, B. M. Babin, D. A. Tirrell and V. J. Orphan, *Environ Microbiol*, 2014, **16**, 2568-2590.
31. Z. P. Demko and K. B. Sharpless, *Angew Chem Int Ed Engl*, 2002, **41**, 2113-2116.
32. C. W. Tornoe, C. Christensen and M. Meldal, *J Org Chem*, 2002, **67**, 3057-3064.
33. Q. Wang, T. R. Chan, R. Hilgraf, V. V. Fokin, K. B. Sharpless and M. G. Finn, *J Am Chem Soc*, 2003, **125**, 3192-3193.
34. W. S. P. Jong, C. M. Ten Hagen-Jongman, T. Den Blaauwen, D. Jan Slotboom, J. R. H. Tame, D. Wickström, J.-W. De Gier, B. R. Otto and J. Luirink, *Molecular Microbiology*, 2007, **63**, 1524-1536.
35. W. S. P. Jong, M. H. Daleke-Schermerhorn, D. Vikström, C. M. ten Hagen-Jongman, K. de Punder, N. N. van der Wel, C. E. van de Sandt, G. F. Rimmelzwaan, F. Follmann, E. M. Agger, P. Andersen, J.-W. de Gier and J. Luirink, *Microbial Cell Factories*, 2014, **13**, 162.
36. K. T. Tokuyasu, *J Cell Biol*, 1973, **57**, 551-565.
37. W. Kukulski, M. Schorb, S. Welsch, A. Picco, M. Kaksonen and J. A. Briggs, *J Cell Biol*, 2011, **192**, 111-119.
38. J. B. Pawlak, G. P. Gential, T. J. Ruckwardt, J. S. Bremmers, N. J. Meeuwenoord, F. A. Ossendorp, H. S. Overkleeft, D. V. Filippov and S. I. van Kasteren, *Angew Chem Int Ed Engl*, 2015, **54**, 5628-5631.
39. P. J. Peters, in *Current Protocols in Cell Biology*, John Wiley & Sons, Inc., 2001.
40. J. Kuipers, T. J. van Ham, R. D. Kalicharan, A. Veenstra-Algra, K. A. Sjollema, F. Dijk, U. Schnell and B. N. Giepmans, *Cell Tissue Res*, 2015, **360**, 61-70.

4

Correlative Light and Electron Microscopy reveals Discrepancy between Gold and Fluorescence Labelling[*]

Introduction

Fluorescence Microscopy (FM) is a powerful imaging tool that can be employed to track, localise and monitor biomolecules within cellular systems. However, with fluorescence measurements only the position of the labelled biomolecules can be studied in relation to other fluorescently-labelled biomolecules, but the morphology of subcellular structures wherein they reside remains invisible. Conversely, Electron Microscopy (EM) enables observations at nanometer-scale resolution and is therefore often employed to gain ultrastructural characterisation of the subcellular environment pertinent to the biomolecules initially investigated with FM.[1-5]

The location of biomolecules within EM imaged specimen can be visualised upon gold labelling. Colloidal gold is electron dense and, due to its punctate and precise labelling pattern, it is favourable for the localisation of biomolecules within structures studied at nanometer scale.[6, 7] Gold labelling can be broadly applied, e.g. in combination with immunocytochemistry (through direct antibody coupling or in combination with protein A), but also with lectins and other binding proteins.[6, 8] This allows recognition of fluorescent reporter proteins (such as green fluorescent protein (GFP)), fluorophores, or direct epitopes studied with FM.[9] The preferred method for preparing biological material for gold labelling is the Tokuyasu cyosectioning technique. This technique is the only post-embedding on-section immunolabelling approach that does not require dehydration by polar solvents before application of affinity markers. It is therefore that thawed crysosections tend to give the highest accessibility of antibodies to the antigens and are the best for most purposes on-section labelling strategies.[10-12]

---

[*] Published as part of: Daphne M. van Elsland, Erik Bos, Joanna B. Pawlak, Herman S. Overkleeft, Abraham J. Koster and Sander I. van Kasteren. *J. Microsc.,* **267**, 307-317 (2017). Prof. Gareth Griffiths, Dr. Urška Repnik, and Dr. I. Berlin are kindly acknowledged for critical reading of the manuscript.

Besides colloidal gold markers, directly visible in the electron microscope, one can also use Correlative Light and Electron Microscopy (CLEM) to directly visualise fluorescent markers on EM imaged specimen. With CLEM, specific biomolecules and cellular structures can be identified at low magnification with FM, followed by ultrastructural assessment of subcellular location and context with EM.[13, 14] CLEM enables the detection of rare cellular events and allows interpretation of fluorescent labelling on low magnification/large overview images in contrast to colloidal gold markers, which are too small to detect at low magnification. A downside of fluorescence-based CLEM is that correlation of images requires enlargement of the FM image to cover the high magnification EM image. This enlargement results in diffuse fluorescent signals with a diameter of a few hundred nanometers that cannot be related to the exact location of proteins of interest, which can be around 4 nm in diameter and may be associated with organelles as small as 30 nm.[15]

It was envisaged that the center of the fluorescent signals could be found by combining gold labelling and fluorescence-based CLEM in a single experiment. Surprisingly, this combination showed for the lysosomal membrane protein LAMP-1 a discrepancy between the distribution of gold and fluorescent label. To understand the scope and implications of this phenomenon, a series of experiments were devised involving bioorthogonal labelling of cryosections.[16] Bioorthogonal labelling is a chemical labelling strategy whereby firstly a small, physiologically inert chemical group is incorporated into a biomolecule of interest, which is subsequently reacted with a detection group using a highly selective chemical reaction. With this approach a wide range of biomolecules can be labelled, with high specificity and minimal perturbations.[17, 18] Through the use of bioorthogonal labelling it was possible to compare fluorescence and immunogold labelling of model membrane-associated or soluble epitopes using the same labelling procedures. It was discovered that in particular membrane-associated antigens are strongly labelled with gold particles, whereas the signal of fluorescence labelling of the same target molecules is weak or not detectable.

Results

Defining the problem

In order to determine the position of fluorophore-tagged antigens within cellular ultrastructures, a previously described CLEM strategy was applied for detection and localisation of fluorescent tags[16] and labelled fluorophore-antigen complexes with immuno gold particles. This strategy involves cryosectioning according to the Tokuyasu technique and thus allows fluorescence-based CLEM and immunogold labelling on the same specimen sections. Labelling strategies employed in this study are schematically displayed in all figures and the corresponding symbol legends are shown in Table 1. The fluorescence-gold labelling strategies employed in this study all rely on indirect fluorophore to gold conjugation upon use of antibodies. This indirect fluorophore to gold conjugation has been shown to minimise the possible quenching of the fluorescence signals and is therefore the method of choice to combine fluorescence-based CLEM and immunogold labelling.[19]

Table 1. Symbols legends labelling strategies.

component	symbol
Protein A conjugated gold	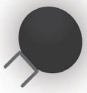
Protein A conjugated AlexaFluor	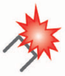
IgG antibody	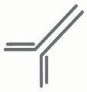
AlexaFluor conjugated IgG antibody	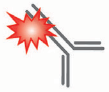
Antigen	
Azide modified antigen	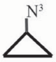
AlexaFluor alkyne	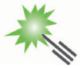

It was chosen to apply this strategy to the lysosomal membrane glycoprotein LAMP-1, a major protein component of the lysosomal membrane.[20] LAMP-1 is widely used as a marker for the identification of late endosomes and lysosomes with FM and EM.[21, 22] Bone Marrow derived Dendritic Cells (BM-DCs) were cultured, processed for cryosectioning[23] and sectioned into 75 nm thick sections, followed by primary labelling with a fluorescent (AlexaFluor 647) rat anti mouse LAMP-1 antibody and secondary labelling with 15 nm protein A-coated gold particles after a rabbit anti-rat IgG binding step (Figure 1A, *Strategy*). Sections were then imaged with a confocal microscope, after which sections were stained with uranylacetate and imaged using an electron microscope. The FM and EM images were superimposed (Figure 1A, *CLEM*), and the corresponding label distributions were analysed (Figure 1A, *Label distribution*). To facilitate interpretation of the gold labelling in relation to the fluorescent signals, all gold particles are highlighted with green dots. Upon the morphological appearance of a visible membrane profile several organelles are depicted white when fluorescent label is associated and yellow when gold label is associated. It was found that the distribution of LAMP-1 gold only partially overlapped with the distribution of LAMP-1 fluorescence, while LAMP-1 fluorescence was always associated with gold label (Figure 1A, *Label distribution*). Note that gold can be localised on fluorescent labels, but not on organelle structures. Moreover, areas with high fluorescence were not highly gold-labelled. Quantification of overlap revealed that only 66% of the gold particles colocalised with fluorescence.

The above results were deemed remarkable, considering that the gold label was directed towards the fluorescent LAMP-1 antibody. To explore whether such label discrepancy represents a general phenomenon associated with combining fluorescence and gold techniques, the CLEM and immunogold approach was tested for non membrane-bound molecules, namely cathepsins papain-like cysteine proteases known to reside within lysosomes. In order to label cathepsins with fluorescence and immunogold, BM-DCs were incubated with a DCG-04 probe, which binds to active cathepsins and contains a bioorthogonal azide-group.[24, 25] After cryo sectioning of BM-DCs, the DCG-04-azide was labelled with an AlexaFluor 488 fluorophore using an on-section copper-catalysed Huisgen cycloaddition (ccHc) reaction.[16] This was followed by an immunogold labelling step directed against the AlexaFluor 488 (Figure 1B, *Strategy*). The distribution of cathepsin gold label corresponded well with the distribution of the cathepsin fluorescence label (Figure 1B, *Label distribution*). Quantification showed that 87% of the gold particles co-localised with the fluorescence signal. These results suggest that the degree of correspondence between gold and fluorescence label distribution may vary with the location of the antigen (i.e. membrane-associated versus soluble).

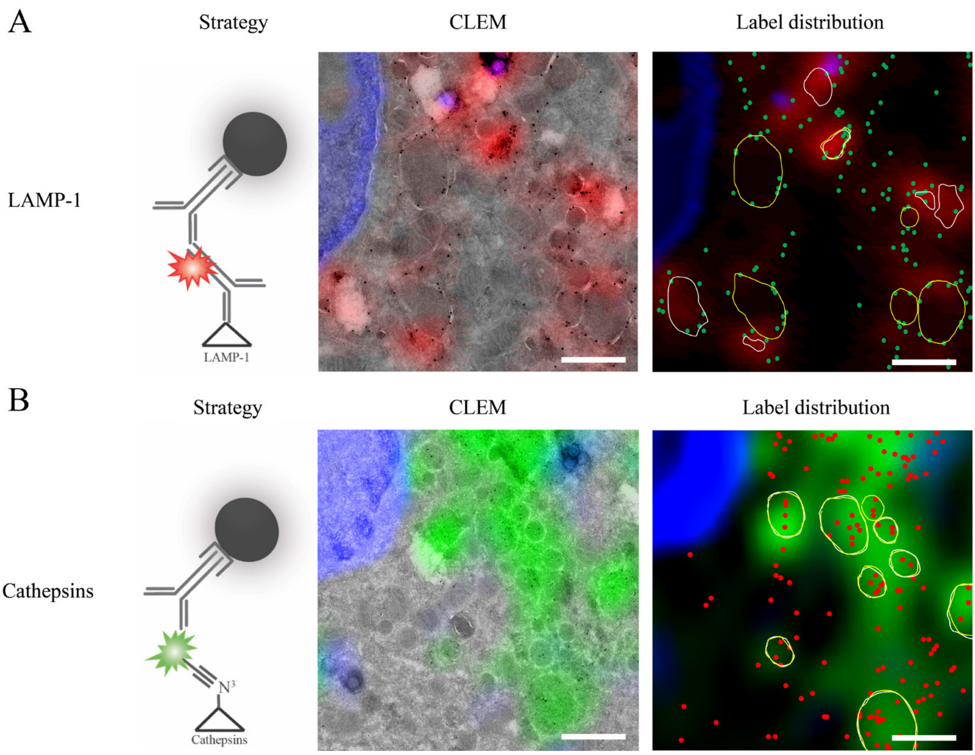

Figure 1. Labelling of LAMP-1 with gold results in different label patterns compared to the labelling of LAMP-1 with fluorescence. (A) BM-DC sections were labelled with a fluorescent AlexaFluor647 (red) rat anti-mouse LAMP-1 antibody, and with protein A-coated gold particles. Gold particle labelling was performed using a rabbit anti-rat binding step (*Strategy*). Representative CLEM image (*CLEM*). Upon the morphological appearance of a visible membrane profile several organelles are depicted white when fluorescent label is associated and yellow when gold label is associated (*Label distribution*). (B) BM-DCs were incubated with DCG-04-azide and were labelled with AlexaFluor488 alkyne (green) and with protein A coated gold directed against AlexaFluor488 using a rabbit anti-AlexaFluor448 binding step (*Strategy*). Representative CLEM image (*CLEM*). Upon the morphological appearance of a visible membrane profile, several organelles are depicted white when fluorescent label is associated, and yellow when gold label is associated (*Label distribution*). Scale bars 500 nm.

Analyzing the problem

In contrast to LAMP-1, the distribution of gold label corresponded well with the distribution of the fluorophore label for cathepsins. Since LAMP-1 and cathepsins are associated with the same organelles, it was anticipated to see predominantly overlap of the LAMP-1 and cathepsin label distributions.[26] To test this, LAMP-1-associated organelles were defined as being positive for cathepsin label and distributions of LAMP-1 gold (Figure 2A, *Strategy*) and LAMP-1 fluorescence

(Figure 2B, *Strategy*) in relation to these cathepsin-positive organelles were analysed. As expected, association of LAMP-1 with cathepsin-positive organelles was confirmed with immunogold labelling (Figure 2A, *CLEM and Label distribution*). However, immunofluorescence labelling of LAMP-1 showed that LAMP-1 also associated with cathepsin-negative organelles and that cathepsin positive vesicles are not always associated with LAMP-1 (Figure 2B). To exclude the possibility that the secondary antibody in the gold label strategy represented in Figure 2A would influence the labelling, the protein A gold was substituted for protein A AlexaFluor 647 (Figure 2C, *Strategy*) and the result of this strategy (Figure 2C, *label distribution*) was compared with the results shown in Figure 2B. Statistical colocalisation analysis (Figure 2C, *colocalisation*) showed that substitution of protein A gold by protein A AlexaFluor 647 resulted in a label distribution similar to the distribution shown in Figure 2B. Collectively, these results indicate that the application of gold particles within a label strategy influences the immunodetection of antigens on sections.

Testing the hypothesis

The results presented so far show that the distribution of immunogold label for LAMP-1 does not completely correlate with immunofluorescent labelling of the same antigen. As this was prominently observed for the LAMP-1 epitope, but not for the cathepsin epitope, it was postulated that there could be an effect of the immediate surrounding of the epitope on the ability of the gold conjugates to bind to cognate epitopes. Since LAMP-1 is a membrane-bound molecule while cathepsin is soluble, it was hypothesised that immunogold labels membrane-bound molecules differently from soluble epitopes. It was thus set out to install the same bioorthogonal group used to label cathepsins via the DCG-04 probe on a membrane-associated epitope, creating the same covalent fluorophore introduction in a membrane associated context. This was achieved by installing the bioorthogonal group on sialylated glycans,[27] as these constitute parts of membrane-bound molecules.

Jurkat cells were incubated with Ac_4-N-azidoacetylmannosamine (Ac_4-ManNAz), to add a bioorthogonal functionality to sialylated glycans under conditions reported previously.[16] Cryo sections from these cells were subjected to the same labelling strategy as used for the cathepsins above. To eliminate the possibility that a different cell type and/or rearrangement of the bioortogonal group would influence either the binding of AlexaFluor 488 alkyne or recognition of AlexaFluor 488 by anti AlexaFluor 488 IgG, modified epitopes were first doublelabelled with AlexaFluor alkyne and protein A AlexaFluor (Figure 3A and B, S*trategy*). Similar overlap of the two fluorophores was observed for both epitopes (Figure 3A and B, *Label distribution*) with no significant difference between the two azide-modified epitopes (Figure 3B, *Colocalisation*), meaning that the affinities of the two labels were not altered upon the epitope or cell type change. Next, the sialylated glycans were doublelabelled and protein A AlexaFluor was substituted for protein A gold (Figure 3C, *Strategy*). It was found that the gold label localised primarily on the plasma membrane, whereas the fluorescent signal predominantly labelled intracellular structures (Figure 3C, *CLEM*). Quantification of colocalisation (Figure 3C, *Label distribution*) revealed that again only 64% of the gold label co-localised with the fluorescent foci, lending credence to the hypothesis that the cellular location of an epitope influences the degree of gold labelling. For soluble epitopes the degree of gold label is relatively low compared to the fluorescent signal, whereas the membrane-bound epitopes get highly labelled with gold, even when the fluorescence label is poorly or not detectable at all with confocal microscopy.

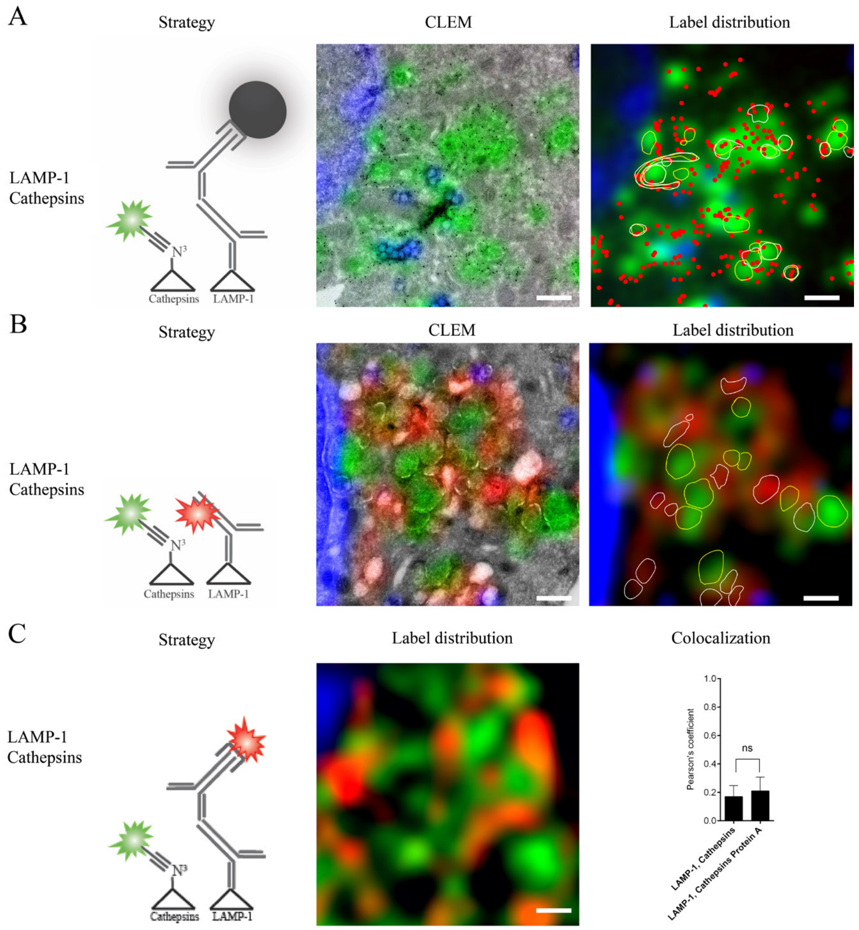
A
Strategy
CLEM
Label distribution
LAMP-1
Cathepsins
N3
Cathepsins
LAMP-1
B
Strategy
CLEM
Label distribution
LAMP-1
Cathepsins
N3
Cathepsins
LAMP-1
C
Strategy
Label distribution
Colocalization
LAMP-1
Cathepsins
N3
Cathepsins
LAMP-1
Pearson's coefficient
1.0
0.8
0.6
0.4
0.2
0.0
ns
LAMP-1, Cathepsins
LAMP-1, Cathepsins Protein A

Figure 2. Labelling with gold particles shows a different antigen distribution than with fluorescent labelling. (A) BM-DCs were incubated with DCG-04-azide and labelled with AlexaFluor488 alkyne (green). Sections were subsequently labelled with anti-LAMP-1 and protein A-coated gold directed against the LAMP-1 antibody using a rabbit anti-rat binding step (*Strategy*). CLEM images obtained (*CLEM*) were analysed for label distribution and gold distribution is marked with red dots. Structures that are positive for LAMP-1 gold are depicted in white and structures positive for cathepsin fluorescence are depicted in yellow. (B) BM-DCs were incubated with DCG-04-azide and were labelled on section with AlexaFluor488 alkyne (green). Sections were subsequently labelled with fluorescent AlexaFluor647 anti-LAMP-1 (red) (*Strategy*). CLEM images obtained (*CLEM*) were analysed for label distribution. Structures positive for LAMP-1 fluorescence are depicted in white and structures positive for cathepsin fluorescence in yellow. (C) BM-DCs were incubated with DCG-04-azide and were labelled on section with TAMRA alkyne (green). Sections were subsequently labelled with anti-LAMP-1 and protein A AlexaFluor488 fluorophore (red) directed against the LAMP-1 antibody using a rabbit anti-rat binding step (*Strategy*). A representative confocal image of this sample is shown in *Fluorescence*. Colocalisation analysis of the labelling sequences in (B) and (C) (*Colocalisation*). Scale bars, 500 nm.

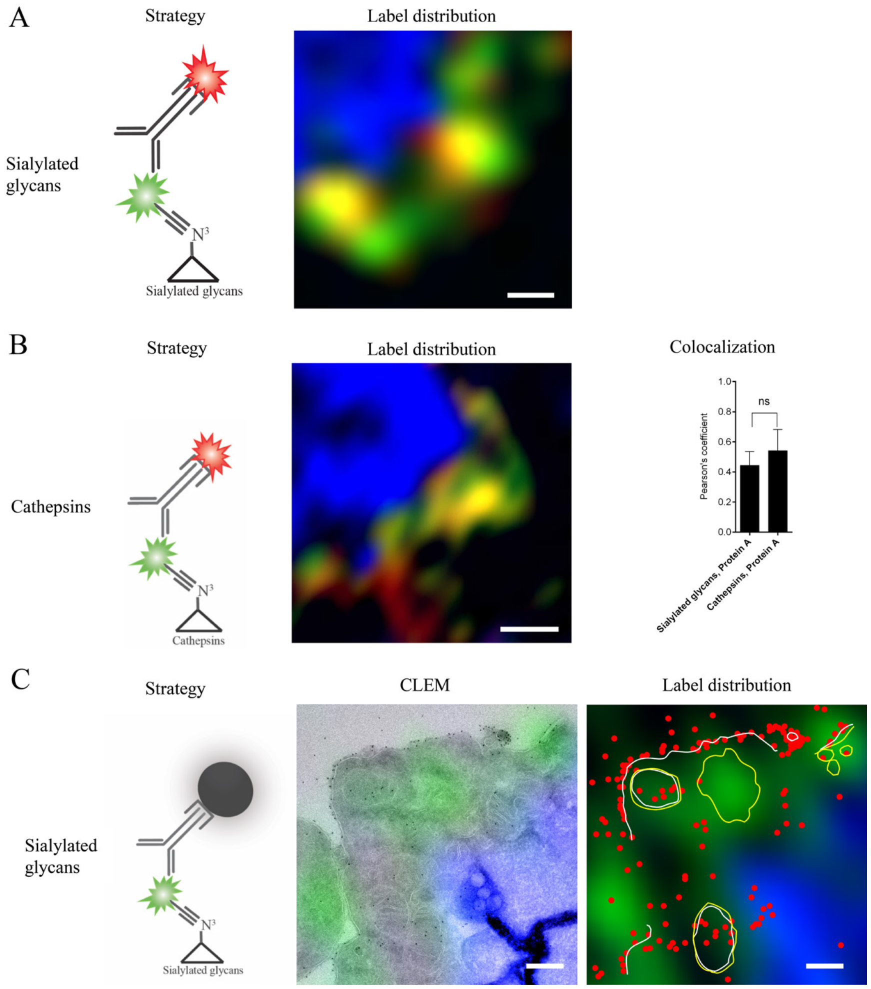
A
Strategy
Label distribution
Sialylated glycans
N3
Sialylated glycans
B
Strategy
Label distribution
Colocalization
Cathepsins
N3
Cathepsins
1.0
0.8
0.6
0.4
0.2
0.0
ns
Pearson's coefficient
Sialylated glycans, Protein A
Cathepsins, Protein A
C
Strategy
CLEM
Label distribution
Sialylated glycans
N3
Sialylated glycans

Figure 3. The cellular location of an epitope influences gold labelling, resulting in a discrepancy between fluorescence and gold label distribution. (A) Jurkat cells were incubated with N-azidoacetylmannosamine and were labelled on section with AlexaFluor488 alkyne (green). Sections were subsequently labelled with a AlexaFluor647 protein A fluorophore directed against the AlexaFluor488 using a rabbit anti-rat binding step (*Strategy*). (B) BM-DCs incubated with DCG-04-azide were labelled on section with AlexaFluor488 alkyne (green) and protein A AlexaFluor647 (red) directed toward AlexaFluor488 using a rabbit anti-AlexaFluor488 binding step. Colocalisation analysis of sialylated glycans and protein A compared to cathepsins and protein A (*Colocalisation*). (C) Jurkat cells were incubated with N-azidoacetylmannosamine and were labelled on section with AlexaFluor488 alkyne (green). Gold particle labelling was performed using a rabbit anti-AlexaFluor448 binding step (*Strategy*). Representative CLEM image (CLEM). Organelles positive for sialylated glycan-fluorescence are depicted in yellow and organelles positive for sialylated glycan-gold are depicted in white. The distribution of these spheres is displayed in the context of the label distribution (*Label distribution*). Scale bar 500 nm.

Conclusion

In order to translate information of FM studies to EM analysis, biomolecules initially observed with the former need to be labelled in a manner compatible with EM. Traditionally this is performed using immunogold labelling of fluorescently detected biomolecules. Here the discrepancies arising between distributions of fluorescence and gold labelling were identified and explored. It was found that a subset of cathepsin-positive organelles is negative for LAMP-1 when labelling is done by fluorescence, but positive for LAMP-1 when labelling is done with gold particles. Variations in label distributions can be explained by marker heterogeneity in phagosomal, endosomal and lysosomal structures.[28-30] However, such heterogeneity cannot explain that the label distribution pattern changes upon changing the type of label (gold vs fluorescent label). It was reasoned that the antigen detection level could change upon changing the type of label, but that the label distribution pattern should not.

In a comparison of fluorescent and gold label it can be argued that the localisation of diffuse enlarged fluorescent signals may result in a less distinct mapping of positive structures, and that fluorescence can be difficult to detect when label density is weak, which is especially the case for fluorescence labelling on non-dense structures such as membranes. However, since the fluorescence intensity is related to the concentration of the epitope, there should still be an overlap of fluorescence and gold label,[31] and this is not expressed by the observed discrepancy.

On top of this gold labelling may show different antigen detection levels. Variations in labelling of conjugated gold particles have been previously reported by Griffiths and Hoppeler, describing variations in immunogold labelling efficiencies for the ER, Golgi apparatus and viral membranes.[32] In their study the ER membranes were found to exhibit the highest labelling efficiency compared to the Golgi apparatus or viral membranes. These observations are supported by others noting profound variations in immunogold labelling efficiency between different cellular compartments and structures.[33-35] It is generally considered that cross-linking of target molecules by fixatives, as well as steric hindrance and valency of both target and ligand molecules constitute factors that influence labelling efficiency.[36] Other investigators report that the density of cellular material affects the labelling efficiency as well. In dense secretory granules, there is almost only surface labelling whereas the less dense endoplasmic reticulum gets more prominently labelled.[37] It was postulated that these epitope availability effects more strongly affect gold labelling compared to fluorescence labelling, resulting in the discrepancies observed between these labelling strategies.

If epitopes of interest are found in various structures within the same specimen, gold labelling may result in a biased detection of target molecules. As a consequence it may be argued that in this context fluorescence labelling is preferable to gold labelling. However, to reach the punctuality of the gold particles, the detection of these fluorescence labels needs to be at a higher resolution. Super-resolution microscopy techniques, such as STORM and PALM, may serve this purpose as these techniques allow to precisely localise molecules at a resolution of a few nanometers. Moreover, examples of their applications to CLEM have yet been explored.[15, 38] Another approach resulting in high resolution labelling includes labels capable of polymerizing diaminobenzidine (DAB) . It has been shown that photooxidation-based polymerisation of DAB occurs within a few nanometers away of the epitope.[39-42] Application of these high resolution methods could pave the way to provide alternative labels for accurate mapping in correlative FM and EM studies.

Experimental

Specimen preparation

BM-DCs and Jurkat cells were cultured as described elsewhere[16]. BM-DCs were incubated for 2 hours with DCG-04-azide [43] (final concentration of 10 µM), after which the cells were washed with PBS and kept for 2 h in fresh medium. Jurkat cells were incubated for 3 days with 50 µM of N-azidoacetylmannosamine (MannAz, Invitrogen) from stock solutions in DMSO.

Samples were prepared for cryosectioning as described elsewhere [16, 44]. Briefly, BM-DCs and Jurkat cells were fixed for 24 h in freshly prepared 2% PFA in 0.1 M phosphate buffer. Fixed cells were embedded in 12% gelatin (type A, bloom 300, Sigma) and cut with a razor blade into 0.5 mm^3 cubes. The sample blocks were infiltrated in phosphate buffer containing 2.3 M sucrose for 3 h. Sucrose-infiltrated sample blocks were mounted on aluminum pins and plunged in liquid nitrogen. The frozen samples were stored in liquid nitrogen.

Ultrathin cell sections of 75 nm were obtained essentially as described elsewhere[16]. Briefly, the frozen sample was mounted in a cryo-ultramicrotome (Leica). The sample was trimmed to yield a squared block with a front face of about 300 x 250 µm (Diatome trimming tool). Using a diamond knife (Diatome) and antistatic device (Leica) a ribbon of 75 nm thick sections was produced that was retrieved from the cryochamber with the lift-up hinge method[45]. A droplet of 1.15 M sucrose was used for section retrieval.

Obtained sections were transferred to a specimen grid previously coated with formvar and carbon grids were additionally coated with 100 nm FluoroSpheres carboxylate-modified (350/440) (Life Technologies).

On-section labelling

Sections that were click-labelled with AlexaFluor488/TAMRA alkyne and immunogold-labelled were labelled as follows; thawed cryosections on an EM grid were left for 30 minutes on the surface of 2% gelatin in phosphate buffer at 37°C. Subsequently grids were incubated on drops of PBS/glycine and PBS/glycine containing 1% BSA. Grids were then incubated on top of the ccHc- cocktail (0.1 M HEPES pH 7.3, 1 mM $CuSO_4$, 10 mM sodium ascorbate, 1 mM THPTA ligand, 10 mM amino-guanidine, 5 µM AlexaFluor488/TAMRA alkyne (Invitrogen) for 1 h and washed 6 times with PBS. Sections were then blocked again with PBS/Glycine containing 1% BSA after which the grids were incubated for 1 h with 0.1 M PBS/glycine 1% BSA (blocking solution) supplemented with a rabbit IgG anti Alexa 488 antibody (Invitrogen). After washing with PBS/Glycine and blocking with PBS/glycine 0.1% BSA, grids were incubated for 20 minutes on PBS/glycine 1% BSA supplemented with protein A coated 10 or 15 nm goldparticles (CMC, Utrecht University). Grids were then washed with PBS, labelled with DAPI and additionally washed with PBS and aquadest. In case of protein A AlexaFluor labelling, protein A-coated goldparticles were replaced with protein A Alexa 488 or protein A Alexa 647 (20 µg/ml).

In case of immunofluorescence and immunogold labelling against LAMP-1 thawed cryosections on an EM grid were left for 30 minutes on the surface of 2% gelatin in phosphate buffer at 37°C. Grids were washed 5 times with PBS/glycine and blocked with PBS/glycine containing 1% BSA after which the grids were incubated for 1 h with PBS/glycine 1% BSA supplemented with a rat anti-mouse LAMP-1 AlexaFluor647 (Biolegend, Cat. 121609). Grids were then washed 5 times with PBS/glycine and blocked again with PBS/glycine containing 1% BSA after which the grids were incubated for 1 h with PBS/glycine 1% BSA supplemented with a rabbit IgG anti-rat (Nordic Immunology). After washing with PBS/glycine and blocking with PBS/glycine 0.1% BSA, grids were incubated for 20 minutes with PBS/glycine 1% BSA supplemented with protein A coated 10/15 nm goldparticles (CMC, Utrecht University). Grids were then washed with PBS, labelled with DAPI and additionally washed with PBS and aquadest. In case of protein A Alexa labelling, protein A-coated 10/15 nm goldparticles were replaced for protein A Alexa 488 or protein A Alexa 647 (20 µg/ml).

In case click labelling and LAMP-1 labelling were performed on the same section, click labelling was preformed prior to the LAMP-1 labelling steps.

Microscopy and correlation

The CLEM approach used was adapted from Vicidomini et al. and has been described elsewhere[16]. Briefly, grids containing the sample sections were washed with 50% glycerol and placed on glass slides (precleaned with 100% ethanol). Grids were then covered with a small drop of 50% glycerol, after which a coverslip was mounted over the grid. Coverslips were fixed using Scotch Pressure-Sensitive Tape. Samples were imaged with a Leica TCS SP8 confocal microscope (63x oil lens, N.A.=1.4). After confocal microscopy the EM grid with the sections was removed from the glass slide, rinsed in distilled water and incubated for 5 minutes on droplets of an aqueous solution containing 2% methylcellulose and 6% uranyl acetate. Excess of methylcellulose/uranyl solution was blotted away and grids were air-dried. EM imaging was performed with a Tecnai 20 transmission electron microscope (FEI) operated at 120 kV acceleration voltage.

Correlation of confocal and EM images was performed in Adobe Photoshop CS6. In Adobe Photoshop, the FM image was copied as a layer into the EM image and made 50% transparent. Transformation of the FM image was necessary to match it to the larger scale of the EM image. This was performed via isotropic scaling and rotation using interpolation settings; bicubic smoother. Alignment at low magnification was carried out with the aid of nuclear DAPI staining in combination with the shape of the fluorescently labelled cells. At high magnification alignment was performed using the fiducial beads [46].

Colocalisation analysis and quantification of label distributions

Upon the morphological appearance of a visible membrane profile organelles were depicted either positive for gold or for fluorescence. For the determination of structures positive for gold only structures positive for two or more particles were depicted.

Colocalisation of gold and fluorescence was calculated as a percentage by quantification of the overlap of gold and fluorescence using the count tool in Photoshop. With this strategy gold particles were counted that either colocalised with fluorescence or did not colocalise with fluorescence.

The Pearson coefficient was determined on magnified confocal images of protein A double labelled samples using the Coloc2 function in ImageJ after background was corrected to eliminate nonspecificity. These images were obtained in Adobe Photoshop CS6 upon CLEM correlation.

References

1. S. A. Predescu, D. N. Predescu, B. K. Timblin, R. V. Stan and A. B. Malik, *Mol Biol Cell*, 2003, **14**, 4997-5010.
2. H. Robenek, O. Hofnagel, I. Buers, M. J. Robenek, D. Troyer and N. J. Severs, *J Cell Sci*, 2006, **119**, 4215-4224.
3. M. Boonen, C. Staudt, F. Gilis, V. Oorschot, J. Klumperman and M. Jadot, *J Cell Sci*, 2016, **129**, 557-568.
4. D. Sarnataro, A. Caputo, P. Casanova, C. Puri, S. Paladino, S. S. Tivodar, V. Campana, C. Tacchetti and C. Zurzolo, *PLoS One*, 2009, **4**, e5829.
5. S. I. Choi, Y. S. Maeng, T. I. Kim, Y. Lee, Y. S. Kim and E. K. Kim, *PLoS One*, 2015, **10**, e0119561.
6. G. Griffiths, in *Fine Structure Immunocytochemistry*, Springer Berlin Heidelberg, 1993, 9-25.
7. T. M. Mayhew and J. M. Lucocq, *Histochem Cell Biol*, 2008, **130**, 299-313.
8. W. P. Faulk and G. M. Taylor, *Immunochemistry*, 1971, **8**, 1081-1083.
9. M. S. Sirerol-Piquer, A. Cebrian-Silla, C. Alfaro-Cervello, U. Gomez-Pinedo, M. Soriano-Navarro and J. M. Verdugo, *Micron*, 2012, **43**, 589-599.
10. K. T. Tokuyasu, *J Cell Biol*, 1973, **57**, 551-565.
11. J. W. Slot and H. J. Geuze, *Nat Protoc*, 2007, **2**, 2480-2491.
12. P. Webster, H. Schwarz and G. Griffiths, *Methods Cell Biol*, 2008, **88**, 45-58.
13. P. de Boer, J. P. Hoogenboom and B. N. Giepmans, *Nat Meth*, 2015, **12**, 503-513.
14. B. N. Giepmans, *Histochem Cell Biol*, 2008, **130**, 211-217.
15. S. Watanabe, A. Punge, G. Hollopeter, K. I. Willig, R. J. Hobson, M. W. Davis, S. W. Hell and E. M. Jorgensen, *Nat Meth*, 2011, **8**, 80-84.
16. D. M. van Elsland, E. Bos, W. de Boer, H. S. Overkleeft, A. J. Koster and S. I. van Kasteren, *Chem Sci*, 2016, **7**, 752-758.
17. M. Grammel and H. C. Hang, *Nat Chem Biol*, 2013, **9**, 475-484.
18. D. M. van Elsland, E. Bos, H. S. Overkleeft, A. J. Koster and S. I. van Kasteren, *J Chem Biol*, 2015, **8**, 153-157.
19. I. K. Kandela and R. M. Albrecht, *Scanning*, 2007, **29**, 152-161.
20. E. L. Eskelinen, *Mol Aspects Med*, 2006, **27**, 495-502.
21. E. van Meel and J. Klumperman, *Histochem Cell Biol*, 2008, **129**, 253-266.
22. H. Appelqvist, P. Wäster, K. Kågedal and K. Öllinger, *J Mol Cell Biol*, 2013, **5**, 214-226.
23. P. J. Peters, in *Curr Protoc Cell Biol*, John Wiley & Sons, Inc., 2001.
24. J. R. Pungercar, D. Caglic, M. Sajid, M. Dolinar, O. Vasiljeva, U. Pozgan, D. Turk, M. Bogyo, V. Turk and B. Turk, *The FEBS journal*, 2009, **276**, 660-668.
25. D. Greenbaum, K. F. Medzihradszky, A. Burlingame and M. Bogyo, *Chem Biol*, 2000, **7**, 569-581.

26. D. Bromme, *Curr Protoc Protein Sci,* **Chapter 21**, Unit 21 22.
27. E. Saxon and C. R. Bertozzi, *Science*, 2000, **287**, 2007-2010.
28. J. Huotari and A. Helenius, *EMBO J*, 2011, **30**, 3481-3500.
29. J. P. Luzio, P. R. Pryor and N. A. Bright, *Nat Rev Mol Cell Biol*, 2007, **8**, 622-632.
30. R. M. Henry, A. D. Hoppe, N. Joshi and J. A. Swanson, *J Cell Biol*, 2004, **164**, 185-194.
31. K. Tohda, H. Lu, Y. Umezawa and M. Gratzl, *Anal Chem*, 2001, **73**, 2070-2077.
32. G. Griffiths and H. Hoppeler, *J Histochem Cytochem*, 1986, **34**, 1389-1398.
33. G. Posthuma, J. W. Slot and H. J. Geuze, *J Histochem Cytochem*, 1984, **32**, 1028-1034.
34. J. Tooze, M. Hollinshead, R. Frank and B. Burke, *J Cell Biol*, 1987, **105**, 155-162.
35. J. Lucocq, *J Anat*, 1994, **184 (Pt 1)**, 1-13.
36. J. G. White, M. D. Krumwiede and G. Escolar, *Am J Pathol*, 1999, **155**, 2127-2134.
37. e. H. Catherine Rabouille, M. A. Nasser *Humana Press*, 1999, 125-144.
38. N. de Souza, *Nat Meth*, 2015, **12**, 37-37.
39. G. M. Gaietta, T. J. Deerinck and M. H. Ellisman, *Cold Spring Harb Protoc*, 2011, **2011**, pdb top94.
40. G. E. Sosinsky, G. M. Gaietta, G. Hand, T. J. Deerinck, A. Han, M. Mackey, S. R. Adams, J. Bouwer, R. Y. Tsien and M. H. Ellisman, *Cell Commun Adhes*, 2003, **10**, 181-186.
41. K. Cortese, A. Diaspro and C. Tacchetti, *J Histochem Cytochem*, 2009, **57**, 1103-1112.
42. J. T. Ngo, S. R. Adams, T. J. Deerinck, D. Boassa, F. Rodriguez-Rivera, S. F. Palida, C. R. Bertozzi, M. H. Ellisman and R. Y. Tsien, *Nat Chemical Biol*, 2016, **12**, 459-465.
43. S. Hoogendoorn, G. H. van Puijvelde, J. Kuiper, G. A. van der Marel and H. S. Overkleeft, *Angew Chem Int Ed Engl*, 2014, **53**, 10975-10978.
44. P. J. Peters, E. Bos and A. Griekspoor, *Curr Protoc Cell Biol*, 2006, **Chapter 4**, Unit 4 7.
45. E. Bos, C. SantAnna, H. Gnaegi, R. F. Pinto, R. B. Ravelli, A. J. Koster, W. de Souza and P. J. Peters, *J Struct Biol*, 2011, **175**, 62-72.
46. J. Kuipers, T. J. Ham, R. D. Kalicharan, A. Veenstra-Algra, K. A. Sjollema, F. Dijk, U. Schnell and B. N. G. Giepmans, *Cell Tissue Research*, 2015, **360**, 61-70.

5

Detection of Bioorthogonal Groups by Correlative Light and Electron Microscopy allows Imaging of Degraded Bacteria in Phagocytes[*]

Introduction

Phagocytic degradation is a question of great biological relevance, as it is one of the key mechanisms by which the immune system keeps pathogens at bay. As a consequence, subversion of the phagolysosomal pathway is a survival strategy employed by a wide range of parasites, which collectively are responsible for a great amount of human morbidity and mortality.[1]

The interaction between immune cells and pathogenic bacteria is very difficult to study[2], as intracellular pathogens can be non-trivial to grow ex vivo[3] and very difficult to genetically alter. Even in (rare) cases where these bacteria can be genetically modified,[4] imaging their encounters with host phagocytes is limited to encounters where successful infection is established. Encounters whereby the pathogens are killed and degraded are difficult to image, as the proteolysis that is a hallmark of successful phagocytic maturation[5] results in the degradation of reporter proteins and epitopes.[6]

---

[*] Published as part of: Daphne M. van Elsland, Erik Bos, Wouter de Boer, Herman S. Overkleeft, Abraham J. Koster and Sander I. van Kasteren. *Chem. Sci*, **7**, 752-758 (2016).

Bioorthogonal chemistry is a powerful tool for labelling of (sub)-populations of biomolecules in complex biological systems[7] and could be employed to circumvent these problems. The approach relies on the introduction of a small, physiologically inert chemical group into a biomolecule of interest that can subsequently be visualised using a selective reaction.[8] The small size, biological stability of the chemical group, and the wide range of biomolecules that can be labelled with this approach makes this method a valuable part of the biochemist's toolkit.[9, 10]

Bolstered by the recent successful imaging of a pathogen inside a host phagocyte through the use of a bioorthogonally-modified cell wall component, D-alanine,[11-13] it was envisaged that bioorthogonal bacteria could also be used to image degradation events in host phagocytes. Bioorthogonal non-canonical amino acid tagging (BONCAT)[14, 15] for pan-proteomic incorporation of bioorthogonal groups[16, 17] would allow the labelling of a wide range of bacterial species without the need for genetic modification.[18] Furthermore, unlike reporter proteins, bioorthogonal groups, such as azides,[19, 20] have been shown to be stable in the harsh chemical environments of the phagolysosomal system and should therefore be detectable even when extensive proteolysis has occurred.

Information about subcellular localisation is of key importance when studying parasite–phagocyte-interactions as movement between organelles may be essential to the life cycle of certain parasites.[1, 21] Only transmission electron microscopy (TEM)-based techniques allows the study of these pathogens in their subcellular context, as it provides substructural information on the position of any label/antigen within the cell.[22] However, in contrast to superresolution imaging,[23, 24] no methods have been reported that allow the visualisation of bacterial degradation using bioorthogonal labelling in combination with EM imaging.[25]

This chapter describes the application of a correlative light electron microscopy (CLEM)-based imaging approach for the visualisation of bioorthogonal groups, which allows the imaging of BONCAT-labelled bacteria inside phagocytes (Figure 1); even as they are being degraded. This approach combines the benefits of confocal microscopy – which allows widefield navigation to areas of interest[26] – with those of EM – which provides narrow-field high-resolution information about the interior of the cell.[22] All approaches described here on the model organism *Escherichia coli* (*E. coli)* are amenable to application to pathogens, which would open new avenues for studying the events leading to bacterial clearance and/or establishment of intracellular residence by intracellular pathogens.

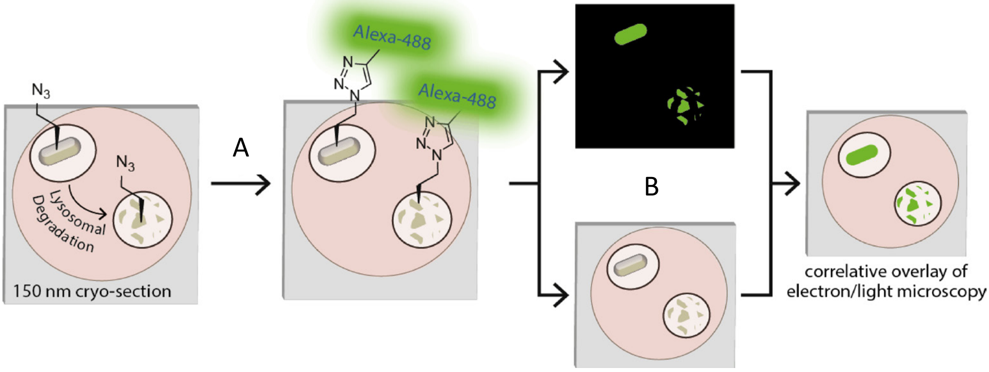

Figure 1: Overview: (A) phagocytosed azido-*E. coli* can be fluorescently visualised in an ultrathin cryosection using a copper-catalysed Huisgen cycloaddition reaction with a fluorophore; (B) overlay of this image on an electron micrograph provides an ultrastructural context for the signal with nanometer-scale resolution. As the bioorthogonal handle is stable to proteolysis, degraded bacteria can be visualised in this manner.

Results

Comparison of GFP-E. coli and azido-E. coli for imaging phagolysosomal degradation

Most CLEM studies employ the fusion of fluorescent proteins to a protein of interest or antibody-based approaches to allow their identification and localisation.[22] These labelling approaches have shown to be of great value for the imaging of specific proteins in their cellular context, but only in the cases where genetic modification of the organism is possible and where the attachment of the fluorescent proteins does not affect protein function.[27] Immunofluorescence has also been used, but combined with CLEM it either compromises ultrastructure (by virtue of the need of fixation and permeabilisation prior to CLEM-sample preparation)[28], or suffers from a notoriously low success rate due to compromised epitope availability in samples prepared for TEM.[29]

To determine whether the BONCAT-based labelling approach has advantages over genetic methods for the detection of phagocytosed bacteria during degradation, the fate of azido-*E. coli* was compared to that of GFP-expressing *E. coli* (Figure 2). Mouse bone marrow-derived dendritic cells (BM-DCs)[30, 31] were incubated with azido-*E. coli* or GFP-*E. coli* for 45 minutes. After washing, the cells were chased for 1 h, 2 h or 3 h prior to fixation, bioorthogonal modification of the azides (where present), and confocal imaging (Figure 2) – time points in which maturation of a phagosome to a phagolysosome is known to take place in these cells.[32]

To assess whether the fluorescent signal originated from intact or (partially) degraded bacteria, extranuclear DAPI staining was analysed: colocalisation of the fluorescent signal with the extra-nuclear DAPI indicates the intactness of the bacterial DNA, which in turn indicates the intactness of the bacterium.[33] Absence of this colocalisation (i.e. 488 nm single-positive foci) indicated the degradation of the bacterial genome and thus death. The azide-based signal persisted significantly more than the GFP-signal after killing of the bacterium; as indicated by the significantly larger number of DAPI-negative/azide-positive foci at all time points of the chase period compared to DAPI-negative/GFP-positive foci (Figure 3). Many of the azide-positive foci were smaller than intact DAPI/azide double positive foci, indicating these signals to originate from partially degraded bacteria.

CLEM imaging of azido-E. coli after uptake by BM-DCs.

We obtained ultrastructural information about the location of these smaller, DAPI-negative foci by performing CLEM analysis on azido-*E. coli*-treated BM-DCs samples at all four time points (Figure 4 and Figure 5). Co-staining with the lysosomal marker Lysosomal Associated Membrane Protein-1 (LAMP-1) revealed that these degraded fragments only partially resided in LAMP-1-positive late endosomes/lysosomes. This ties in with previous studies showing the existence of a second population of phagosomes in DCs, which do not acidify and never become LAMP-1 positive.[34] This set of phagosomes has been implicated in DC-specific functions, such as cross-presentation.[35, 36] Morphological information obtained from TEM showed that the azide-positive/DAPI-positive foci were intact bacteria, whereas the DAPI-negative foci showed no identifiable bacterial morphology, indicating that this technique allows the imaging of partially degraded bacteria inside mammalian phagocytes (Figure 4 and Figure 5) .

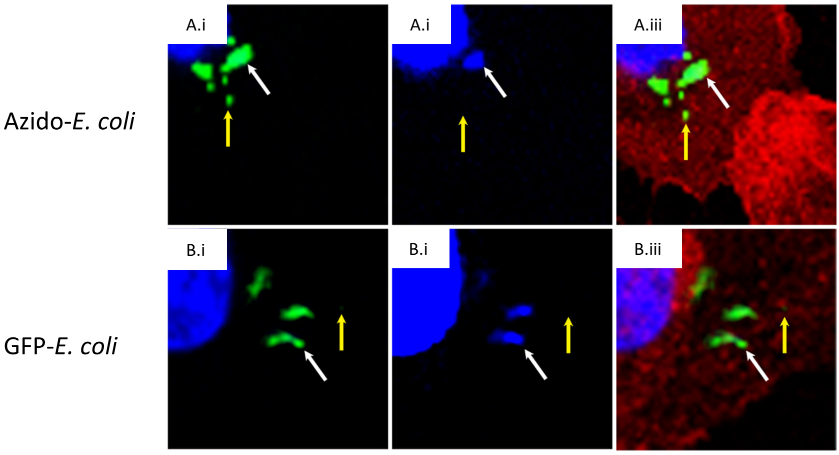

Figure 2: Confocal microscopy of (A) azido-*E. coli* or (B) GFP-*E. coli* after phagocytosis. BM-DCs were pulsed with either azido-*E. coli* or GFP-*E. coli* (45 minutes pulse). Cells were fixed after a 2 h chase and stained with DAPI (blue), anti-actin (red) and, in case of azido-*E. coli* , AlexaFluor-488 alkyne (green = either GFP or AlexaFluor-488). (i) DAPI/488 nm overlay; (ii) DAPI only; (iii) all fluorescent channels overlay. Yellow arrows indicate a 488-single positive focus, white arrows a DAPI/488 nm double positive focus.

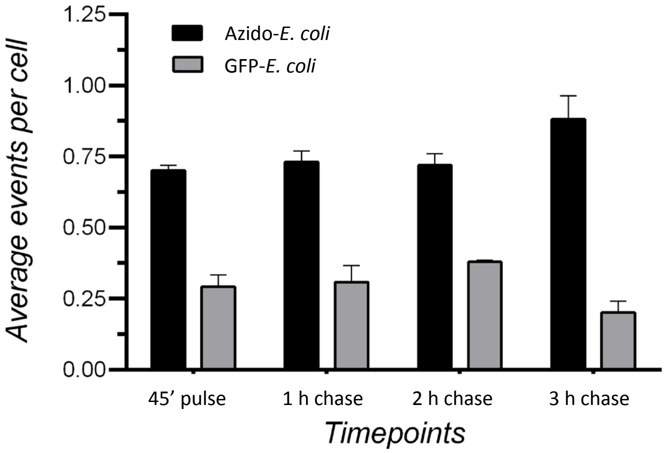

Figure 3: Comparison of GFP-*E. coli* and azido-*E. coli* for imaging phagolysosomal degradation in BM-DCs. BM-DCs were incubated with either GFP-*E. coli* or azido-*E.coli* cells for 45 minutes. Cells were washed with PBS to remove unbound/non-internalised *E. coli*. After a 45 minutes pulse, 1 h chase, 2 h chase or 3 h chase cells were fixed with 4% PFA for 15 minutes. Azido-*E. coli* containing cells were labelled with AlexaFluor-488 alkyne using copper-catalysed Huisgen cycloaddition-conditions. From each condition confocal microscopy pictures were made. Based on these pictures the average number of green foci, that represented degraded bacteria per cell, was determined. Only the foci that were within the focus plane of the cell (determined by the actin staining) were counted and had no overlap with extra-nuclear DAPI stain. Per condition 50 cells were counted. N=2.

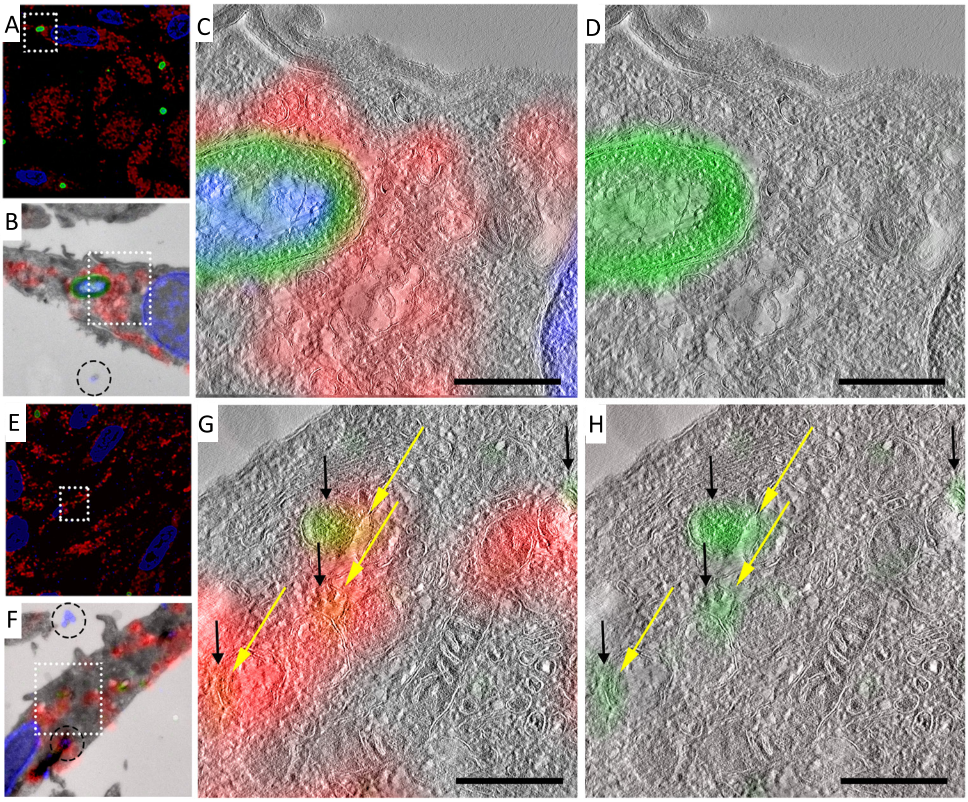

Figure 4: CLEM imaging of phagocytosed azido-*E. coli*: BM-DCs were pulsed with azido-*E. coli* (45 minutes pulse). Cells were washed with PBS to remove unbound/non-internalised *E. coli*. Samples were fixed immediately after pulsing (A–D) or after a 3 h chase (E–H). Cells were subjected to Tokuyasu sample preparation and cryosectioned into 150 nm sections. Sections were reacted with AlexaFluor-488 alkyne using ccHc-conditions (green), anti-LAMP-1 (red) and DAPI (blue). DAPI staining and blue fiducials (indicated with circles in B and F) were used for correlation purposes. (A/E) Confocal microscopy images; (B/F) CLEM image obtained from overlay LM and EM pictures; (C, D, G and H) CLEM details from (B/F), showing LAMP-1 and 488 nm channels (C/G) or 488 nm alone (D/H). Green = AlexaFluor-488, Red = LAMP-1, Blue = nuclear DAPI stain and fiducial beads. Scale bar 500 nm.

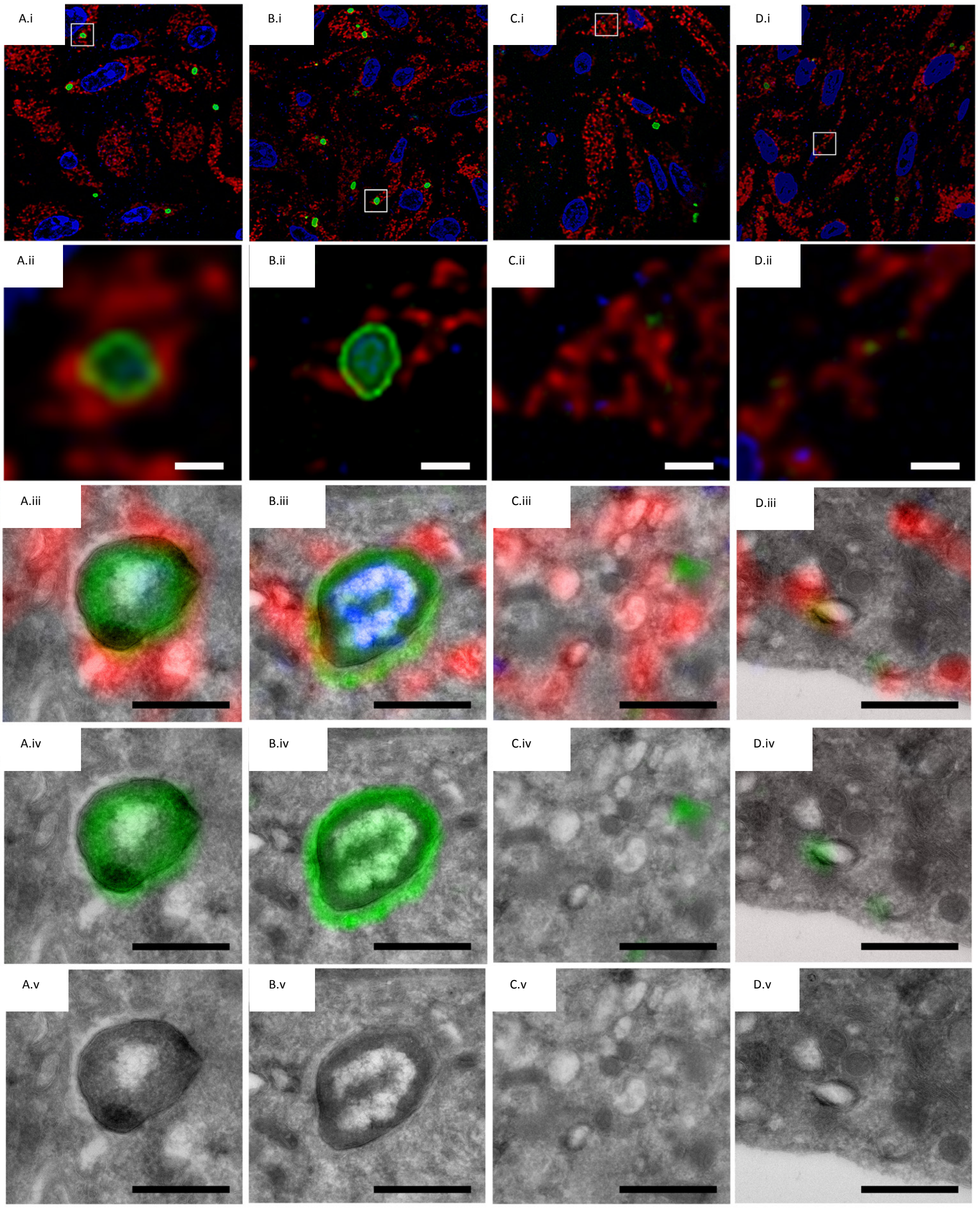

Figure 5: CLEM imaging of mouse BM-DCs infected with azido-*E. coli*. BM-DCs were incubated with *E. coli* cells for 45 minutes. Cells were washed with PBS to remove unbound/non-internalised *E. coli*. After a 45 minutes pulse (A.i-v), 1 h chase (B.i-v), 2 h chase (C.i-v) or 3 h chase (D.i-v) cells were fixed in 2% PFA, subjected to Tokuyasu sample preparation (including gelatin embedding and sucrose infiltration) and crysectioned into 150 nm sections. Sections were reacted with AlexaFluor-488 (green) alkyne using copper-catalysed Huisgen cycloaddition reaction, anti-LAMP-1 (red) and DAPI (blue). DAPI staining and blue fiducials were used for correlation purposes. (A.i-D.i) Confocal microscopy image of bioorthogonally tagged *E. coli* B834 incubated with mouse BM-DCs (A.i) 45

minutes pulse (B.i) 1 h chase (C.i) 2 h chase (D.i) 3 h chase. Green = AlexaFluor-488, Red = LAMP-1, Blue = nuclear DAPI stain and fiducial beads. (ii) Detail from i. (iii) CLEM image obtained from overlay EM picture and figure ii, using blue fiducials and DAPI stain for correlation. (iv) Similar detail from a.iii-d.iii without red and blue signals. (v) Similar detail from a.iii-d.iii EM image only. Scale bar 500 nm.

Conclusion

By combining BONCAT with CLEM-imaging, we have established a new approach that allowed us to visualise bioorthogonally modified bacteria in an ultrastructural cellular context, even during late stages of bacterial degradation. With this approach degradation events in a cell can be identified at low magnification with confocal microscopy using bioorthogonal labelling, after which ultrastructural information about their subcellular location and context can be obtained with EM. This is of great interest for the study of obligate intracellular parasites that are very hard to study by any other means.

As the application of bioorthogonal chemistry is ever expanding, the CLEM-imaging method of bioorthogonal groups described here could also be of great benefit to the study of labelled biomolecules in other fields in which bioorthogonal imaging has proven its value.[25] Application of this approach to other bioorthogonal assays (for instance, lipid imaging[37] and the imaging of newly synthesised proteins[38]), and perhaps in combination with some of the more recently developed bioorthogonal chemistries[39] will allow the provision of additional structural information to the current imaging methods available for these types of biomolecules.

Experimental

E. coli culturing conditions and growth measurements

E. coli B834(DE3) bacteria were grown overnight at 37°C in Lysogeny Broth (LB) medium. The following day cultures were diluted 1:50 in LB medium and grown at 37°C till an OD_{600} between 0.3-0.5. Subsequently cells were collected and resuspended in Selenomet medium (Molecular Dimensions) and supplemented with either 4 mM Azidohomoalanine (Aha) (Bachem) or 4 mM Methionine (Met) (Sigma-Aldrich). After 1 h OD_{600} were measured and cells were collected by centrifugation for BM-DC infection experiments.

E. coli B834(DE3) GFP_{A206K} was grown overnight at 37°C in LB medium. The following day cultures were diluted 1:50 in LB medium and grown at 37 °C till an OD_{600} between 0.3-0.5. Throughout culturing, cultures were supplemented with 100 µg/ml Ampicillin. The vector pRD35 for the constitutive expression of GFP_{A206K}, was constructed by cloning GFP into pUC21 using NsiI and MluI restriction sites. An A206K mutation was introduced by site-directed mutagenesis PCR to prohibit dimerisation of GFP.[40] The constitutive *hns* promoter and ribosomal binding site (the 258 bases upstream of the *E. coli hns* gene), were amplified by PCR, using *E. coli* K12 as a template, and positioned upstream of GFP by way of XhoI and NsiI. Used primers are indicated in Table 1.

GFP fw NsiI	ACA-ATG-CAT-AGT-AAA-GGA-GAA-GAA-CTT-TTC-ACT-GGA-GTT-G
A206K fw	CCT-GTC-CAC-ACA-ATC-TAA-ACT-TTC-GAA-AGA-TCC-C
A206K rev	GGG-ATC-TTT-CGA-AAG-TTT-AGA-TTG-TGT-GGA-CAG-G
GFP R	CAC-ACG-CGT-TTA-TTT-GTA-TAG—TTC-ATC-CAT-GCC-ATG-TGT-AAT-CC
HNS-Chrom-Fw-XhoI	GAA-CTC-GAG-GGT-CGT-CAG-CCT-ACG-ATA-ATC-TCC-CC
HNS-Chrom-Rev-NsiI	ACT-ATG-CAT-TCT-AGT-AAT-CTC-AAA-CTT-ATA-TTG-GGG-TGG-TTT-G

Table 1: Primers used for GFP-plasmid construction.

Mammalian cell culture conditions

Mouse bone marrow derived dendritic cells (BM-DCs) were generated from B57BL/6 mice bone marrow essentially as described[30] with some modifications. Briefly, bone marrow was flushed from femurs and tibia and cells were cultured in IMDM (Sigma Aldrich) supplemented with 8% heat-inactivated fetal calf serum, 2 mM L-glutamine, 20 µM 2-Mercaptoethanol (Life Technologies), penicillin 100 I.U./mL and streptomycin 50 µg/mL in the presence of 20 ng/mL GM-CSF (ImmunoTools). Medium was replaced on day 3 and 7 of culture and the cells were used between days 10 and 13.

E. coli B834(DE3) cells were added to the BM-DCs as suspensions in PBS in a ratio of approximately 25:1, respectively. After 45 minutes of incubation unbound/non-internalised *E. coli* cells were washed off (2x PBS) and medium was replaced. At the indicated time points cells were subjected to confocal microscopy or Tokuyasu sample preparation.

Whole cell confocal microscopy

BM-DCs were seeded (7 x 10^4) on a 12-well removable chamber slide (Ibidi) and left to grow O/N. The following day *E. coli* B834 cells harboring either GFP/Aha/Met were added to the BM-DCs as suspensions in PBS in a ratio of approximately 25:1, respectively. After 45 minutes of incubation unbound/non-internalised *E. coli* cells were washed off (2x PBS) and medium was replaced. At the indicated time points cells were fixed in 4% PFA for 15 minutes. Until further analysis cells were kept in PBS at 4°C. When all slides were collected, fixed cells were incubated for 30 minutes with blocking buffer (1% BSA, 1% gelatin cold water fish skin), for 1 h with click cocktail (0.1 M HEPES pH 7.3, 1 mM $CuSO_4$, 10 mM sodium ascorbate, 1 mM THPTA ligand, 10 mM amino-guanidine, 5 µM AlexaFluor-488 Alkyne (Invitrogen)), O/N with anti-actin antibody (abcam), 1 h with goat anti-rabbit AlexaFluor-568 (Invitrogen) and DAPI (1 µg/ml). After the staining procedures chambers were removed and cells were covered with a small drop of 50% glycerol, after which a coverslip was mounted over the grid. Coverslips were fixed using Scotch Pressure-Sensitive Tape. Samples were imaged with a Leica TCS SP8 confocal microscope (63x oil lens, N.A.=1.4).

Bioorthogonal labelling on cryosections

Samples were prepared for cryosectioning as described elsewhere.[41] Briefly, BM-DCs were fixed for 24 h in freshly prepared 2% PFA in 0.1 M phosphate buffer. Fixed cells were embedded in 12% gelatin (type A, bloom 300, Sigma) and cut with a razor blade into 0.5 mm^3 cubes. The sample blocks were infiltrated in phosphate buffer containing 2.3 M sucrose for 3 h. Sucrose-infiltrated sample blocks were mounted on aluminum pins and plunged in liquid nitrogen. The frozen samples were stored under liquid nitrogen.

Ultrathin cell sections were obtained as described elsewhere. Briefly, the frozen sample was mounted in a cryo-ultramicrotome (Leica). The sample was trimmed to yield a squared block with a front face of about 300 x 250 µm (Diatome trimming tool). Using a diamond knife (Diatome) and antistatic device (Leica) a ribbon of 150 nm thick sections was produced that was retrieved from the cryochamber with a droplet of 1.15 M sucrose containing 1% methylcellulose. Obtained sections were transferred to a specimen grid previously coated with formvar and carbon. Grids were additionally coated as indicated with either 100 nm TetraSpeck beads or 100 nm FluoroSpheres (blue) carboxylate-modified (350/440) (Life Technologies).

To further improve the structural integrity of the ultrathin cryosections a novel micromanipulator (Manip, Diatome) was used that was mounted on the cryochamber of the ultramicrotome.[42] This device facilitated section retrieval from the cryochamber and resulted in less overstretching of the sections during thawing.[43]

Sections were labelled as follows; thawed cryosections on an EM grid were left for 30 minutes on the surface of 2% gelatin in phosphate buffer at 37°C. Subsequently grids were incubated on drops of PBS/glycine and PBS/glycine containing 1% BSA. Grids were then incubated on top of the ccHc-cocktail (0.1 M HEPES pH 7.3, 1 mM $CuSO_4$, 10 mM sodium ascorbate, 1 mM THPTA ligand, 10 mM amino-guanidine, 5 µM AlexaFluor-488 alkyne (Invitrogen) for 1 h and washed 6 times with PBS. Sections containing BM-DCs and Jurkat cells were then labelled with DAPI (2 µg/ml), and additionally washed with PBS and aquadest.

In case of additional immune-labelling against LAMP-1 grids were subjected to the following steps directly after the ccHc reaction. Grids were washed 5 times with PBS/glycine and blocked again with PBS/glycine containing 1% BSA after which the grids were incubated for 1 h with PBS/glycine 1% BSA supplemented with a rat anti-mouse LAMP-1 (BioLegend). Sections were subsequently washed 6 times with PBS, labelled with DAPI (2 µg/ml) and finally washed again with PBS and aquadest.

Microscopy and correlation

The CLEM approach used was adapted from Vicidomini et al.[44] Grids containing the sample sections were washed with 50% glycerol and placed on glass slides (pre- cleaned with 100% ethanol). Grids were then covered with a small drop of 50% glycerol, after which a coverslip was mounted over the grid. Coverslips were fixed using Scotch Pressure-Sensitive Tape. Samples were imaged with a Leica TCS SP8 confocal microscope (63x oil lens, N.A.=1.4). Confocal microscopy was used as it allowed to make image stacks from the sections at different focus planes; this was convenient as the sections were found to be in different focus planes whilst placed between the glass slides and coverslip. Confocal stacks were deconvolved with theoretical point spread functions using Huygens Essential deconvolution software (SVI, Hilversum, Netherlands). After fluorescence microscopy the EM grid with sections was removed from the glass slide, rinsed in distilled water and incubated for 5 minutes on droplets of unranylacetate/methylcellulose.

Excess of uranylacetate/methylcellulose was blotted away and grids were air-dried. EM imaging was performed with a Tecnai 12 Biotwin transmission electron microscope (FEI) at 120 kV acceleration voltage. Tilt series for electron tomography were collected using Xplore3D (FEI Company) software. The angular tilt range was set from -60˚ to 60˚ with 2˚ increments, and an objective lens defocus of -2 µm at a magnification of 20 K (pixel size is 1 nm). Alignments of the tilt series and weighted-back projection reconstructions for tomography were performed using IMOD software.[45]

Correlation of confocal and EM images was performed in Adobe Photoshop CS6. In Adobe Photoshop, the LM image was copied as a layer into the EM image and made 50% transparent. Transformation of the LM image was necessary to match it to the larger scale of the EM image. This was performed via isotropic scaling and rotation. Interpolation settings; bicubic smoother. Alignment at low magnification was carried out with the aid of nuclear DAPI staining in combination with the shape of the cells, at high magnification alignment was performed using fiducial beads.[46]

References

1. D. M. Walker, S. Oghumu, G. Gupta, B. S. McGwire, M. E. Drew and A. R. Satoskar, *Cell Mol Life Sci*, 2014, **71**, 1245-1263.
2. M. B. Johnson and A. K. Criss, *J Vis Exp*, 2013, **79**, 50729.
3. R. W. Truman and J. L. Krahenbuhl, *Int J Lepr Other Mycobact Dis*, 2001, **69**, 1-12.
4. O. Lamrabet and M. Drancourt, *Tuberculosis (Edinb)*, 2012, **92**, 365-376.
5. O. V. Vieira, R. J. Botelho and S. Grinstein, *Biochem J*, 2002, **366**, 689-704.
6. H. Katayama, A. Yamamoto, N. Mizushima, T. Yoshimori and A. Miyawaki, *Cell Struct Funct*, 2008, **33**, 1-12.
7. R. K. Lim and Q. Lin, *Chem Commun (Camb)*, 2010, **46**, 1589-1600.
8. H. C. Kolb, M. G. Finn and K. B. Sharpless, *Angew Chem Int Ed Engl*, 2001, **40**, 2004-2021.
9. E. M. Sletten and C. R. Bertozzi, *Angew Chem Int Ed Engl*, 2009, **48**, 6974-6998.
10. C. P. Ramil and Q. Lin, *Chem Commun (Camb)*, 2013, **49**, 11007-11022.
11. G. W. Liechti, E. Kuru, E. Hall, A. Kalinda, Y. V. Brun, M. VanNieuwenhze and A. T. Maurelli, *Nature*, 2014, **506**, 507-510.
12. P. Shieh, M. S. Siegrist, A. J. Cullen and C. R. Bertozzi, *Proc Natl Acad Sci U S A*, 2014, **111**, 5456-5461.
13. M. S. Siegrist, S. Whiteside, J. C. Jewett, A. Aditham, F. Cava and C. R. Bertozzi, *ACS Chem Biol*, 2013, **8**, 500-505.
14. D. C. Dieterich, A. J. Link, J. Graumann, D. A. Tirrell and E. M. Schuman, *Proc Natl Acad Sci U S A*, 2006, **103**, 9482-9487.
15. P. Landgraf, E. R. Antileo, E. M. Schuman and D. C. Dieterich, *Methods Mol Biol*, 2015, **1266**, 199-215.
16. K. L. Kiick, E. Saxon, D. A. Tirrell and C. R. Bertozzi, *Proc Natl Acad Sci U S A*, 2002, **99**, 19-24.
17. K. L. Kiick and D. A. Tirrell, *Tetrahedron*, 2000, **56**, 9487-9493.
18. R. Hatzenpichler, S. Scheller, P. L. Tavormina, B. M. Babin, D. A. Tirrell and V. J. Orphan, *Environ Microbiol*, 2014, **16**, 2568-2590.
19. J. B. Pawlak, G. P. Gential, T. J. Ruckwardt, J. S. Bremmers, N. J. Meeuwenoord, F. A. Ossendorp, H. S. Overkleeft, D. V. Filippov and S. I. van Kasteren, *Angew Chem Int Ed Engl*, 2015, **54**, 5628-5631.
20. S. P. Ouellette, F. C. Dorsey, S. Moshiach, J. L. Cleveland and R. A. Carabeo, *PLoS One*, 2011, **6**, e16783.
21. N. van der Wel, D. Hava, D. Houben, D. Fluitsma, M. van Zon, J. Pierson, M. Brenner and P. J. Peters, *Cell*, 2007, **129**, 1287-1298.
22. P. de Boer, J. P. Hoogenboom and B. N. Giepmans, *Nat Methods*, 2015, **12**, 503-513.

23. I. Nikic, T. Plass, O. Schraidt, J. Szymanski, J. A. Briggs, C. Schultz and E. A. Lemke, *Angew Chem Int Ed Engl*, 2014, **53**, 2245-2249.
24. R. S. Erdmann, H. Takakura, A. D. Thompson, F. Rivera-Molina, E. S. Allgeyer, J. Bewersdorf, D. Toomre and A. Schepartz, *Angew Chem Int Ed Engl*, 2014, **53**, 10242-10246.
25. D. M. van Elsland, E. Bos, H. S. Overkleeft, A. J. Koster and S. I. van Kasteren, *J of Chem Biol*, 2015, **8**, 153-157.
26. B. N. Giepmans, *Histochem Cell Biol*, 2008, **130**, 211-217.
27. C. L. Thomas and A. J. Maule, *J Gen Virol*, 2000, **81**, 1851-1855.
28. U. Schnell, F. Dijk, K. A. Sjollema and B. N. Giepmans, *Nat Methods*, 2012, **9**, 152-158.
29. G. Griffiths and J. M. Lucocq, *Histochem Cell Biol*, 2014, **142**, 347-360.
30. M. B. Lutz, N. Kukutsch, A. L. Ogilvie, S. Rossner, F. Koch, N. Romani and G. Schuler, *J Immunol Methods*, 1999, **223**, 77-92.
31. M. A. West, R. P. Wallin, S. P. Matthews, H. G. Svensson, R. Zaru, H. G. Ljunggren, A. R. Prescott and C. Watts, *Science*, 2004, **305**, 1153-1157.
32. L. P. Erwig, K. A. McPhilips, M. W. Wynes, A. Ivetic, A. J. Ridley and P. M. Henson, *Proc Natl Acad Sci U S A*, 2006, **103**, 12825-12830.
33. E. Y. Seo, T. S. Ahn and Y. G. Zo, *Appl Environ Microbiol*, 2010, **76**, 1981-1991.
34. A. Savina, C. Jancic, S. Hugues, P. Guermonprez, P. Vargas, I. C. Moura, A. M. Lennon-Dumenil, M. C. Seabra, G. Raposo and S. Amigorena, *Cell*, 2006, **126**, 205-218.
35. I. Cebrian, G. Visentin, N. Blanchard, M. Jouve, A. Bobard, C. Moita, J. Enninga, L. F. Moita, S. Amigorena and A. Savina, *Cell*, 2011, **147**, 1355-1368.
36. E. Saxon and C. R. Bertozzi, *Science*, 2000, **287**, 2007-2010.
37. S. Ito, L. Shen, Q. Dai, S. C. Wu, L. B. Collins, J. A. Swenberg, C. He and Y. Zhang, *Science*, 2011, **333**, 1300-1303.
38. K. E. Beatty, J. C. Liu, F. Xie, D. C. Dieterich, E. M. Schuman, Q. Wang and D. A. Tirrell, *Angew Chem Int Ed Engl*, 2006, **45**, 7364-7367.
39. K. Lang and J. W. Chin, *ACS Chem Biol*, 2014, **9**, 16-20.
40. D. A. Zacharias, J. D. Violin, A. C. Newton and R. Y. Tsien, *Science*, 2002, **296**, 913-916.
41. P. J. Peters, E. Bos and A. Griekspoor, in *Current Protocols in Cell Biology*, John Wiley & Sons, Inc., 2001,.
42. D. Studer, A. Klein, I. Iacovache, H. Gnaegi and B. Zuber, *J Struct Biol*, 2014, **185**, 125-128.
43. E. Bos, C. SantAnna, H. Gnaegi, R. F. Pinto, R. B. Ravelli, A. J. Koster, W. de Souza and P. J. Peters, *J Struct Biol*, 2011, **175**, 62-72.

44. G. Vicidomini, M. C. Gagliani, K. Cortese, J. Krieger, P. Buescher, P. Bianchini, P. Boccacci, C. Tacchetti and A. Diaspro, *Microsc Res Tech*, 2010, **73**, 215-224.
45. J. R. Kremer, D. N. Mastronarde and J. R. McIntosh, *J Struct Biol*, 1996, **116**, 71-76.
46. J. Kuipers, T. J. van Ham, R. D. Kalicharan, A. Veenstra-Algra, K. A. Sjollema, F. Dijk, U. Schnell and B. N. Giepmans, *Cell Tissue Res*, 2015, **360**, 61-70.

6

Towards Ultrastructural Imaging of *Salmonella*-Host Interactions using Bioorthogonal Labelling and Super-Resolution CLEM [*]

Introduction

The immune system is the defence mechanism that protects the human body against illness and infection. Through a series of steps called the immune response, it attacks pathogens and potentially harmful commensals. When rapid and effective, the infection will be eliminated quickly and disease will not occur. However, many bacterial pathogens have evolved strategies to subvert and exploit the immune response in order to enter and replicate in eukaryotic cells.

A prime example of such a bacterial pathogen is *Salmonella enterica* (*Salmonella*). *Salmonella* is a Gram-negative facultative intracellular pathogen that infects both humans and animals.[1] More than 2500 *Salmonella* serotypes exist, which can be broadly grouped in non-typhoidal and typhoidal.[2] Non-typhoidal *Salmonella* serotypes cause localised gastrointestinal infections in healthy human adults, whereas typhoidal serotypes have evolved to enter and exploit intestinal macrophages and cause life-threatening systemic infections.[3, 4]

---

[*] D.M. van Elsland, S. Pujals, I. Berlin, L. Albertazzi, J.J.C. Neefjes, H.S. Overkleeft, A.J. Koster and S.I. van Kasteren contributed to the work described in this chapter.

Typhoidal *Salmonella* establishes a systemic infection upon the temporal and spatial injection of bacterial proteins into macrophage cells.[5] This temporal and coordinated delivery of effector proteins modulates the functions of the macrophage cell organelles and promotes *Salmonella* replication and its subsequent dissemination throughout the host.[6] *Salmonella* can enter macrophages by several endocytic routes, which are triggered by the secretion of several effector proteins via both pathogenicity island 1 (SPI1) and non-SPI1 type III secretion systems (T3SS) (Figure 1, (*1*)).[7] Once intracellular, *Salmonella* remains inside the spacious phagosome (SP) (Figure 1, (*2*)). This vacuolar compartment shrinks over minutes to hours to form an adherent membrane around one or more bacteria, which is then referred to as the *Salmonella*-containing vacuole (SCV) (Figure 1, (*3*)). Upon the injection of effector proteins *Salmonella* modulates the interaction of the SCV with the endocytic environment and the ER-Golgi network and as such ensures the maturation of the SCV and its own replication (Figure 1, (*4*)).[3]

Understanding the mechanisms by which *Salmonella* modulates and interacts with host cell organelles is thus of key importance for the understanding of *Salmonella*-virulence mechanisms in the development of systemic *Salmonella* infections.[6] To unravel these mechanisms injected and secreted bacterial proteins need to be labelled and traced.

Proteome-wide labelling of injected and secreted bacterial proteins can be established using bioorthogonal non-canonical amino acid tagging (BONCAT). With BONCAT bioorthogonally functionalised amino acid analogs such as azidohomoalanine (Aha) and homopropargylglycine (Hpg) are incorporated in the proteomes of prokaryotic and eukaryotic cells (Figure 2A). These bioorthogonal amino acid analogs are incorporated by wild-type methionyl-tRNA synthetase (metRS) at the sites where naturally methionine amino acids are incorporated. After incorporation, bioorthogonally functionalised amino acids can be labelled with a detection group using chemical ligation (Figure 2C).[8, 9]

Recently, Grammel et al. reported that the BONCAT labelling strategy can even be used to selectively label and study the proteome wide expression levels of bacterial pathogens inside mammalian immune cells.[8-12] By mutating the methionyl-tRNA synthetase (NLL-MetRS) of bacteria, non-canonical amino acid such as azidonorleucine (ANL) and 2-aminoocytynoic acid (AOA) (Figure 2B) were specifically incorporated in *Salmonella Typhimurium* and *Yersinia enterocolitica* whilst present in the environment of a host cell. Recently, Mahdavi et al. reported that this bioorthogonal labelling approach even enabled the identification of distinct secretion profiles for intracellular and extracellular bacteria, and showed that it allows the analysis of the temporal order of bacterial protein expression during different stages of infection.[11, 13]

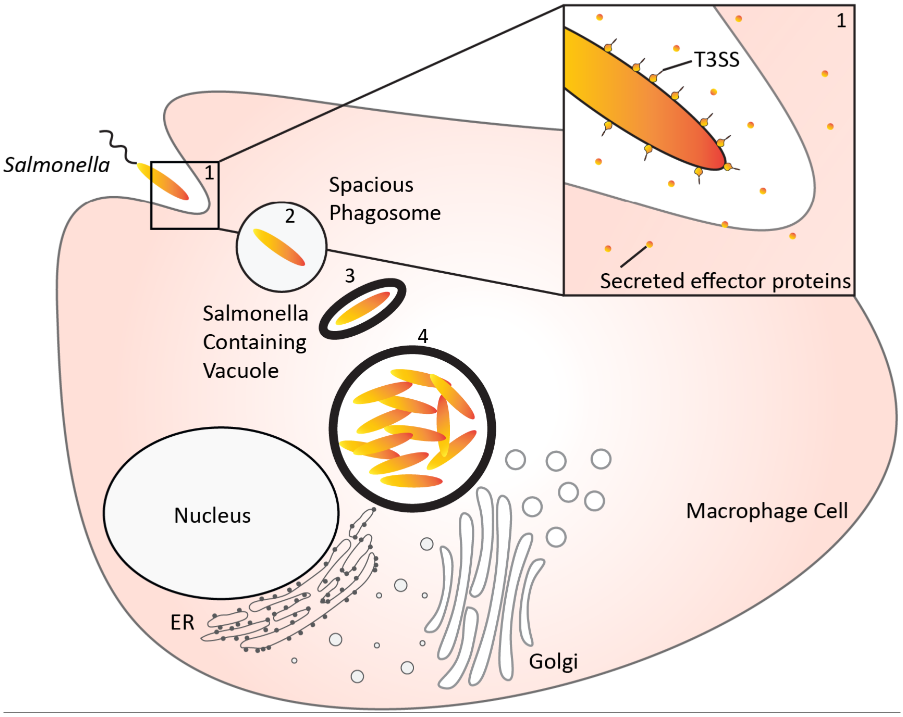

Figure 1: Schematic overview of interactions between *Salmonella* and host macrophage cells. *Salmonella* gets internalised by endocytosis upon secretion of effector proteins trough the T3SS (*1*). Subsequently *Salmonella* is enclosed in a spacious phagosome (SP) that is formed by membrane ruffles (*2*). Later, the phagosome fuses with lysosomes, acidifies and shrinks to become adherent around the bacterium. This is called the *Salmonella*-containing vacuole (SCV) (*3*). Upon the injection of effector proteins through the T3SS *Salmonella* modulates the interaction of the SCV with the endocytic environment and the ER-Golgi network and as such ensures the maturation of the SCV and its own replication (*4*).

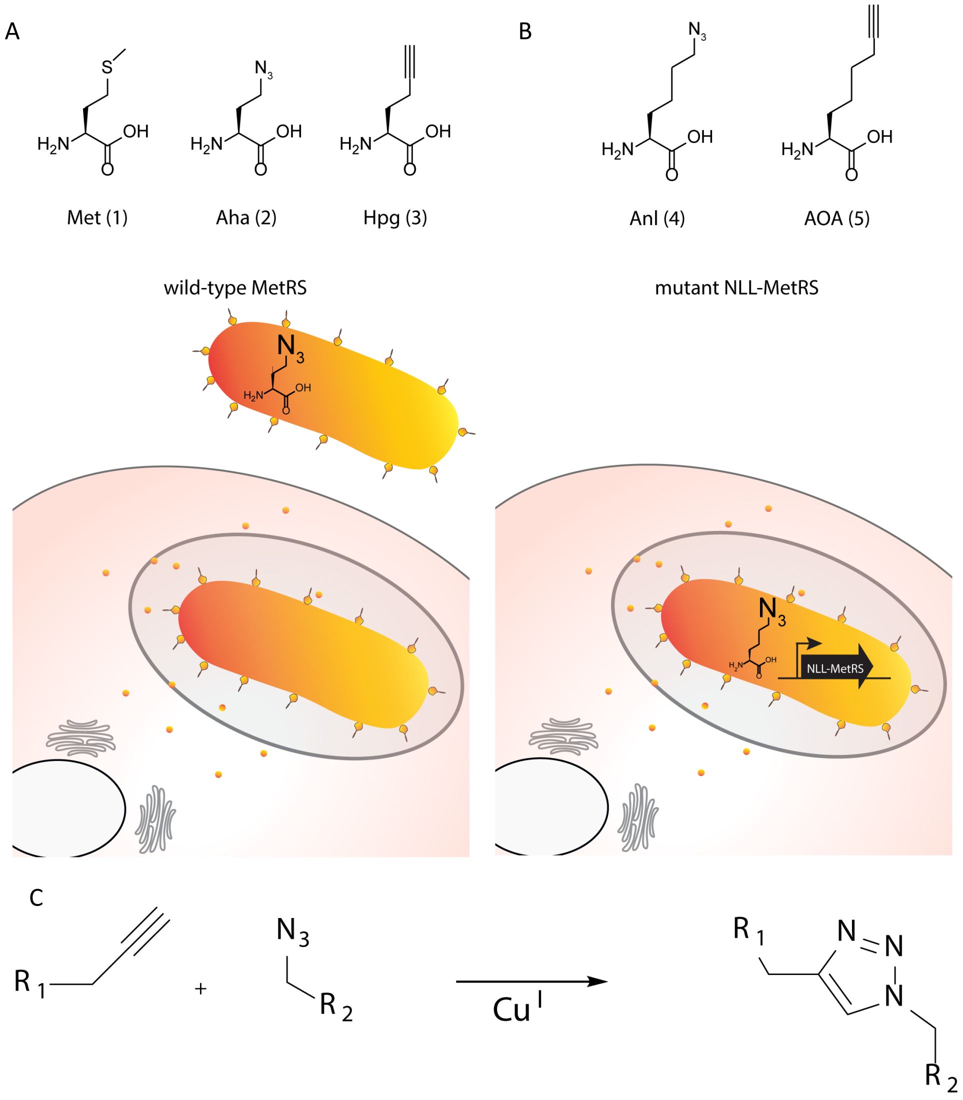
A
Met (1)
Aha (2)
Hpg (3)
B
Anl (4)
AOA (5)
wild-type MetRS
mutant NLL-MetRS
NLL-MetRS
C
Cu I

Figure 2: BONCAT for the identification of secreted bacterial effector proteins. (A) Structures of natural amino acid Met (1) and bioorthogonal amino acid analogs Aha (2) and Hpg (3) that can all be charged to tRNAMet by the wild-type MetRS. (B) Structure of Anl, which can be utilised only by a mutant synthetase like MetRSNLL and can therefore be incorporated cell-specifically in the bacterial proteome during infection. (C) Reaction scheme of Cu-catalyzed cycloaddition reaction between proteins that contain (azide- or alkyne-) modified amino acids with an azide- or alkyne-functionalised reporter.

BONCAT is thus a very powerful tool to unravel the temporal expression of *Salmonella* effector proteins. However, to investigate the interaction of these effector proteins with the host-environment, tools are needed that allow for their detection within the context of the hostcell. Recently, an approach was reported that enables the visualisation of BONCAT-labelled bacteria in the context of a host cell with correlative light and electron microscopy (CLEM).[14] This correlative transmission electron microscopy (TEM) technique allows for the wide field navigation to areas of interest with fluorescence microscopy and provides narrow field high-resolution information on the interior of the cell with TEM, and would thus allow for the visualisation of BONCAT-labelled *Salmonella* in the context of host cell organelles. However, the resolution of the fluorescence detection within this strategy, which is around 250 nm[15], is not sufficient to unravel the existence of secreted virulence factors, which can be around 2-20 nm in diameter.[16]

Recent developments in the field of CLEM have shown that upon implementing super-resolution imaging in CLEM, the detection resolution of fluorescent probes can be improved 10-fold, resulting in a more accurate and sensitive ultrastuctural localisation of fluorescent labels.[17] Since its initial inception it was shown that, depending on the research question, super-resolution imaging strategies can be combined with TEM in various ways.[18] It has been reported that upon lowering osmium tetroxide (OsO_4) concentrations and optimisation of embedding resin, fluorescence quenching could be prevented and fluorescence was preserved. This sample preparation technique was used with both PALM (photoactivated localisation microscopy)[17] and STED (stimulated emission depletion) microscopy.[19-21] Another example described the use of PALM, or STORM (stochastic optical reconstruction microscopy)[22], after Tokuyasu sectioning and subsequent OsO_4 contrast enhancement prior to scanning electron microscopy measurements.[23, 24] Since this latter technique uses Tokuyasu sample preparation as also reported for the BONCAT-CLEM strategy, it could be implemented in the CLEM strategy for the visualisation of secreted virulence factors. The aim of this study is therefore to apply the BONCAT-CLEM strategy for the imaging of BONCAT-labelled *Salmonella* virulence factors upon implementation of STORM imaging in the CLEM imaging sequence.

Results

In order to monitor *Salmonella*-host interactions with bioorthogonal amino acid tagging and CLEM, it was first tested whether bioorthogonal amino acids could be incorporated into the *Salmonella* proteome without the need of tRNA/tRNA synthetase engineering. To this end, the incorporation of the bioorthogonal amino acid Hpg into the bacterial proteome was monitored, analogous to the method outlined for *E. coli* in Chapter 3.[25]

It was decided to explore the incorporation of Hpg into the *Salmonella* model bacterium *S. Typhimurium*, as it represents a useful model to characterise the molecular mechanisms that underpin the interactions between thyphoidal *Salmonella* species and phagocytic cells.[3] Incorporation into the proteome was optimised with respect to cell viability and incorporation levels as assessed using SDS-PAGE analysis. In line with previous findings, extended incubation times resulted in reduced viability (Figure 3A), suggesting negative effects on protein expression upon prolonged exposure to bioorthogonal amino acids.[10, 14] Surprisingly, lowering the concentration of the bioorthogonal amino acid Hpg resulted in a higher incorporation level (Figure 3B). Thus, optimal conditions in terms of viability and incorporation levels were 30 minutes incubation with 0.4 mM Hpg, and these conditions were used for all further imaging studies.

To address whether the alkyne-*S. Typhimurium* bacteria could be imaged within a host cell using bioorthogonal labelling and confocal microscopy analysis, mouse bone marrow-derived dendritic cells (BM-DCs) were incubated with alkyne-modified *S. Typhimurium* expressing the fluorescent protein DsRed.[26] Subsequently, cells were washed, fixed and labelled with AlexaFluor-488 azide using the optimised copper-catalysed Huisgen cycloaddition (ccHc) reactions described in Chapter 3 of this thesis.[14] Confocal analysis revealed colocalisation of the DsRed-expressing *S. Typhimurium* and the bioorthogonal AlexaFluor-488 label (Figure 4). However, the signal of the AlexaFluor-488 was faint, which is most probably a result of the presence of endogenous Met that competes with Hpg for its incorporation. Despite this competition, these results show that the alkyne-*S. Typhimurium* bacteria can be labelled detectably with AlexaFluor-488-azide in the environment of a host cell using a ccHc reaction.

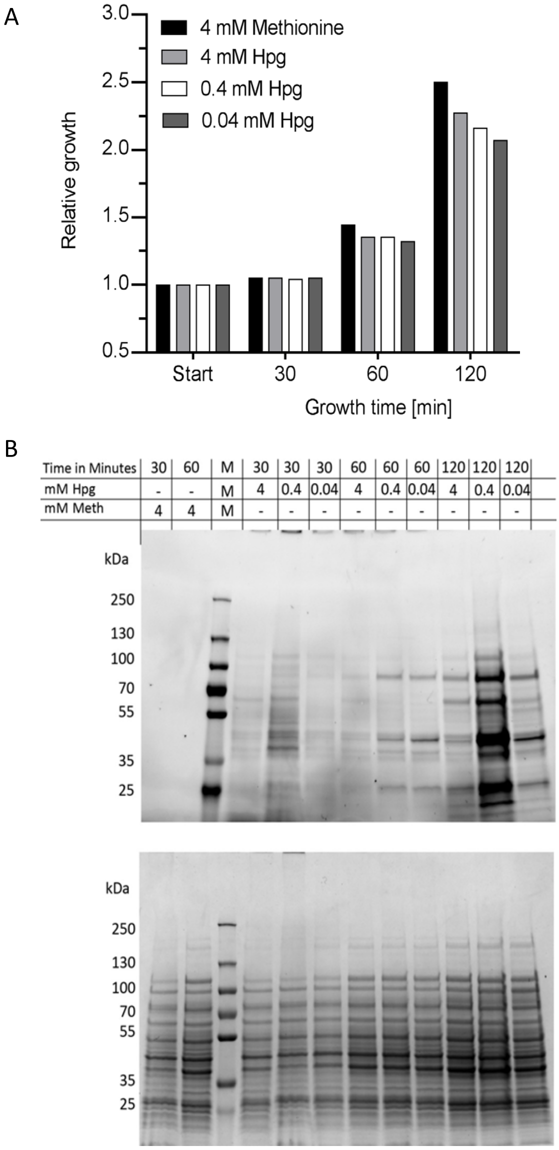

Figure 3: Hpg incorporation in *S. Typhimurium* A) *S. Typhimurium* cells were grown to an OD_{600} of 0.3-0.5. Cultures were then incubated with the indicated Hpg or Met concentrations. OD_{600} were measured at indicated time points and relative generations were calculated (first generation was set at 1 at timepoint 0). B) Top: Fluorescence gel of AlexaFluor-647 alkyne-labelled *S. Typhimurium* cells grown in the presence of the indicated concentrations of Hpg and Met. Bottom: Coomassie-staining loading control shows relative amounts of total protein per sample.

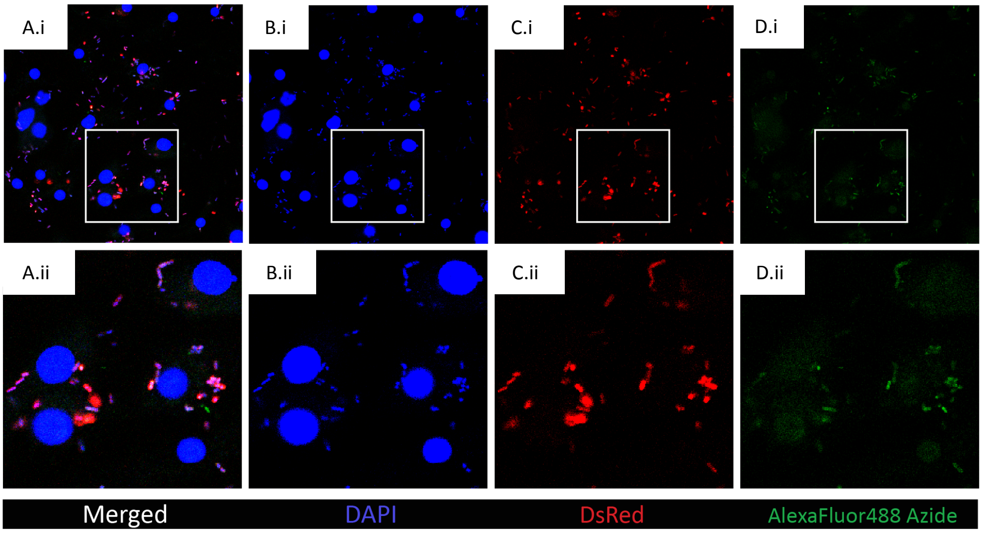

Figure 4: Confocal microscopy of BM-DCs incubated with alkyne-*S. Typhimurium*. BM-DCs were incubated with alkyne-*S. Typhimurium* expressing DsRed. After a 45 minutes pulse cells were washed and fixed. Cells were subsequently labelled with AlexaFluor-488 azide (green = AlexaFluor-488) and DAPI. A) merged channels, B) DAPI only, C) DsRed, D) AlexaFluor-488 azide. A.i-D.i) low magnification overview, A.ii-D.ii) high magnification overview.

For analysis of alkyne-*S. Typhimurium* bacteria on ultrastructures, bioorthogonally tagged *S. Typhimurium* has to be specifically labelled after Tokuyasu sample preparation and cryosectioning. To test the feasibility of this approach BM-DCs were again incubated with alkyne-*S. Typhimurium* and subjected to Tokuyasu sample preparation: after cryosectioning, the samples were transferred to an EM grid and labelled with AlexaFluor-488-azide using a ccHc-reaction. These sections were then imaged in the confocal microscope. This revealed a very low signal-to-noise ratio of the AlexaFluor-488-azide (Figure 5A), in line with the whole cell confocal microscopy findings.

In an attempt to increase the intensity of fluorescence of the bioorthogonal handles, an additional labelling step was included to enhance the signal. First the sections were incubated with anti-AlexaFluor-488 IgG, which was then visualised using the IgG-binding protein A conjugated with-AlexaFluor-647. This approach resulted in an improvement of the signal-to-noise ratio and provided sufficient fluorescence to perform CLEM analysis (Figure 5B). After this successful confocal imaging, the sections were embedded in methylcellulose with uranylacetate and subjected to EM imaging. Correlation of the confocal and EM images was performed using nuclear DAPI stain (Figure 6). Images were successfully correlated and morphological information obtained from the EM images showed that the alkyne-positive foci located on intact *S. Typhimurium*, as well as smaller non double-membrane containing structures (Figure 6D/E, yellow arrows). These results show that, upon use of a combination of bioorthogonal labelling and CLEM, ultrastructural information of *S. Typhimurium* and of the host phagocyte could successfully be obtained.

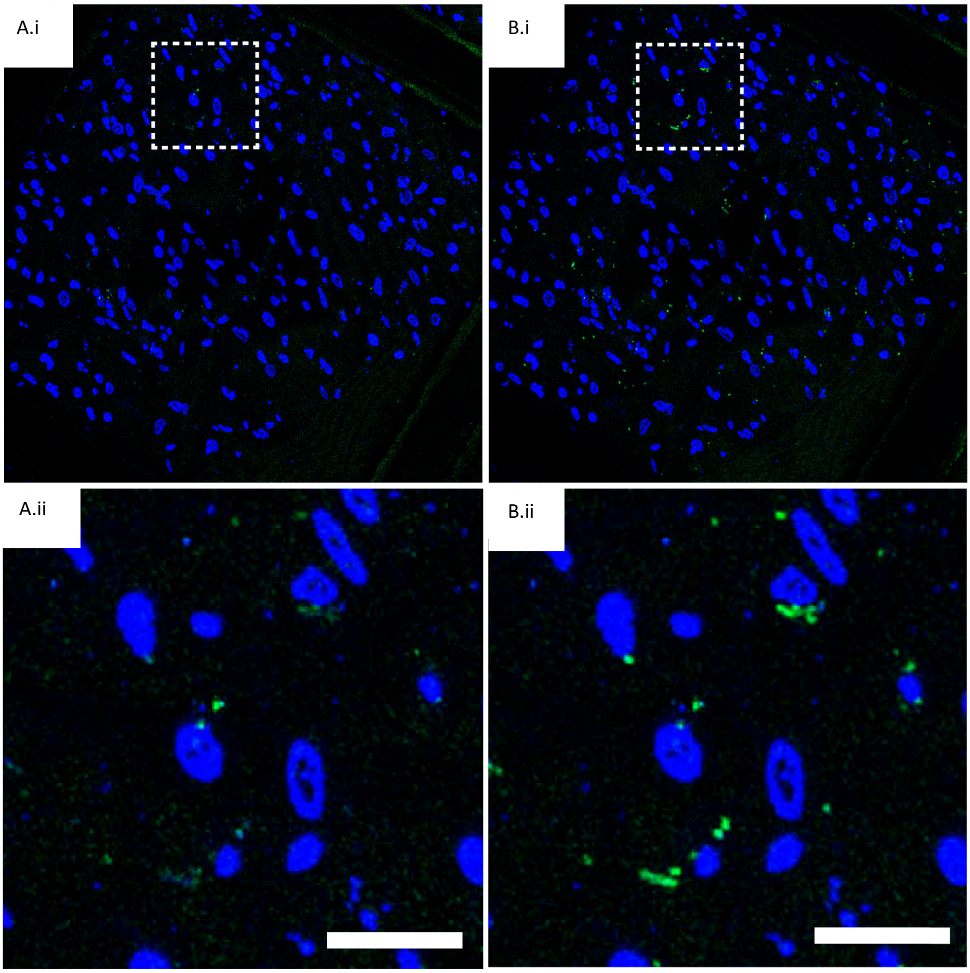

Figure 5: Protein A-AlexaFluor-647 enhancement of bioortohogonal labelling. BM-DCs were incubated with alkyne-*S. Typhimurium* and washed with PBS to remove unbound/non-internalised *S. Typhimurium*. Cells were fixed, subjected to Tokuyasu sample preparation and cryosectioned into 75 nm sections. A.i) Sections were reacted with AlexaFluor-488 azide using ccHc-conditions (green), and stained with DAPI (blue). B.i) To enhance the fluorescence signal of the bioorthogonal label sections were additionally labelled with Protein A-AlexaFluor-647 (green) using a rabbit anti AlexaFluor-488 antibody. (ii) Details of i. Scale bar: 7 µm.

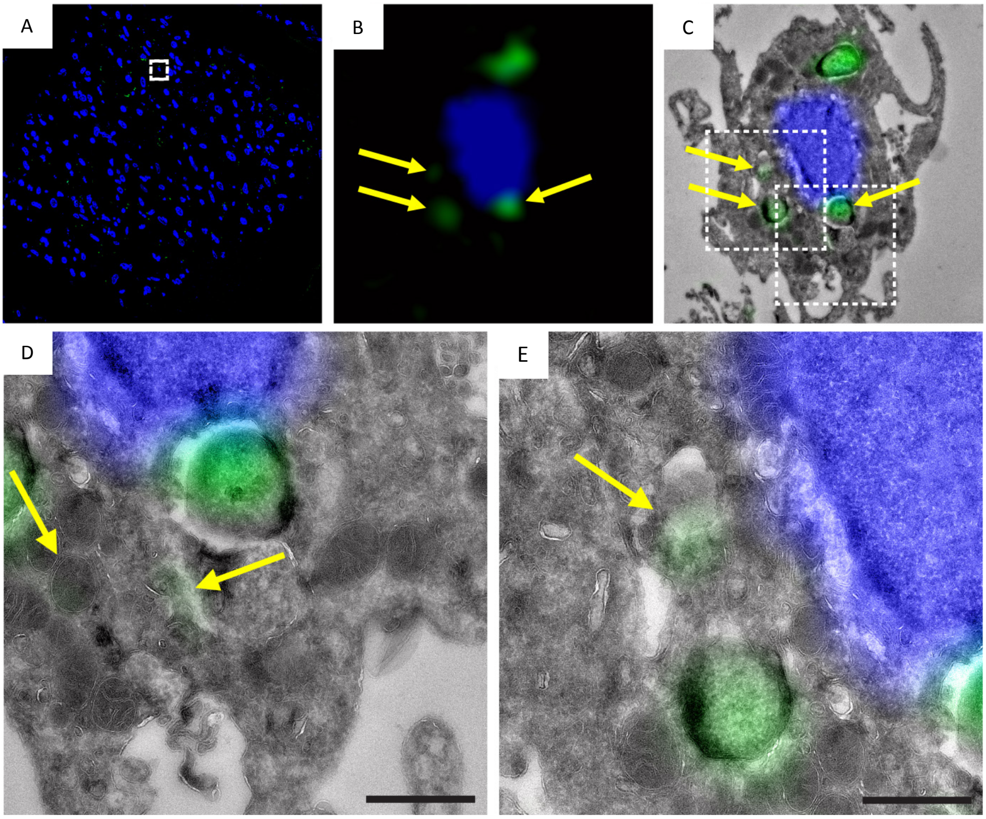

Figure 6: CLEM imaging of phagocytosed alkyne-*S. Typhimurium.* BM-DCs were incubated with alkyne-*S. Typhimurium* and washed with PBS to remove unbound/non-internalised *S. Typhimurium*. Cells were fixed and subjected to Tokuyasu sample preparation and cryosectioned into 75 nm sections. Sections were reacted with AlexaFluor-488 azide using ccHc-conditions (green) and stained with DAPI (blue). The fluorescence signal of the AlexaFluor-488 was enhanced with protein A AlexaFluor-647 using a rabbit anti-AlexaFluor-488 antibody. DAPI staining was used for correlation purposes. A) low magnification confocal image, B) high magnification confocal image, C) CLEM image of B correlated with EM image, D) detail of C, E) detail of D. Yellow arrows indicate label that derived from alkyne-*S. Typhimurium*. Scale bar 500 nm.

The resolution of the fluorescence signal that was used for the correlation of the bioorthogonal signal results in accuracies around 250 nm, due to the van Abbe diffraction limit of visible light. Since the main envisaged goal of the method development was to reveal the location of secreted virulence factors that are around 2-20 nm in size[16], the detection level of the fluorescence signal had to be improved. It was therefore explored whether the photoactivated localisation microscopy (PALM)-CLEM imaging of fluorescent proteins initially reported by Betzig and co-workers[17], could be modified to the use of detecting the bioorthogonal labels. For this the related Nikon N-STORM was explored on the Tokuyasu-sections that were previously imaged by confocal microscopy (Figure 6). Sections were now labelled with AlexaFluor-647 and embedded between a glass slide and coverslip with a glucose oxidase (GLOX) buffer. The use of STORM imaging on the sample sections resulted in a drastic improvement of both the accuracy and detection levels of the fluorescently labelled alkyne-*S. Typhimurium* (Figure 7). Additionally, distinctions in label intensities could be observed within the individual bacteria. Since alkyne handles were incorporated prior to infection, non-labelled regions within the bacteria might represent regions where newly synthesised, untagged, proteins are formed.[27]

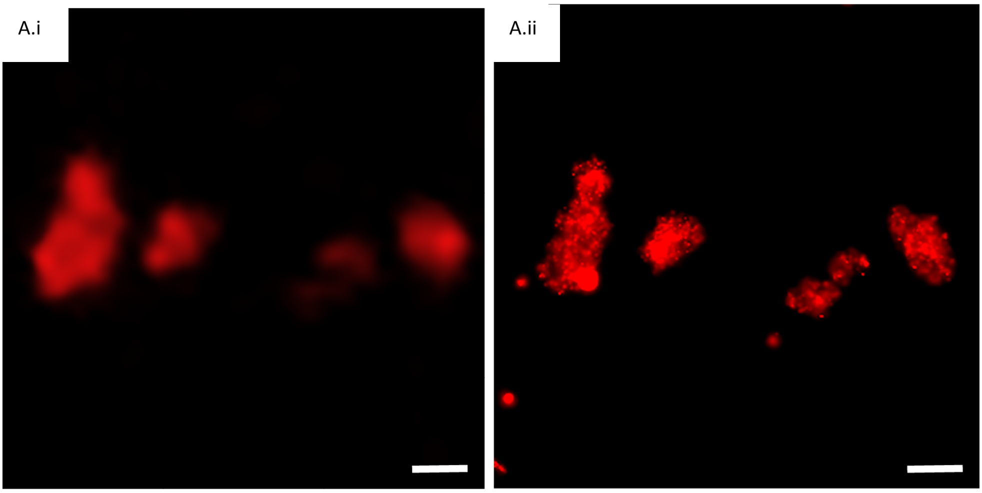

Figure 7: Super-resolution N-STORM image of 75 nm cryosection of BMDCs incubated with alkyne-*S. Typhimurium*. BM-DCs were incubated with alkyne-*S. Typhimurium* and washed with PBS to remove unbound/non-internalised *S. Typhimurium*. Cells were fixed and subjected to Tokuyasu sample preparation and cryosectioned into 75 nm sections. Sections were reacted with AlexaFluor-647 azide using ccHc-conditions (red). A.i) Wide field low resultion image of alkyne-*S. Typhimurium* A.ii) Super resolution N-STORM image of alkyne-*S. Typhimurium.* Scale bar: 500 nm.

Sample sections were subsequently treated as for the previously reported CLEM strategy and EM structure were analysed (Figure 8). It seemed that STORM imaging did not affect the appearance of the ultrastructures. Membranes were intact and no structural alterations could be observed between STORM-imaged regions compared to non-imaged ones. Moreover, host cell organelles were still recognisable by their distinct morphological appearances. Upon correlation of the STORM images, signals were primarily present on the *S. Typhimurium* bacteria.

Moreover, small labels surrounding the bacteria were present on small structures with a diameter of around 10-20 nm, which were both present on membranes of vesicular host structures and were seemingly unattached within the spacious phagosome.

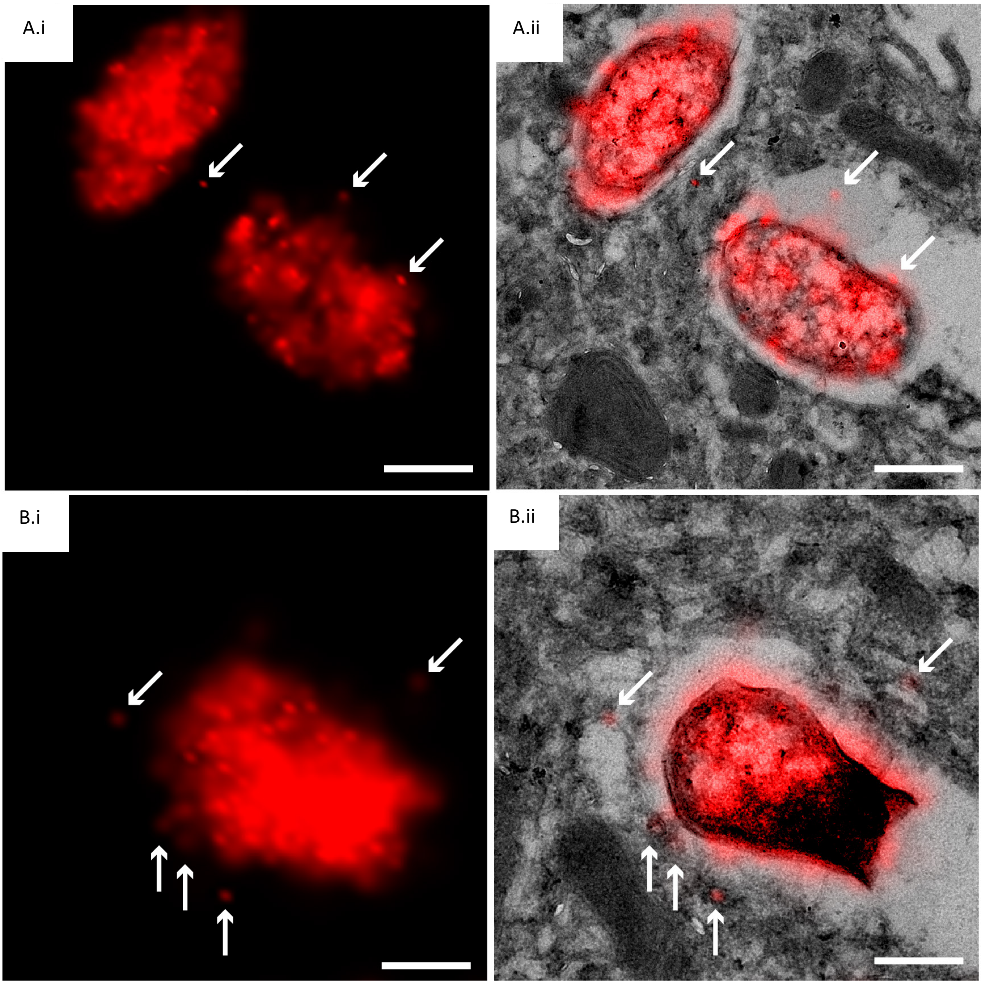

Figure 8: Super-resolution N-STORM-CLEM image of 75 nm cryosection of BMDCs incubated with alkyne-*S. Typhimurium*. BM-DCs were incubated with alkyne-*S. Typhimurium* and washed with PBS to remove unbound/non-internalised *S. Typhimurium*. Cells were fixed and subjected to Tokuyasu sample preparation and cryosectioned into 75 nm sections. Sections were reacted with AlexaFluor-647 azide using ccHc-conditions (red). A.i) Example 1 of super-resolution N-STORM image of alkyne-*S. Typhimurium*. A.ii) super-resolution CLEM image of A.i. B.i) Example 2 of super-resolution N-STORM image of alkyne-*S. Typhimurium*. B.ii) super-resolution CLEM image of B.i. Arrows indicate fragments of alkyne-*S. Typhimurium* that have been internalised by the host-cell. Scale bar: 250 nm.

Conclusion

The results presented show that upon implementation of STORM imaging in a CLEM setting, BONCAT-labelled *S. Typhimurium* can be imaged within the context of the host cell with high sensitivity and accuracy. This strategy has great potential to further elucidate the temporal and spatial injection of *Salmonella* virulence factors and their interactions with host organelles. In the presented experimental setup the *S. Typhimurium* bacteria were BONCAT labelled prior to their encounter with phagocytic host cells. This setup primarily allows for the monitoring of effector protein secretion during early stages of infection. However, since strategies have been reported to specifically BONCAT label a bacterium whilst interacting with a host cell, this imaging approach would also allow monitoring of effector protein secretion during later stages of infection.[11] Moreover, due to the broad applicability of BONCAT labelling, this strategy can also be combined with several mutant strains that have been shown to have attenuated virulence. In this fashion information can be obtained on the host-interaction and secretion patterns of these attenuated strains. In addition, the site-specific incorporation of bioorthogonal handles in virulence factors of interest would even allow for a more targeted CLEM-imaging approach between virulence factors and host cell organelles.[28] For example, a single virulence factor of interest can be specifically BONCAT-labelled and using the STORM-CLEM approach quantitative information can be extracted on their expression levels in the context of the infected host cell.[29, 30]

Experimental

Salmonella Typhimurium culturing conditions

Salmonella Typhimurium expressing DsRed[26, 31, 32] were grown overnight at 37°C in Lysogeny Broth (LB) medium. The following day cultures were diluted 1:33 in LB medium and grown at 37°C till an OD_{600} between 0.3-0.5. Subsequently cells were collected and resuspended in Selenomet medium (Molecular Dimensions) and supplemented with either 0.04, 0.4 or 4 mM Homopropargylglycine (Hpg) (Chiralix) or 4 mM Methionine (Met) (Sigma-Aldrich). After 30, 60 and 120 minutes OD_{600} were measured and cells were collected by centrifugation for gel analysis and bone marrow dendritic cell (BM-DC) infection experiments. Throughout culturing, cultures were supplemented with 100 µg/ml Ampicillin.

Mammalian cell culture conditions

Mouse BM-DCs were generated from B57BL/6 mice bone marrow essentially as described[33] with some modifications. Briefly, bone marrow was flushed from femurs and tibia and cells were cultured in IMDM (Sigma Aldrich) supplemented with 8% heat-inactivated fetal calf serum, 2 mM L-glutamine, 20 µM 2-mercaptoethanol (Life Technologies), penicillin 100 l.U./mL and streptomycin 50 µg/mL in the presence of 20 ng/mL GM-CSF (ImmunoTools). Medium was replaced on day 3 and 7 of culture and the cells were used between days 10 and 13.

S. Typhimurium expressing DsRed and cultured in the presence of 0.4 mM Hpg for 30 minutes were added to the BM-DCs as suspensions in PBS at a multiplicity of infection (MOI) of 50. After 45 minutes of incubation unbound/non-internalised *S. Typhimurium* cells were washed away (2x PBS) and medium was replaced. Subsequently cells were subjected to confocal microscopy or Tokuyasu sample preparation.

SDS-PAGE analysis

At the indicated time points *S. Typhimurium* were collected and cells were lysed with lysis buffer (50 mM HEPES pH 7.3, 150 mM NaCl and 1% NP-40) and incubated on ice for 1 h. Subsequently protein concentrations were determined with a Quibit 2.0 fluorimeter (Life Technologies), after which 20 µg of the protein was incubated for 1 h with copper catalysed Huisgen cycloaddition (ccHc)-cocktail (0.1 M HEPES pH 7.3, 1 mM $CuSO_4$, 10 mM sodium ascorbate, 1 mM THPTA ligand, 10 mM amino-guanidine, 5 µM AlexaFluor-647 azide (Invitrogen)). Samples were then resuspended in 4x SDS Sample buffer (250 mM TrisHCl pH 6.8, 8% w/v SDS, 40% glycerol, 0.04% w/v bromophenolblue, 5% 2-mercaptoethanol) and incubated at 100°C for 5 minutes. After the samples were run through a Hamilton syringe multiple times to shear genomic DNA, samples were subjected to SDS-PAGE. Gels were then directly imaged with a Biorad Universal Hood III for in-gel visualisation of the fluorescent labelling. As a loading control gels were stained with Coomassie Brilliant Blue. PageRuler Plus Prestained Protein Ladder (Thermo Scientific) was used as a protein standard.

Whole-cell confocal microscopy

BM-DCs were seeded (7 x 10^4) on a 12 well removable chamber slide (Ibidi) and left to grow O/N. The following day *S. Typhimurium* expressing DsRed and cultured in the presence of 0.4 mM Hpg for 30 minutes were added to the BM-DCs as suspensions in PBS at an MOI of 50. After 45 minutes of incubation unbound/non-internalised *S. Typhimurium* were washed away (2x PBS) and cells were fixed in 4% PFA for 15 minutes. Until further analysis cells were kept in PBS at 4°C. Fixed cells were incubated for 30 minutes with blocking buffer (1% BSA, 1% gelatin cold water fish skin, 0.3% Triton X-100), for 1 h with click cocktail ((0.1 M HEPES pH 7.3, 1 mM $CuSO_4$, 10 mM sodium ascorbate, 1 mM THPTA ligand, 10 mM amino-guanidine, 5 µM AlexaFluor-647 Azide (Invitrogen)) and DAPI (1 µg/ml). After the staining procedures chambers were removed and cells were covered with a small drop of 50% glycerol, after which a coverslip was mounted over the grid. Coverslips were fixed using Scotch Pressure-Sensitive Tape. Samples were imaged with a Leica TCS SP8 confocal microscope (63x oil lens, N.A.=1.4).

Bioorthogonal labelling on cryosections

Samples were prepared for cryosectioning as described elsewhere[34]. Briefly, BM-DCs infected with *S. Typhimurium* were fixed for 24 h in freshly prepared 2% PFA in 0.1 M phosphate buffer. Fixed cells were embedded in 12% gelatin (type A, Bloom 300, Sigma) and cut with a razor blade into 0.5 mm^3 cubes. The sample blocks were infiltrated in phosphate buffer containing 2.3 M sucrose for

3 h. Sucrose-infiltrated sample blocks were mounted on aluminum pins and plunged in liquid nitrogen. Frozen samples were stored under liquid nitrogen.

Ultrathin cell sections were obtained as described elsewhere.[34] Briefly, the frozen sample was mounted in a cryo-ultramicrotome (Leica). The sample was trimmed to yield a squared block with a front face of about 300 x 250 µm (Diatome trimming tool). Using a diamond knife (Diatome) and antistatic device (Leica) a ribbon of 150 nm thick sections was produced that was retrieved from the cryochamber with a droplet of 1.15 M sucrose containing 1% methylcellulose. Obtained sections were transferred to a specimen grid previously coated with formvar and carbon. Grids were additionally coated as indicated with carboxylate-modified fluorescent fiducial beads (350/440)(Life Technologies).

Sections were labelled as follows: thawed cryosections on an electron microscopy (EM) grid were left for 30 minutes on the surface of 2% gelatin in phosphate buffer at 37°C. Subsequently grids were incubated on drops of PBS/glycine and PBS/glycine containing 1% BSA. Grids were then incubated on top of the ccHc-cocktail (0.1 M HEPES pH 7.3, 1 mM $CuSO_4$, 10 mM sodium ascorbate, 1 mM THPTA ligand, 10 mM amino-guanidine, 5 µM AlexaFluor-488 Azide or AlexaFluor-647 Azide (Invitrogen) for 1 h and washed 6 times with PBS. In preparation for confocal microscopy the grids were blocked again with PBS/glycine containing 1% BSA after which the grids were incubated for 1 h with PBS/glycine 1% BSA supplemented with an AlexaFluor-488 antibody (Invitrogen). After washing with PBS/Glycine and blocking with PBS/glycine 0.1 % BSA, grids were incubated for 20 minutes on PBS/Glycine 1% BSA supplemented with AlexaFluor-647 Protein A (Invitrogen) to enhance the fluorescence signal. Sections were then labelled with DAPI (2 µg/ml), and additionally washed with PBS and aquadest.

Microscopy and correlation

The correlative light and electron microscopy (CLEM) approach used was adapted from Vicidomini et al.[35] Grids containing the sample sections were washed with 50% glycerol and placed on glass slides (pre-cleaned with 100% ethanol). Grids were then covered with a small drop of 50% glycerol after which a coverslip was mounted over the grid. Coverslips were fixed using Scotch Pressure-Sensitive Tape. Samples were imaged with a Leica TCS SP8 confocal microscope (63x oil lens, N.A.=1.4). Confocal microscopy was used as it allowed to make image stacks from the sections at different focus planes; this was convenient as the sections were found to be in different focus planes whilst placed between the glass slides and coverslip.

In case of STORM imaging grids containing the sample sections were washed with glucoseoxidase (GLOX) buffer (100 µl PBS, 20 µl 50% glucose, 20 µl 1M MEA (monoethanolamine) and 2µl GLOX (0.7 mg/ml GLOX, 5 mg/ml catalase in PBS) supplemented with 30% glycerol (60 µL) and placed on glass slides. Grids were then covered with a small drop of GLOX buffer, after which a coverslip was mounted over the grid. STORM images were acquired using a Nikon N-STORM system configured for total internal reflection fluorescence (TIRF) imaging. Excitation inclination was tuned to adjust focus and to maximise the signal-to-noise ratio. AlexaFluor-647 was excited illuminating the sample with a 647 nm (~160 mW) laser line built into the microscope. Fluorescence was collected by means of a Nikon 100x, 1.4 NA oil immersion objective and passed through a quad-band-pass dichroic filter (97335 Nikon). 20,000 frames were acquired for the 647 channel. Images were recorded onto a 256 × 256 pixel region (pixel size 160 nm) of a CMOS camera. STORM images were analysed with the STORM module of the NIS element Nikon software.[30]

After fluorescence or STORM microscopy the EM grid with the sections was removed from the glass slide, rinsed in distilled water and incubated for 5 minutes on droplets of uranylacetate/methylcellulose. Excess of uranylacetate/methylcellulose was blotted away and grids were air-dried. EM imaging was performed with a Tecnai 12 Biotwin transmission electron microscope (FEI) at 120 kV acceleration voltage.[36]

Correlation of confocal and EM images was performed in Adobe Photoshop CS6. In Adobe Photoshop, the light microscopy (LM) image was copied as a layer into the EM image and made 50 % transparent. Transformation of the LM image was necessary to match it to the larger scale of the EM image. This was performed via isotropic scaling and rotation. Interpolation settings; bicubic smoother. Alignment at low magnification was carried out with the aid of nuclear DAPI staining in combination with the shape of the cells; at high magnification alignment was performed using fiducial beads.[37]

References

1. R. Rotger and J. Casadesus, *Int Microbiol*, 1999, **2**, 177-184.
2. G. M. Haeusler and N. Curtis, *Adv Exp Med Biol*, 2013, **764**, 13-26.
3. A. Haraga, M. B. Ohlson and S. I. Miller, *Nat Rev Microbiol*, 2008, **6**, 53-66.
4. H. K. de Jong, C. M. Parry, T. van der Poll and W. J. Wiersinga, *PLoS Pathog*, 2012, **8**, e1002933.
5. C. G. Forest, E. Ferraro, S. C. Sabbagh and F. Daigle, *Microbiology*, 2010, **156**, 3689-3698.
6. P. Escoll, S. Mondino, M. Rolando and C. Buchrieser, *Nat Rev Micro*, 2016, **14**, 5-19.
7. C. M. Alpuche-Aranda, E. L. Racoosin, J. A. Swanson and S. I. Miller, *J Exp Med*, 1994, **179**, 601-608.
8. J. A. Johnson, Y. Y. Lu, J. A. Van Deventer and D. A. Tirrell, *Curr Opin Chem Biol*, 2010, **14**, 774-780.
9. D. C. Dieterich, A. J. Link, J. Graumann, D. A. Tirrell and E. M. Schuman, *Proc Natl Acad Sci U S A*, 2006, **103**, 9482-9487.
10. M. Grammel, M. M. Zhang and H. C. Hang, *Angew Chem Int Ed Engl*, 2010, **49**, 5970-5974.
11. A. Mahdavi, J. Szychowski, J. T. Ngo, M. J. Sweredoski, R. L. Graham, S. Hess, O. Schneewind, S. K. Mazmanian and D. A. Tirrell, *Proc Natl Acad Sci U S A*, 2014, **111**, 433-438.
12. D. C. Dieterich, J. J. Lee, A. J. Link, J. Graumann, D. A. Tirrell and E. M. Schuman, *Nat Protoc*, 2007, **2**, 532-540.
13. A. G. Chande, Z. Siddiqui, M. K. Midha, V. Sirohi, S. Ravichandran and K. V. S. Rao, 2015, **5**, 13430.
14. D. M. van Elsland, E. Bos, W. de Boer, H. S. Overkleeft, A. J. Koster and S. I. van Kasteren, *Chem Sci*, 2016, **7**, 752-758.
15. E. J. Guggenheim, A. Khan, J. Pike, L. Chang, I. Lynch and J. Z. Rappoport, *PLoS One*, 2016, **11**, e0159980.
16. H. P. Erickson, *Biol Proced Online*, 2009, **11**, 32-51.
17. E. Betzig, G. H. Patterson, R. Sougrat, O. W. Lindwasser, S. Olenych, J. S. Bonifacino, M. W. Davidson, J. Lippincott-Schwartz and H. F. Hess, *Science*, 2006, **313**, 1642-1645.
18. N. de Souza, *Nat Meth*, 2015, **12**, 37-37.
19. S. Watanabe, A. Punge, G. Hollopeter, K. I. Willig, R. J. Hobson, M. W. Davis, S. W. Hell and E. M. Jorgensen, *Nat Meth*, 2011, **8**, 80-84.
20. K. A. Sochacki, G. Shtengel, S. B. van Engelenburg, H. F. Hess and J. W. Taraska, *Nat Meth*, 2014, **11**, 305-308.
21. S. Watanabe, J. Richards, G. Hollopeter, R. J. Hobson, W. M. Davis and E. M. Jorgensen, *J Vis Exp*, 2012.

22. H. Suleiman, L. Zhang, R. Roth, J. E. Heuser, J. H. Miner, A. S. Shaw and A. Dani, *Elife*, 2013, **2**, e01149.
23. B. G. Kopek, G. Shtengel, C. S. Xu, D. A. Clayton and H. F. Hess, *Proc Natl Acad Sci U S A*, 2012, **109**, 6136-6141.
24. B. G. Kopek, G. Shtengel, J. B. Grimm, D. A. Clayton and H. F. Hess, *PLoS One*, 2013, **8**, e77209.
25. N. J. Agard, J. A. Prescher and C. R. Bertozzi, *J Am Chem Soc*, 2004, **126**, 15046-15047.
26. S. Méresse, O. Steele-Mortimer, B. B. Finlay and J. P. Gorvel, *The EMBO Journal*, 1999, **18**, 4394-4403.
27. S. Bakshi, H. Choi and J. C. Weisshaar, *Front Microbiol*, 2015, **6**.
28. F. Wang, S. Robbins, J. Guo, W. Shen and P. G. Schultz, *PLoS ONE*, 2010, **5**, e9354.
29. W. Vandenberg, M. Leutenegger, T. Lasser, J. Hofkens and P. Dedecker, *Cell Tissue Res*, 2015, **360**, 151-178.
30. D. van der Zwaag, N. Vanparijs, S. Wijnands, R. De Rycke, B. G. De Geest and L. Albertazzi, *ACS Appl Mater Interfaces*, 2016, **8**, 6391-6399.
31. M. Sorensen, C. Lippuner, T. Kaiser, A. Misslitz, T. Aebischer and D. Bumann, *FEBS Lett*, 2003, **552**, 110-114.
32. H. M. Albers, C. Kuijl, J. Bakker, L. Hendrickx, S. Wekker, N. Farhou, N. Liu, B. Blasco-Moreno, T. Scanu, J. den Hertog, P. Celie, H. Ovaa and J. Neefjes, *ACS Chem Biol*, 2014, **9**, 414-422.
33. M. B. Lutz, N. Kukutsch, A. L. Ogilvie, S. Rossner, F. Koch, N. Romani and G. Schuler, *J Immunol Methods*, 1999, **223**, 77-92.
34. P. J. Peters, in *Current Protocols in Cell Biology*, John Wiley & Sons, Inc., 2001.
35. G. Vicidomini, M. C. Gagliani, K. Cortese, J. Krieger, P. Buescher, P. Bianchini, P. Boccacci, C. Tacchetti and A. Diaspro, *Microsc Res Tech*, 2010, **73**, 215-224.
36. J. R. Kremer, D. N. Mastronarde and J. R. McIntosh, *J Struct Biol*, 1996, **116**, 71-76.
37. J. Kuipers, T. J. van Ham, R. D. Kalicharan, A. Veenstra-Algra, K. A. Sjollema, F. Dijk, U. Schnell and B. N. Giepmans, *Cell Tissue Res*, 2015, **360**, 61-70.

7

Towards Ultrastructural Imaging of Enzyme Activity with Correlative Light and Electron Microscopy [*]

Introduction

Enzymes are proteins that are involved in the metabolic pathways of living systems, and catalyse chemical reactions that modify, take apart and construct biomolecules. Their activity is regulated by post-translational modifications, protein-protein interactions and/or endogenous small-molecule inhibitors, and as a consequence their expression levels do not necessarily correlate with their activity.[1] Labelling methods such as genetically-encoded reporter proteins and/or antibodies can therefore not be used to obtain information on their active populations.[2] To this end chemical probes termed activity-based probes (ABPs) have been developed, which target the active site of an enzyme and only label its catalytically active form.[3] ABPs consist of three essential structural elements; (1) a recognition element, (2) a reactive group or 'warhead' and (3) a detectable group. The recognition element is recognised as substrate by the enzyme of interest and ensures the selectivity of the ABP. The warhead ensures (covalent) binding of the ABP to the enzyme of interest upon reaction with the catalytically-active amino acid residue of the enzyme. The detectable group can either be a bioorthogonal ligation handle or a reporter (e.g. biotin or a fluorophore) (Figure 1A/B, respectively).[2] If the detectable group is a bioorthogonal ligation handle, the strategy is referred to as two-step ABP labelling and the modification of the ABP takes place after the ABP has reacted with its target enzyme (Figure 1A). Bioorthogonal ligation handles are mostly azide- or alkyne moieties and can be ligated to a fluorescent group or an affinity handle depending on the experimental setup. When the detectable group itself is a reporter moiety, the ABP labelling strategy is referred to as direct ABP labelling, as enzymes are directly labelled with the ABP and can be directly visualised or isolated (Figure 1B). The main advantage of this strategy is that no additional labelling steps are necessary; however, the direct attachment of reporter groups may result in a lower binding affinity and/or specificity of the ABP.[4, 5]

---

[*] D.M. van Elsland, E. van Meel, M.E. Artola Perez de Azanza, H.A.V. Kistemaker, J.M. Aerts, H.S. Overkleeft, A.J. Koster and S.I. van Kasteren contributed to the work described in this chapter.

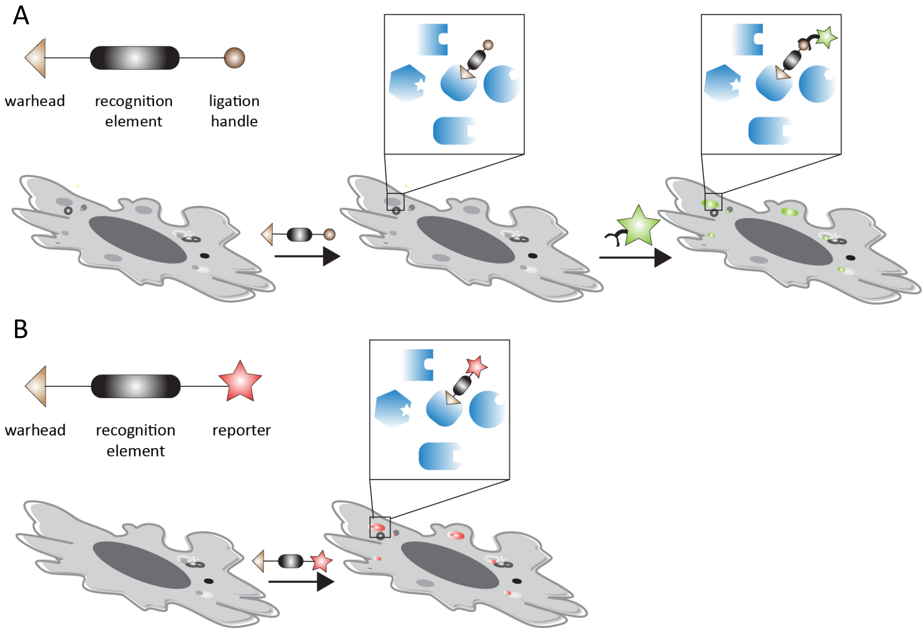

Figure 1: Two-step and direct labelling of enzymes with ABPs. A) The installation of a chemical reporter on active enzyme populations can be achieved upon use of two-step ABPs. Two-step ABPs consist of a warhead, recognition element and a chemical ligation handle. B) Direct ABPs consist of a warhead, recognition element and a detection group.

Over the past decades, a large number of ABPs have been developed that enabled the identification and monitoring of enzyme activity in various disease states.[3, 6-8] Moreover, fluorescence imaging of enzyme activity with ABPs has yielded valuable information on subcellular enzyme localisation.[9, 10] For example, imaging of cathepsin S activity has revealed the existence of distinct populations of cathepsin S-positive vesicles in bone marrow-derived immune cells.[10] However, these imaging studies did not reveal any information on the cellular ultrastructures in which these active enzymes reside. To this end correlative light and electron microscopy (CLEM) imaging of active enzyme populations is explored in this chapter. It is demonstrated that CLEM imaging of both two-step and direct ABP labelling is feasible. With both strategies active populations of cysteine proteases could be identified in their ultrastructural cellular context. Moreover, upon combining direct ABP and CLEM the relative ultrastructural localisation of glucocerebrosidases and cathepsins could be revealed.

Results

CLEM imaging of enzyme activity with two-step ABPs

To verify whether enzyme activity could be imaged with CLEM, a two-step ABP labelling sequence was implemented in the previously reported bioorthogonal on-section labelling strategy.[11] Mouse bone marrow-derived dendritic cells (BM-DCs), which express high levels of active cathepsins in their endolysosomal system, were incubated with the azide-functionalised ABP E-64 (Figure 2A). This irreversible cysteine protease inhibitor reacts selectively with cysteine proteases of the cathepsin family,[12] that localise inside lysosomes and have the ability to degrade internalised matrix proteins.[13] After incubation with E-64-azide, cells were washed, fixed and subjected to Tokuyasu sample preparation and cryosectioning. After cryosectioning, the E-64-azide incubated cells were labelled with an AlexaFluor-488 alkyne fluorophore using an on-section copper-catalysed Huisgen cycloaddition (ccHc) reaction (Figure 2B).[11] This reaction ensured covalent attachment of the AlexaFluor-488 fluorophore to the E-64-azide probe (Figure 2C) and thus to the active population of cathepsins. Sections were subsequently imaged with confocal microscopy (Figure 2D, left upper panel), after which a methylcellulose/uranylacetate embedding step was performed. The sections were then EM imaged and correlation of the confocal and EM-images was performed using fluorescent electron-dense beads as reference markers (Figure 2D, lower left panel/right panel).

The results show that E-64-azide could be successfully imaged using CLEM after on-section bioorthogonal ligation with an AlexaFluor-488 alkyne fluorophore. CLEM images show that the cysteine proteases of the cathepsin family -labelled by E-64- solely localised in membrane-limited lysosome-like structures of around 50-250 nm in diameter (Figure 2D). The intensity of the fluorescent signal varied between these ultrastuctures, which possibly reflects the variations in cysteine protease activity within lysosomes.

CLEM imaging of enzyme activity with a direct ABP

To determine whether direct ABP labelling was also applicable with the CLEM protocol, CLEM imaging of a BODIPY-TMR functionalised E-64 probe was performed (Figure 3A). With exception of the bioorthogonal ligation step, CLEM images of the E-64-BODIPY-TMR treated BM-DCs were obtained according to the exact same protocol as for E-64-azide. The CLEM results show that upon labelling with E-64-BODIPY-TMR membrane-limited lysosome-like structures of around 50-250 nm in diameter were marked cysteine protease-positive. E-64-BODIPY-TMR-labelled structures were detected with varying fluorescence intensities, again indicating differences in cysteine protease activity throughout these organelles. These results are in accordance with the results obtained with the two-step protocol and indicate that with both direct and two-step E-64 variants ultrastructures can be labelled and CLEM-imaged in a similar fashion.

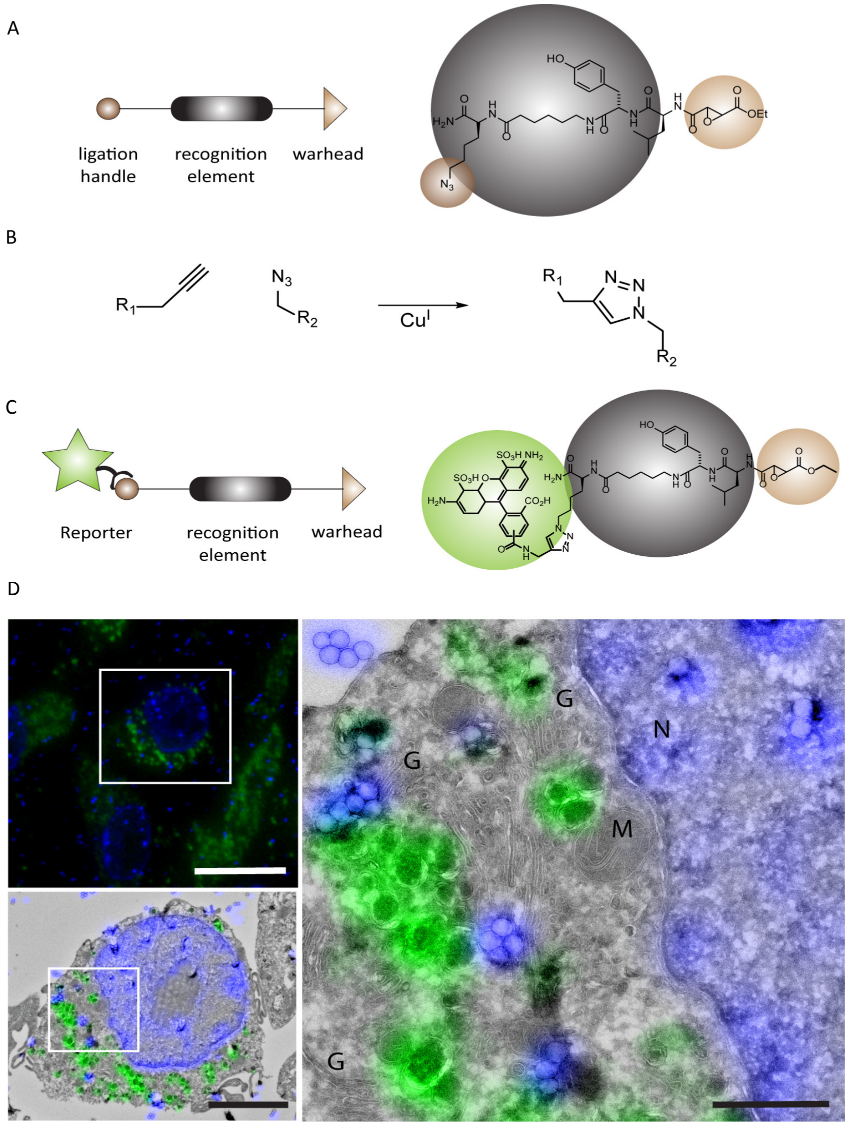
A
ligation handle
recognition element
warhead
HO
H_2N
N_3
OEt
B
R_1
N_3
R_2
Cu^I
C
Reporter
recognition element
warhead
SO_3H
NH_2
H_2N
CO_2H
HO
D
G
N
M

Figure 2: CLEM imaging of active populations of cysteine proteases in BM-DCs using a two-step ABP. A) Azide functionalised E-64 probe. The recognition element of the E-64 probe contains a leucine side chain that ensures its selectivity to cysteine proteases. The warhead is an epoxide moiety that forms a stable covalent bond between enzyme and probe. The ligation handle is represented by an azide moiety that -after covalent interaction of the warhead with the enzyme- can be ligated to a detection group of interest upon a bioorthogonal ligation reaction. B) Bioorthogonal ligation strategy for the covalent attachment of a detection moiety on the azide functionality of the E-64 probe. C) Product formed after ligation of the E-64-azide with a AlexaFluor-488 fluorophore. D) BM-DCs were incubated for 2 h with 10 µM E-64-azide. Cells were fixed in 2% PFA, subjected to Tokuyasu sample preparation and cryosectioned into 75 nm sections. Sections were reacted with

AlexaFluor-488 alkyne (green) using ccHc-conditions and DAPI (blue). DAPI staining and blue fiducials were used for correlation purposes. D) (Upper left) Confocal microscopy image of sample section; scale bar 5 µm. D) (Lower left) CLEM image obtained from overlay of confocal and EM pictures; scale bar 2 µm. D) (Right) High magnification detail showing the following structures: M, mitochondria; N, nucleus; G, Golgi. Scale bar 500 nm .

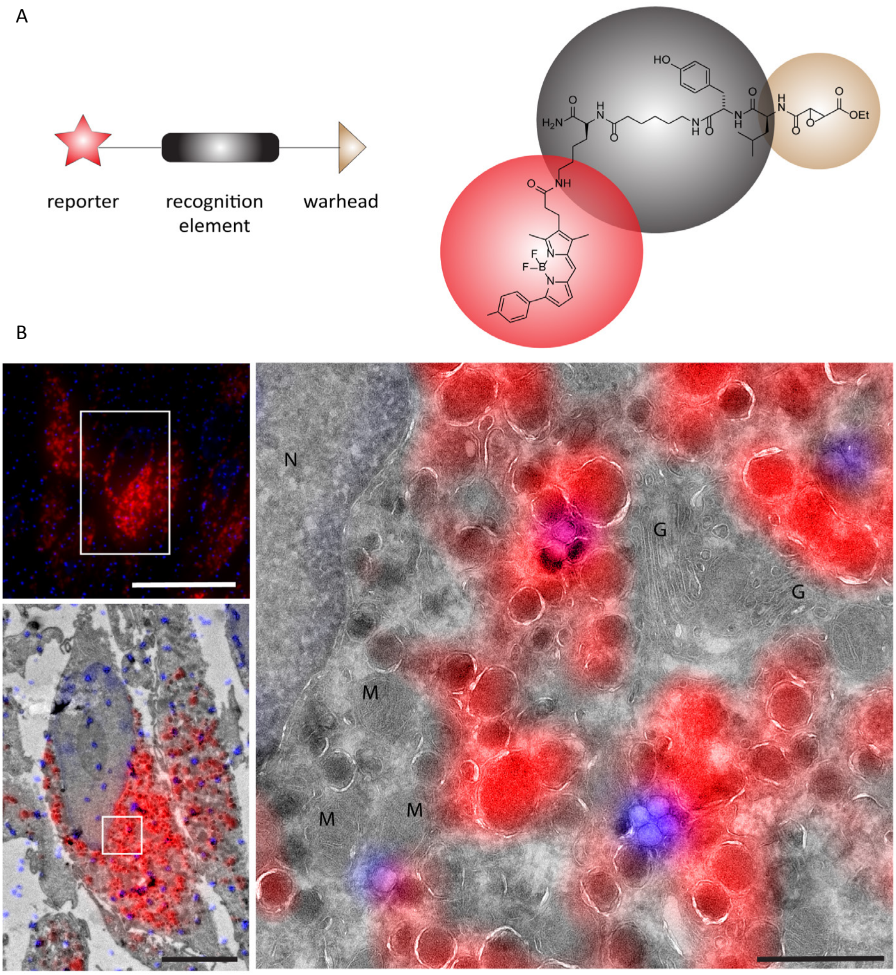

Figure 3: CLEM imaging of active populations of cysteine proteases in BM-DCs using a direct ABP. A) BODIPY-TMR-functionalised E-64 probe. B) BM-DCs were incubated for 2 h with 10 µM E-64-BODIPY-TMR (red). Cells were fixed in 2% PFA, subjected to Tokuyasu sample preparation and cryosectioned into 75 nm sections. Sections were additionally stained with DAPI (blue). DAPI staining and blue fiducials were used for correlation purposes. B) (Upper left) Confocal microscopy image of sample section; scale bar 10 µm. B) (Lower left) CLEM image obtained from overlay of confocal and EM pictures; scale bar 5 µm. B) (Right) High magnification detail showing the following structures; M, mitochondria; N, nucleus; G, Golgi. Scale bar 500 nm.

Comparison of direct and two-step ABP labelling for the CLEM imaging

To further analyse whether CLEM-sample preparation and CLEM-imaging influences the labelling efficiencies of the direct and two-step ABP E-64-BODIPY-TMR was modified with an additional azide moiety (Figure 4).[14] After ABP incubation and CLEM sample preparation the azide was functionalised with an AlexaFluor-488 fluorophore, using the exact same protocol as for the on-section labelling of the E-64-azide. In this manner, fluorescence signals of the direct and two-step ABP labelling strategies could be compared in one single experiment. The results show that both fluorescent signals label the exact same membrane-limited lysosome-like structures (Figure 5). Colocalisation analysis of two signals resulted in a Pearson's R value of 0.82. Most probably this slightly lowered colocalisation is due to the high magnification of the confocal image, whereby chromatic aberration distortions of the fluorescent signals become visible. Overall these results corroborated that CLEM imaging of direct ABP labelling results in similar labelling efficiencies as CLEM imaging of two-step ABPs.

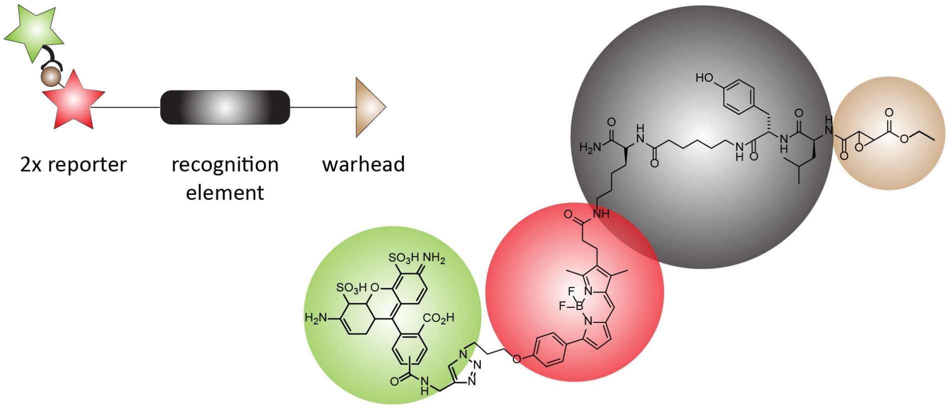

Figure 4: Azide-functionalised E-64-BODIPY-TMR ABP[14] conjugated to AlexaFluor-488 alkyne upon a ccHc reaction.

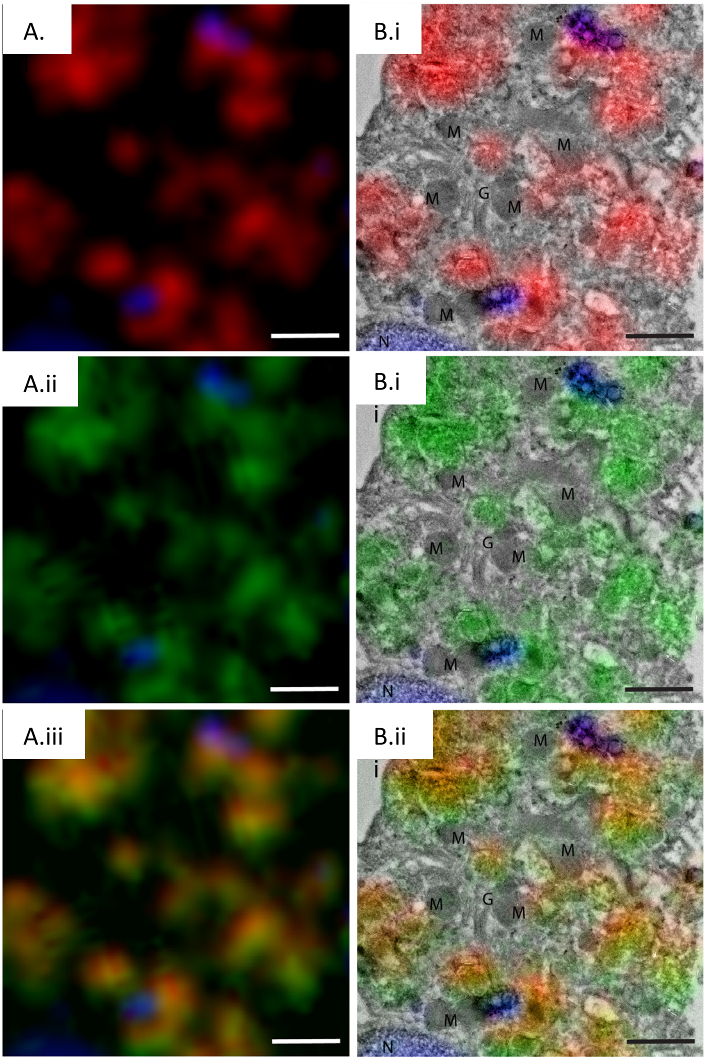

Figure 5: CLEM imaging of active populations of cysteine proteases in BM-DCs using direct and two-step ABPs in a single experiment. BM-DCs were incubated for 2 h with 10 µM E-64-BODIPY-TMR-azide (red). Cells were fixed in 2% PFA, subjected to Tokuyasu sample preparation and cryosectioned into 75 nm sections. Sections were labelled with DAPI (blue) and AlexaFluor-488 alkyne (green) using ccHc conditions. DAPI staining and blue fiducials were used for correlation purposes. (A.i) Confocal microscopy of direct ABP labelling of cysteine proteases (red); scale bar 500 nm. (B.i) CLEM image of direct ABP labelling of cysteine proteases (red); scale bar 500 nm. (A.ii) Confocal microscopy of two-step ABP labelling of cysteine proteases (green), scale bar 500 nm. (B.ii) CLEM image of two-step ABP labelling of cysteine proteases (green), scale bar 500 nm. (A.iii) Confocal microscopy of simultaneous direct and two-step cysteine protease labelling, scale bar 500 nm. (B.iii) CLEM image of direct and two-step cysteine protease labelling, scale bar 500 nm. M, mitochondria; N, nucleus; G, golgi.

Simultaneous CLEM imaging of glucocerebrosidase and cathepsins using ABP-CLEM

Glucocerebrosidase (GBA) is a lysosomal hydrolase that hydrolyses glucocerebrosides. Mutations in the GBA gene result in Gaucher disease, a lysosomal storage disease that is characterised by buildup of glucocerebrosides in lysosomes. GBA is a relatively short-lived enzyme in lysosomes[15] and is subject to intra-lysosomal proteolytic degradation by cathepsins.[16, 17] In case of the very common N370S GBA mutation in Caucasian Gaucher disease patients, resistance against intra-lysosomal proteolytic degradation is reduced. Inhibition of intra-lysosomal turnover of GBA through cathepsin inhibition is therefore considered a therapeutic option for some Gaucher disease patients. Insight in the actual (co-)localisation of reactive cathepsins and active GBA is therefore of great interest.

Monitoring of GBA activity using ABPs has been described using a fluorophore-functionalised cyclophellitol ABP (INHIBODY) that targets active variants of GBA (Figure 6).[18] In a preliminary experiment to determine whether GBA and cathepsin co-localisation can be monitored using ABP-CLEM, HeLa and MelJuSo cells were labelled with both INHIBODY and E-64 probes. These cells were then subjected to the same imaging strategy described above for the CLEM imaging of E-64-BODIPY-TMR-treated BM-DCs. CLEM images of labelled HeLa cells show that cysteine proteases and GBA co-localised in membrane-limited lysosome-like structures (Figure 7). This colocalisation of GBA and cysteine proteases in HeLa cells was confirmed with whole-cell confocal microscopy (Figure 8). In contrast to HeLa cells, conventional confocal microscopy and CLEM of dual-labelled MelJuSo cells showed only a partial colocalisation of cysteine proteases and GBA in lysosome-like structures (Figure 9 and 10). Labelling of cysteine proteases was primarily associated with lysosome structures, indicated with solid arrows (Figure 10A/B). However, in case of GBA labelling, GBA was shown to be present in both lysosome-like cysteine protease-positive structures and cysteine protease-negative ultrastructures. These cysteine protease-negative structures were found to be in very close proximity to the cysteine protease-positive structures, but had a distinct morphology. These results show that with direct ABP-CLEM multiple enzyme populations can be simultaneously imaged and reveal differences in the relative ultrastructural localisation of enzyme populations.

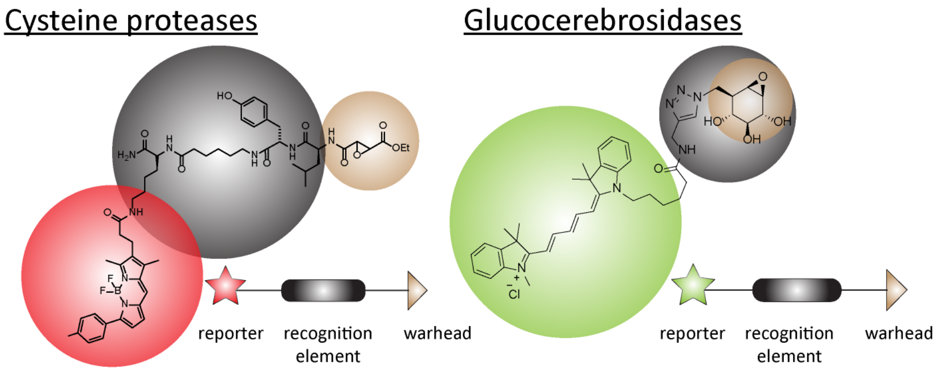
Cysteine proteases
reporter
recognition element
warhead
Glucocerebrosidases
reporter
recognition element
warhead

Figure 6: E-64-BODIPY-TMR ABP and INHIBODY-Cy5 ABP. E-64-BODIPY-TMR: The recognition element of the E-64 probe contains a leucine side chain that ensures its selectivity to cysteine proteases. The warhead is an epoxide moiety that forms a stable covalent bond between enzyme and probe. The reporter is a BODIPY-TMR fluorophore. INHIBODY-Cy5: the warhead is a cyclophellitol moiety that forms a stable covalent bond between the enzyme and the probe upon interaction with the nucleophile of glucocerebrosidases. The reporter functionality is a Cy5 fluorophore.

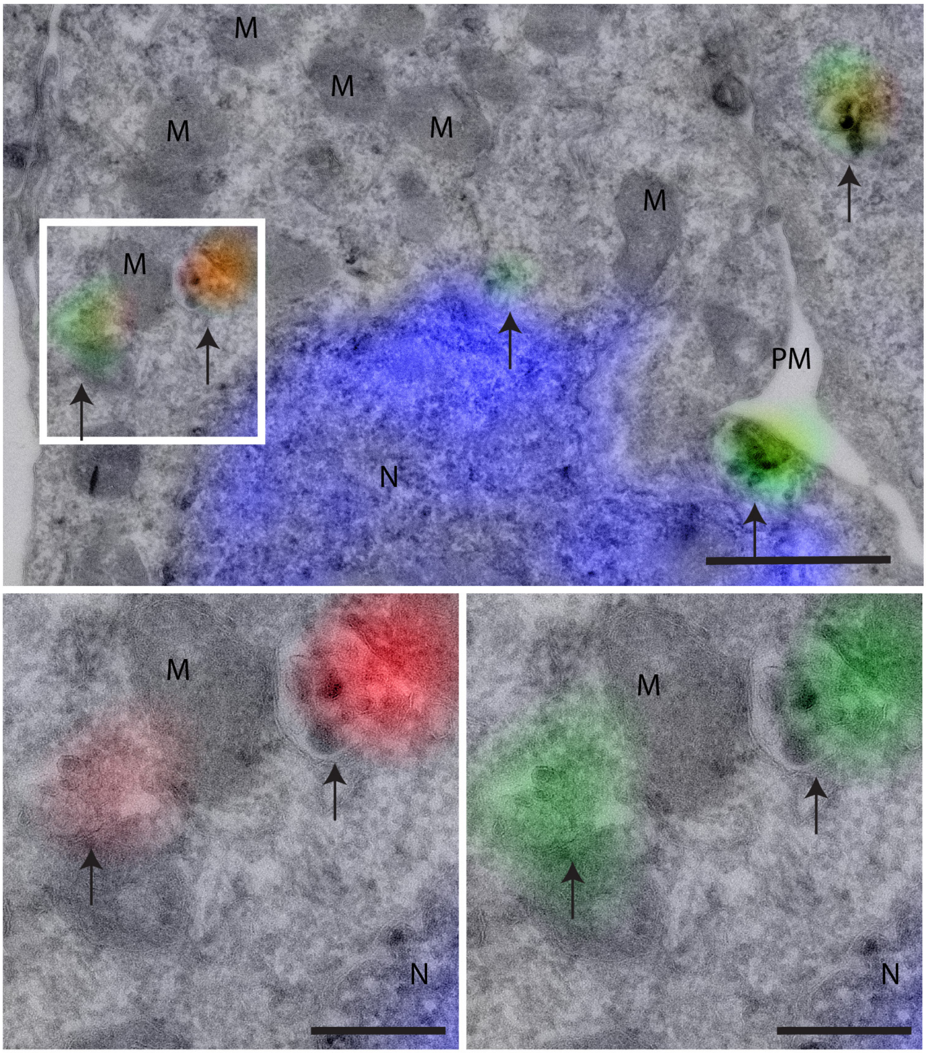

HeLa

Cysteine proteases

Glucocerebrosidases

Figure 7: CLEM imaging of cysteine proteases and glucocerebrosidases (GBAs) in HeLa cells using direct ABPs. HeLa cells were incubated for 2 h with 10 µM E-64-BODIPY-TMR (red) and 100 nM INHIBODY-Cy5 (green). Cells were fixed in 2% PFA, subjected to Tokuyasu sample preparation and cryosectioned into 75 nm sections. Sections were additionally stained with DAPI (blue). (Upper) CLEM image of cysteine proteases (red) and GBA (green) in HeLa cells; arrows indicate locations of cysteine proteases and GBA labelling. Scale bar 500 nm. Lower left) High magnification detail of upper image showing ultrastructural context of E-64-BODIPY-TMR (red) labelling of cysteine proteases (arrows). M, mitochondria; N, nucleus, scale bar, 200 nm. Lower right) High magnification detail of upper image showing GBA labelling (arrows). Scale bar 200 nm. M, mitochondria; N, nucleus; PM, plasma membrane.

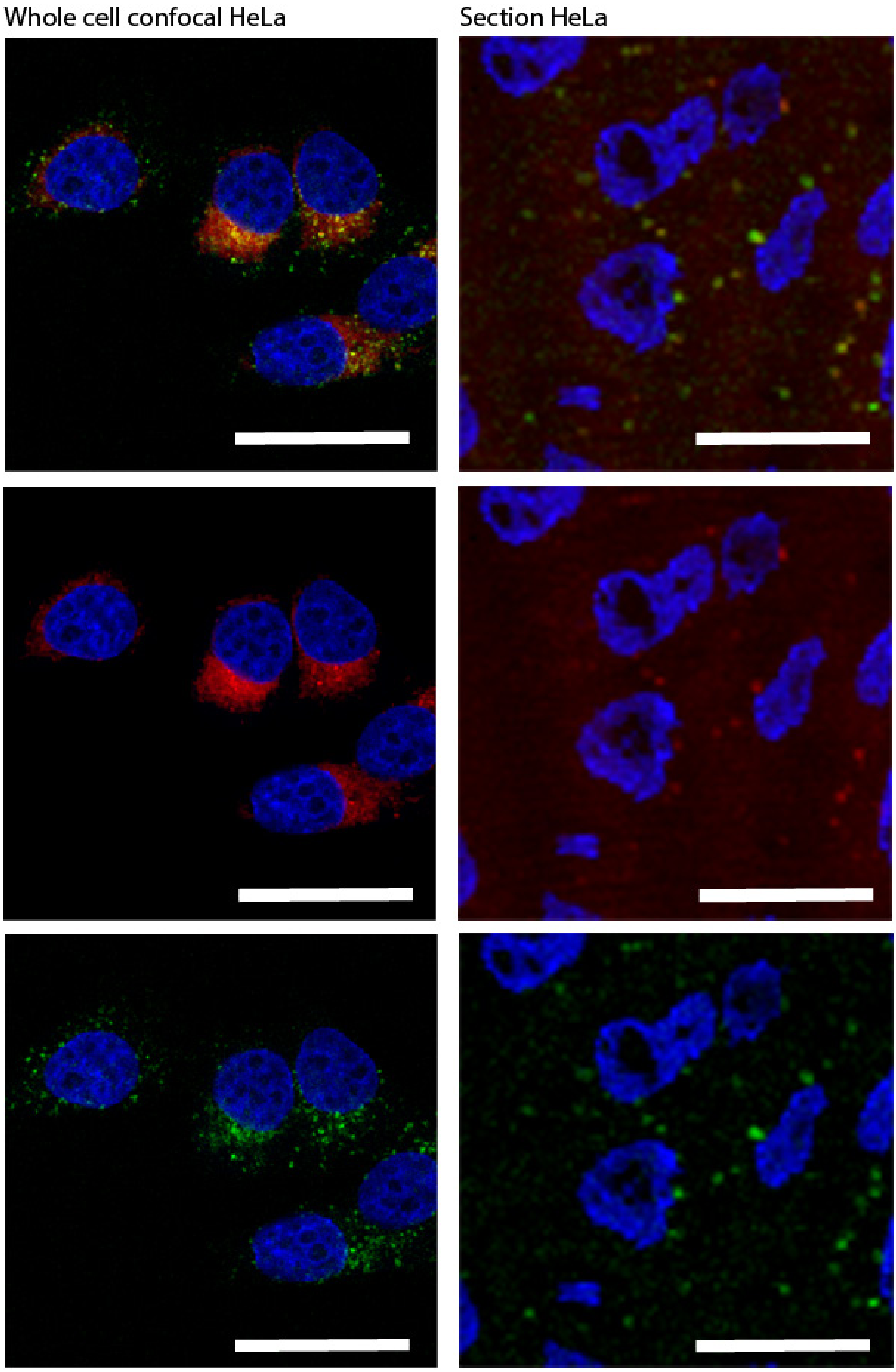
Whole cell confocal HeLa
Section HeLa

Figure 8: Whole cell and on-section confocal microscopy of HeLa cells incubated for 2 h with 10 µM E-64-BODIPY-TMR (red) and 100 nM INHIBODY-Cy5 (green). Cells were additionally stained with DAPI (blue). Scale bars, 25 µm.

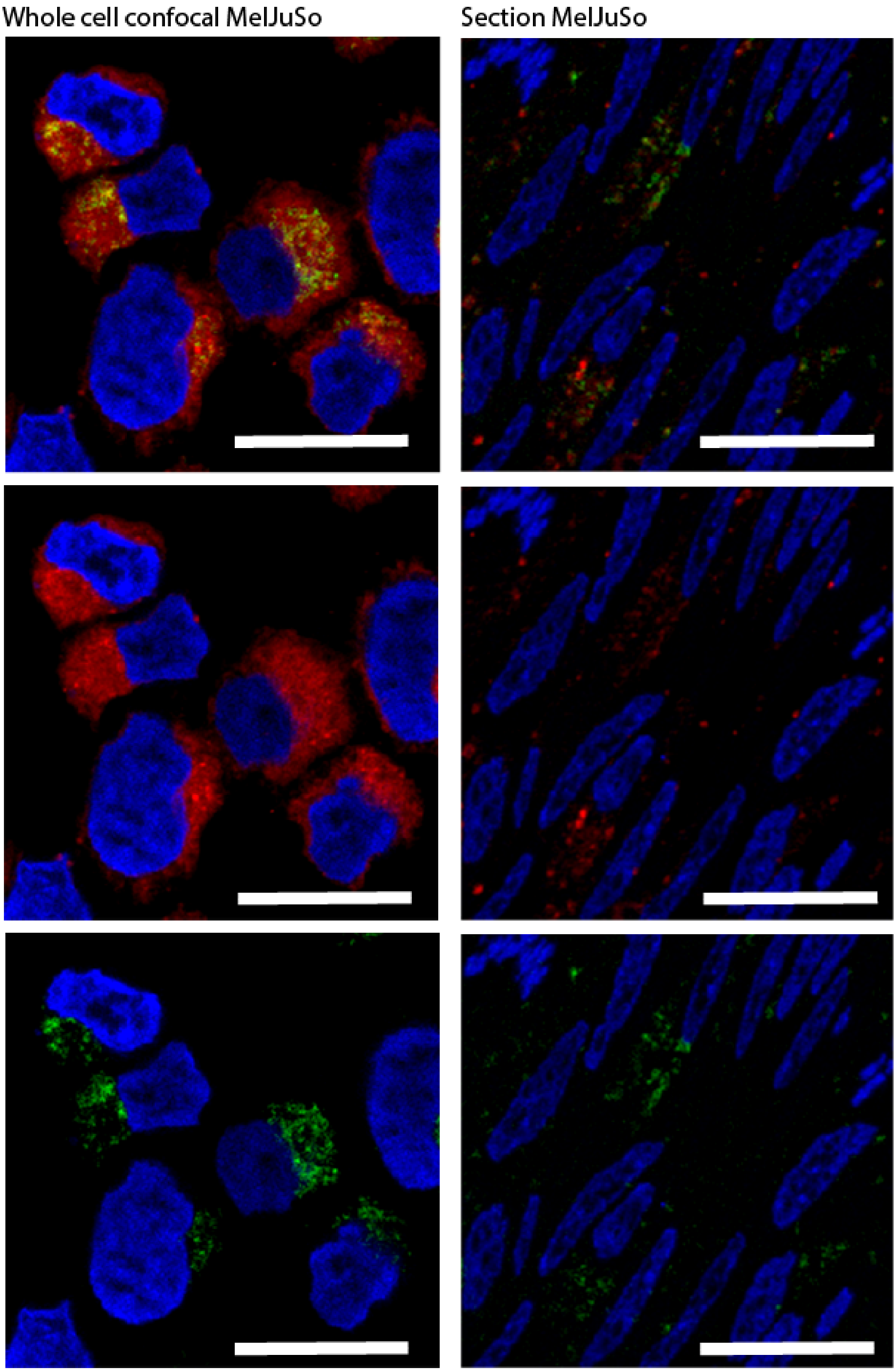
Whole cell confocal MelJuSo
Section MelJuSo

Figure 9: Whole-cell and on-section confocal microscopy of MelJuSo cells incubated for 2 h with 10 µM E-64-BODIPY-TMR (red) and 100 nM INHIBODY-Cy5 (green). Cells were additionally stained with DAPI (blue). Scale bars, 25 µm.

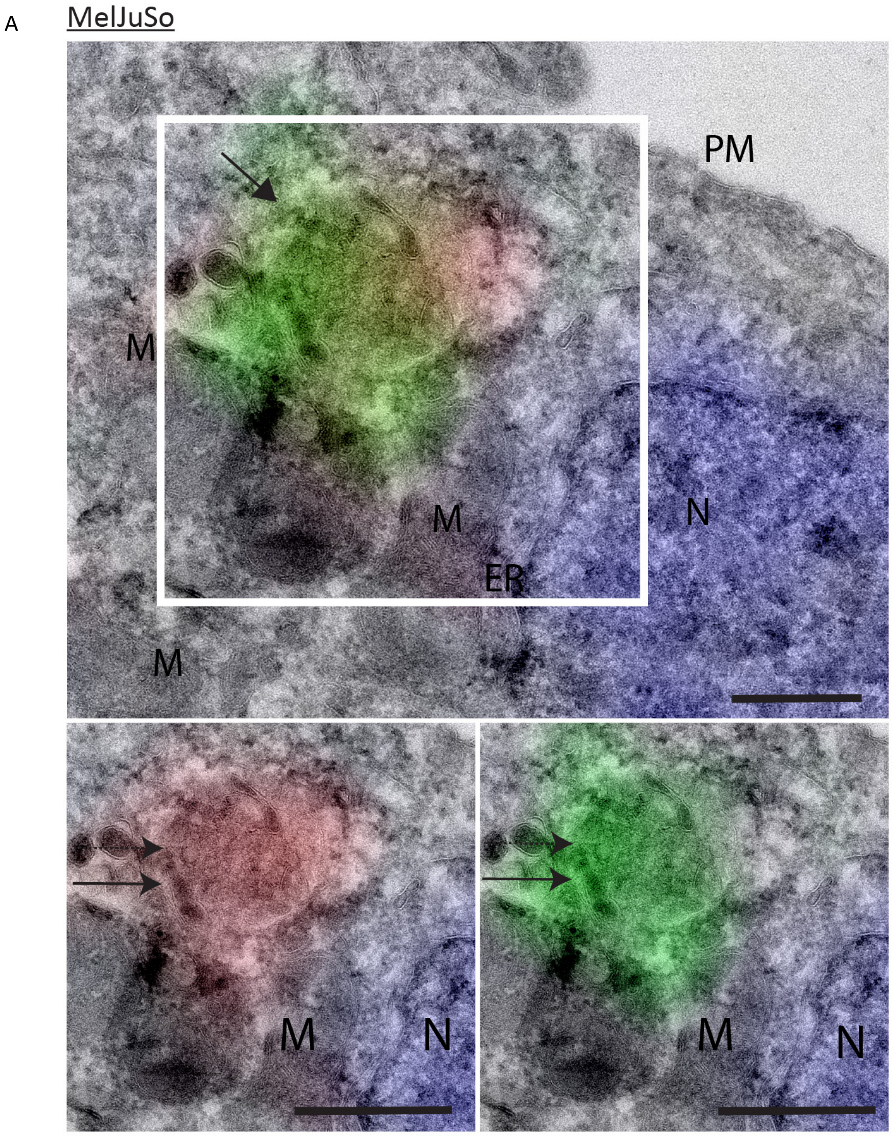
A
MelJuSo
PM
M
M
N
ER
M
M
N
M
N

Cysteine proteases

Glucocerebrosidases

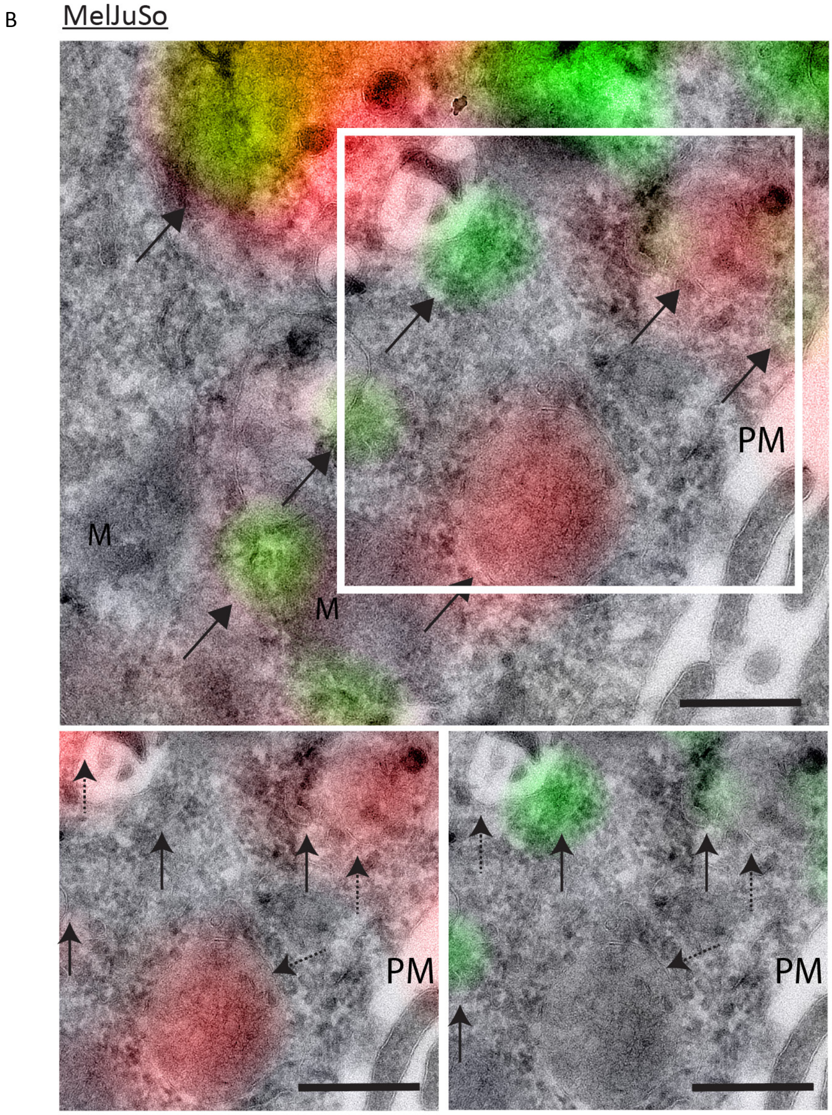

Cysteine proteases Glucocerebrosidases

Figure 10 A/B: CLEM imaging of cysteine proteases and glucocerebrosidases (GBAs) in MelJuSo cells using direct ABP labelling. MelJuSo cells were incubated for 2 h with 10 µM E-64-BODIPY-TMR (red) and 100 nM INHIBODY-Cy5 (green). Cells were fixed in 2% PFA, subjected to Tokuyasu sample preparation and cryosectioned into 75 nm sections. Sections were additionally stained with DAPI (blue). Upper; CLEM image of cysteine proteases (red) and GBA (green) in HeLa cells; arrows indicate locations of cysteine proteases and GBA labelling. Scale bar 500 nm. (Lower left) High magnification detail of upper image showing ultrastructural context of E-64-BODIPY-TMR labelling of cysteine proteases (red, arrows). M, mitochondria; N, nucleus, scale bar, 200 nm. (Lower right) High magnification detail of upper image showing GBA (green, arrows). M, mitochondria; N, nucleus; PM, plasma membrane. Scale bar 200 nm.

Conclusion

In this chapter the first examples of ABP-CLEM are described. Firstly, populations of active cysteine proteases were imaged within the ultrastructural cellular context of dendritic cells using both a two-step and a direct ABP approach. It was shown that cysteine proteases reside inside membrane-limited lysosome-like structures of around 50-250 nm in diameter. It was additionally demonstrated that with both direct and two-step labelling enzyme activity can be labelled with high selectivity and efficiency, indicating that bioorthogonal labelling does not suffer from section penetration limits that have been reported for on-section antibody labelling strategies.[19]

CLEM imaging of multiple enzyme classes showes that HeLa cells have a complete overlap in ultrastructural cellular location of cysteine proteases and GBA, whereas in MelJuSo cells a partial colocalisation could be observed. This partial colocalisation of GBA with E-64-BODIPY-TMR reactive cathepsins is not surprising as it is well established that there is a fundamental difference in the transport of newly synthesised cathepsins and of GBA to lysosomes. Cathepsins acquire mannose-6-phosphate (M6P) moieties in their N-linked glycans in the Golgi apparatus, which ensures the mannose-6-phosphate receptor (M6PR)-mediated transport to late endosomes/lysosomes.[20] In sharp contrast, GBA enzymes depend on binding to the membrane protein LIMP-2 in the endoplasmic reticulum for their transport to lysosomes.[21, 22] Upon LIMP-2 binding, newly formed GBA is transported to acidic late endosomes/lysosomes where low pH dependent dissociation of the complex occurs. It is therefore that distinct vesicular structures are reported to be involved in transport of cathepsins/M6PR and GBA/LIMP-2.[20] ABP-CLEM may provide new insights into the routing biology of these enzymes, and this information is crucial for research on enzyme activity in the lysosomal storage disorder Gaucher disease. It is foreseen that ABP-CLEM can be applied to monitor various Gaucher disease hallmarks and can be used for both diagnostic and therapeutic applications whereby information of GBA activity relative to the activity of other enzyme populations is of interest.

Experimental

Cell culture

Mouse bone marrow derived dendritic cells (BM-DCs) were generated from B57BL/6 mouse bone marrow essentially as described[23] with some modifications. Briefly, bone marrow was flushed from femurs and tibia and cells were cultured in IMDM (Sigma Aldrich) supplemented with 8% heat-inactivated fetal calf serum (FCS, Greiner), 2 mM L-glutamine, 20 µM 2-mercaptoethanol (Life Technologies), penicillin 100 I.U./mL and streptomycin 50 µg/mL in the presence of 20 ng/mL GM-CSF (ImmunoTools). Medium was replaced on day 3 and 7 of culture and the cells were used between days 10 and 13. BM-DCs were incubated for 2 h with E-64-azide[24] (final concentration of 10 µM) or E-64-TMR-azide after which the cells were washed with PBS and kept for 2 h in fresh medium.

HeLa cells were cultured in DMEM (Gibco) supplemented with 7.5% FCS (Greiner). MelJuSo (human melanoma cell line) cells were cultured in IMDM (Sigma Aldrich) supplemented with 7.5% FCS (Greiner). HeLa and MelJuSo cells were incubated for 2 h with 100 nM INHIBODY-Cy5 and 10 µM E-64-BODIPY-TMR from stock solutions in DMSO. After incubation cells were washed and subjected to further analysis.

Whole cell confocal microscopy

Cells were seeded (7 x 10^4) on a 12-well removable chamber slide (Ibidi) and left to grow O/N. The following day activity based probes (ABPs) were added at the indicated time and concentration. Cells were fixed in 4% PFA for 15 minutes and kept in PBS at 4 °C until further analysis. In case of click-labelling with AlexaFluor-488, fixed cells were incubated for 30 minutes with blocking buffer (1% BSA, 1% gelatin cold water fish skin), for 1 h with click cocktail ((0.1 M HEPES pH 7.3, 1 mM $CuSO_4$, 10 mM sodium ascorbate, 1 mM THPTA ligand, 10 mM amino-guanidine, 5 µM AlexaFluor-488 alkyne (Invitrogen)), and DAPI (1 µg/ml). In case of one-step ABP labelling cells were only labelled with DAPI. After the staining procedures chambers were removed and cells were covered with a small drop of 50% glycerol, after which a coverslip was mounted over the grid. Coverslips were fixed using Scotch Pressure-Sensitive Tape. Samples were imaged with a Leica TCS SP8 confocal microscope (63x oil lens, N.A.=1.4).

Bioorthogonal labelling on cryosections

Samples were prepared for cryosectioning as described elsewhere.[11, 25] Briefly, cells were fixed for 24 h in freshly prepared 2% PFA in 0.1 M phosphate buffer. Fixed cells were embedded in 12% gelatin (type A, Bloom 300, Sigma) and cut with a razor blade into 0.5 mm^3 cubes. The sample blocks were infiltrated in 0.1 M phosphate buffer containing 2.3 M sucrose for 3 h. Sucrose-infiltrated sample blocks were mounted on aluminum pins and plunged in liquid nitrogen. The frozen samples were stored under liquid nitrogen.

Ultrathin cell sections of 75 nm were obtained essentially as described elsewhere.[11] Briefly, frozen samples were mounted in a cryo-ultramicrotome (Leica). Samples were trimmed to yield a squared block with a front face of about 300 x 250 µm (Diatome trimming tool). Using a diamond knife (Diatome) and antistatic device (Leica) a ribbon of 75 nm thick sections was produced that was retrieved from the cryo-chamber with the lift-up hinge method.[26] A droplet of 1.15 M sucrose was used for section retrieval.

Obtained sections were transferred to a specimen grid previously coated with formvar and carbon. Grids were additionally coated with 100 nm carboxylate-modified FluoroSpheres (350/440) (Life Technologies).

Sections that were click-labelled with AlexaFluor-488 were labelled as follows: thawed cryosections on an EM grid were left on the surface of 2% gelatin in phosphate buffer at 37°C for 30 minutes. Subsequently grids were incubated on drops of PBS/glycine and PBS/glycine containing 1% BSA. Grids were then incubated on top of the ccHc-cocktail (0.1 M HEPES pH 7.3, 1 mM $CuSO_4$, 10 mM sodium ascorbate, 1 mM THPTA ligand, 10 mM amino-guanidine, 5 µM AlexaFluor-488 Alkyne (Invitrogen) for 1 h and washed 6 times with PBS. Sections were then labelled with DAPI (5 minutes) (2 µg/ml) and additionally washed with PBS and aquadest. In case of one-step ABP labelling cells were only labelled with DAPI.

Microscopy and correlation

The Correlative Light and Electron Microscopy (CLEM) approach used has been described elsewhere.[11] Briefly, grids containing the sample sections were washed with 50% glycerol and placed on glass slides (pre- cleaned with 100% ethanol).

Grids were then covered with a small drop of 50% glycerol, after which a coverslip was mounted over the grid. Coverslips were fixed using Scotch Pressure-Sensitive Tape. Samples were imaged with a Leica TCS SP8 confocal microscope (63x oil lens, N.A.=1.4). After confocal microscopy the electron microscopy (EM) grid with the sections was removed from the glass slide, rinsed in distilled water and incubated for 5 min on droplets of an aqueous solution containing 2% methylcellulose and 6% uranyl acetate. Excess of methylcellulose/uranylacetate solution was blotted away and grids were air-dried. EM imaging was performed with a Tecnai 20 transmission electron microscope (FEI) operated at 120 kV acceleration voltage.

Correlation of confocal and EM images was performed in Adobe Photoshop CS6. In Adobe Photoshop, the fluorescence microscopy image was copied into the EM image as a layer and made 50% transparent. Transformation of the FM image was necessary to match it to the larger scale of the EM image. This was performed via isotropic scaling and rotation using interpolation settings; bicubic smoother. Alignment at low magnification was carried out with the aid of nuclear DAPI staining in combination with the shape of the fluorescently labelled cells. At high magnification alignment was performed using fiducial beads.[27]

Colocalisation analysis

The Pearson coefficient was determined on magnified confocal images (obtained in Adobe Photoshop CS6) using the Coloc2 function in ImageJ after background correction.

References

1. B. D. Alberts B., Hopkin K., Johnson A., Lewis J., Raff M., Roberts K., Walter P., *Garland Science*, 2004, Second Edition.
2. L. I. Willems, H. S. Overkleeft and S. I. van Kasteren, *Bioconjug Chem*, 2014, **25**, 1181-1191.
3. B. F. Cravatt, A. T. Wright and J. W. Kozarich, *Annu Rev Biochem*, 2008, **77**, 383-414.
4. M. Verdoes, L. I. Willems, W. A. van der Linden, B. A. Duivenvoorden, G. A. van der Marel, B. I. Florea, A. F. Kisselev and H. S. Overkleeft, *Org Biomol Chem*, 2010, **8**, 2719-2727.
5. D. J. Vocadlo and C. R. Bertozzi, *Angew Chem Int Ed Engl*, 2004, **43**, 5338-5342.
6. M. Fonovic and M. Bogyo, *Expert Rev Proteomics*, 2008, **5**, 721-730.
7. H. Schmidinger, A. Hermetter and R. Birner-Gruenberger, *Amino Acids*, 2006, **30**, 333-350.
8. W. P. Heal, T. H. Dang and E. W. Tate, *Chem Soc Rev*, 2011, **40**, 246-257.
9. H. C. Hang, J. Loureiro, E. Spooner, A. W. van der Velden, Y. M. Kim, A. M. Pollington, R. Maehr, M. N. Starnbach and H. L. Ploegh, *ACS Chem Biol*, 2006, **1**, 713-723.
10. K. Oresic Bender, L. Ofori, W. A. van der Linden, E. D. Mock, G. K. Datta, S. Chowdhury, H. Li, E. Segal, M. Sanchez Lopez, J. A. Ellman, C. G. Figdor, M. Bogyo and M. Verdoes, *J Am Chem Soc*, 2015, **137**, 4771-4777.
11. D. M. van Elsland, E. Bos, W. de Boer, H. S. Overkleeft, A. J. Koster and S. I. van Kasteren, *Chem Sci*, 2016, **7**, 752-758.
12. D. Greenbaum, K. F. Medzihradszky, A. Burlingame and M. Bogyo, *Chem Biol*, 2000, **7**, 569-581.
13. W. H. t. Humphries and C. K. Payne, *Anal Biochem*, 2012, **424**, 178-183.
14. U. Hillaert, M. Verdoes, B. I. Florea, A. Saragliadis, K. L. Habets, J. Kuiper, S. Van Calenbergh, F. Ossendorp, G. A. van der Marel, C. Driessen and H. S. Overkleeft, *Angew Chem Int Ed Engl*, 2009, **48**, 1629-1632.
15. M. J. Ferraz, W. W. Kallemeijn, M. Mirzaian, D. Herrera Moro, A. Marques, P. Wisse, R. G. Boot, L. I. Willems, H. S. Overkleeft and J. M. Aerts, *Biochimica et biophysica acta*, 2014, **1841**, 811-825.
16. L. M. Jonsson, G. J. Murray, S. H. Sorrell, A. Strijland, J. F. Aerts, E. I. Ginns, J. A. Barranger, J. M. Tager and A. W. Schram, *Eur J Biochem*, 1987, **164**, 171-179.
17. M. A. Hajibagheri, J. L. Hall and T. J. Flowers, *Journal of Experimental Botany*, 1984, **35**, 1547-1557.
18. M. D. Witte, W. W. Kallemeijn, J. Aten, K. Y. Li, A. Strijland, W. E. Donker-Koopman, A. M. van den Nieuwendijk, B. Bleijlevens, G. Kramer, B. I.

Florea, B. Hooibrink, C. E. Hollak, R. Ottenhoff, R. G. Boot, G. A. van der Marel, H. S. Overkleeft and J. M. Aerts, *Nat Chem Biol*, 2010, **6**, 907-913.

19. G. Griffiths, in *Fine Structure Immunocytochemistry*, Springer Berlin Heidelberg, 1993, 9-25.
20. P. Saftig and J. Klumperman, *Nat Rev Mol Cell Biol*, 2009, **10**, 623-635.
21. J. M. Aerts, A. W. Schram, A. Strijland, S. van Weely, L. M. Jonsson, J. M. Tager, S. H. Sorrell, E. I. Ginns, J. A. Barranger and G. J. Murray, *Biochimica et biophysica acta*, 1988, **964**, 303-308.
22. D. Reczek, M. Schwake, J. Schroder, H. Hughes, J. Blanz, X. Jin, W. Brondyk, S. Van Patten, T. Edmunds and P. Saftig, *Cell*, 2007, **131**, 770-783.
23. M. B. Lutz, N. Kukutsch, A. L. Ogilvie, S. Rossner, F. Koch, N. Romani and G. Schuler, *J Immunol Methods*, 1999, **223**, 77-92.
24. S. Hoogendoorn, G. H. van Puijvelde, J. Kuiper, G. A. van der Marel and H. S. Overkleeft, *Angew Chem Int Ed Engl*, 2014, **53**, 10975-10978.
25. P. J. Peters, E. Bos and A. Griekspoor, *Curr Protoc Cell Biol*, 2006, Chapter 4, Unit 4 7.
26. E. Bos, C. SantAnna, H. Gnaegi, R. F. Pinto, R. B. Ravelli, A. J. Koster, W. de Souza and P. J. Peters, *J Struct Biol*, 2011, **175**, 62-72.
27. J. Kuipers, T. J. Ham, R. D. Kalicharan, A. Veenstra-Algra, K. A. Sjollema, F. Dijk, U. Schnell and B. N. G. Giepmans, *Cell and Tissue Research*, 2015, **360**, 61-70.

8

Summary and Future Prospects

In this thesis the combinatorial use of bioorthogonal labelling and Electron Microscopy (EM)-based imaging techniques is explored to enable observations of specific molecular targets in their ultrastructural context within the cell. In **chapter 1** the principles of EM imaging for biological research are discussed, including two different types of electron microscopes and various techniques to prepare specimens for transmission electron microscopy (TEM). **Chapter 1** additionally describes several labelling strategies that can be employed to identify biomolecules within EM-revealed structures. One of these approaches; correlative light and electron microscopy (CLEM) imaging, is explained by means of two generally used CLEM strategies; live-cell CLEM and on-section CLEM.

In **chapter 2** the importance and potential of bioorthogonal chemistry for CLEM imaging is emphasised. In this review an overview is given of frequently used bioorthogonal ligation strategies for imaging, including the copper-catalysed Huisgen cycloaddition (ccHc), the strain-promoted cycloaddition, the inverse electron-demand Diels-Alder cycloaddition, and the photoclick reaction. **Chapter 2** further highlights the advances that have been made towards CLEM imaging of bioorthogonal functionality, including azide-modified gold particles, bioorthogonally-functionalised selenide/zinc sulphide core-shell quantum dots and bioorthogonally-functionalised fluorophores that are capable of photooxidising diaminobenzidine (DAB).

Chapter 3 describes the development of two methods for EM detection of bioorthogonal labels. The first method is a gold labelling strategy that allows for the direct detection of bioorthogonal tags in the EM. The second method is a CLEM-based imaging method in which bioorthogonal tags are detected with fluorescence microscopy (FM), after which EM imaging is performed and images of both FM and EM are correlated. Both methods show that bioorthogonal labelling can be used to selectively label and localise the presence of bioorthogonal tags with EM in a non-homogenous sample of tagged and untagged *E. coli* bacteria.

The methods described in **chapter 3** are based on the ccHc-reaction. This chemical ligation strategy is well-known for its high reaction rate and selectivity and makes use of a very small bioorthogonal ligation handle, which minimally perturbs the structural integrity of the tagged biomolecule. Nevertheless, as stated in **chapter 2**, a variety of alternative labelling strategies exist, which might also be amenable to the bioorthogonal labelling of ultrathin cryosections. Investigation into these alternatives is desirable, since application of different bioorthogonal labelling strategies within one single specimen allows for the simultaneous bioorthogonal labelling of multiple different biomolecules.[1] One of the most promising alternative bioorthogonal labelling strategies that can serve this purpose is the reaction between a tetrazine and a strained alkene. In this type of reaction an electron-deficient diene, a tetrazine, is reacted with a strained alkene such as norbornene. This reaction does not interfere with thiol groups and has evolved in both selectivity and fast kinetics. Moreover, the tetrazine reaction has been well exploited and optimised for several *in situ* and *in vivo* applications.[2, 3]

In **chapter 4** an in-depth analysis of gold and fluorescence labelling for EM-imaging is presented. Upon comparison of both labelling strategies it is shown that, if epitopes of interest are found in various structures within the same specimen, there exist inherent discrepancies between the fluorescence signals and the distribution of gold particles. However, since gold labelling has great advantages regarding its punctate readout, it is desirable to look into alternative methods that can reach the punctuality benefits of the gold particles. One of these alternative strategies; the implementation of super-resolution imaging in a CLEM imaging sequence[4], has been demonstrated in **chapter 6**, where it is shown that stochastic optical reconstruction microscopy (STORM) imaging can be succesfully perfomed on ultrathin cryosections without affecting EM-detectable cellular ultrastructures. In addition to this STORM-CLEM strategy, labels capable of polymerising DAB could also serve as a suitable alternative for gold particle labelling. Recently Ngo et al. have reported the use of a DAB polymerisation strategy for the EM detection of bioorthogonally-labelled biomolecules.[5, 6] Ngo et al. labelled bioorthogonal groups with fluorophores capable of photoconverting triplet oxygen to singlet oxygen. These singlet-oxygen species can precipitate DAB which results in the formation of insoluble DAB precipitates within four nanometers of the original fluorophore. Due to the close proximity at which DAB precipitation occurs, biomolecules -tagged with bioorthogonal functionality- are labelled with high resolution, making this strategy a suitable alternative to gold labelling (Figure 1).[6] However, since Ngo et al. use resin polymerisation for their study, this strategy is not compatible with on-section CLEM, precluding any type of additional on-section (immuno)-labelling and the ability to retrieve the exact same region of interest with both fluorescent and EM detection.

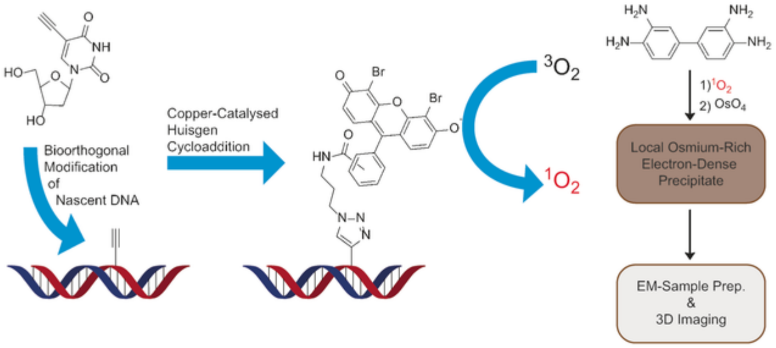
Bioorthogonal Modification of Nascent DNA
Copper-Catalysed Huisgen Cycloaddition
$^3O_2$
$^1O_2$
1) $^1O_2$
2) OsO_4
Local Osmium-Rich Electron-Dense Precipitate
EM-Sample Prep. & 3D Imaging

Figure 1: Detection of bioorthogonal groups in resin embedded EM samples: A) First, a bioorthogonal uridine analogue is metabolicially incorporated in nascent DNA. This handle was modified at the end of the experiment with dibromofluorescein, which can efficiently convert triplet oxygen into singlet oxygen. This singlet oxygen can then convert a 3,3'-diaminbenzidine (DAB) substrate into an insoluble polymer with high affinity for osmium. This osmium is electron dense and can thus be used to visualise the original bioorthogonal group.

In **chapter 5** the CLEM detection of bioorthogonal labels described in **chapter 3**, is applied to the imaging of bacterial degradation in the phagolysosomal system of phagocytic cells. The in situ study of bacteria in the phagocytic pathway is very difficult, as genetic modification is complicated for certain pathogens and -if successful- only allows tracking of pathogen phagocytosis until the point where the genetically-introduced reporter proteins are degraded by the proteolysis that is the hallmark of normal phagosomal maturation. In **chapter 5** it is shown that detection of bioorthogonal groups by CLEM allows one to obtain high resolution information on the subcellular location of the degrading bacteria, even after the signal of the genetically encoded protein reporters has gone.

In **chapter 6** the CLEM strategy reported in **chapter 5** is applied to the imaging of bioorthogonally-labelled *Salmonella Typhimurium* upon implementation of STORM super-resolution imaging. This strategy has great potential to elucidate the temporal and spatial injection of *Salmonella* virulence factors and their interactions with host cells organelles. To further characterise the effects of single virulence factors on host-organelle organisation and morphology it is desirable to additionally apply this strategy on host cells infected with *Salmonella* mutant strains, such as Δssej and ΔsopB that are known for their attenuated virulence.[7, 8] Of additional importance would be to unravel how *Salmonella* affects the architecture of host-cell organelles. Although the in **chapter 6** reported CLEM strategy can provide valuable information on the ultrastructural 2D architecture of the host-cell organelles, it does not provide comprehensive information on relative organelle organisation and their alterations upon *Salmonella* infection. This information can only be obtained upon reconstructing a volumetric 3D image of the obtained cellular ultrastructures. The classic approach for doing this, is by the reassembly and 3D reconstruction of TEM images from sequential sections.[9] This classic 3D reconstruction strategy is compatible with the here presented CLEM imaging of bioorthogonal labels; however, with this method only a limited number of sections can be reconstructed into a 3D volume. Other approaches, such as serial block-face (SBF) and focused-ion beam (FIB) milling and scanning electron microscopy (SEM) might therefore serve as good alternatives. With these approaches faster reconstruction can be performed of large volumes with a resolution that is close to that obtained with TEM.[9] However, the main disadvantage of these approaches is that they are poorly compatible with fluorescence labelling and imaging due to chemical fixation, resin embedding and block staining.[9] In case fluorescence imaging is desirable, it must therefore be performed prior to SBF- and FIB-SEM imaging.[10] Staining upon DAB precipitation, as presented by Ngo et al., therefore serves as a good staining alternative for SBF- and FIB-SEM imaging, albeit that with this type of labelling only one single biomolecule (class) of interest can be labelled per specimen.[5, 6]

In **chapter 7**, CLEM imaging of active enzyme populations is explored. CLEM imaging of active cysteine protease populations are demonstrated using both two-step and direct activity based probe (ABP)-labelling approaches. It is shown that with both strategies active populations of cysteine proteases can be labelled in a similar fashion with high selectivity and efficiency. In addition it is shown that with direct ABPs multiple enzyme populations can be simultaneously CLEM imaged. Further improvement of the ultrastructural detection of active enzyme populations could be achieved upon use of ABPs that become fluorescent upon binding of the enzymatic product. These quenched ABPs (qABPs) are intrinsically quenched, but fluorescently label the target enzyme upon binding by a mechanism-based nucleophilic displacement of the quencher group. In this manner background levels of unbound ABP are lowered, resulting in an improved signal to noise ration. The development of such probes has been initially described by Blum et al., who developed qABPs to dynamically image cysteine protease activity in real time with decreased background levels.[11, 12] Since the development of these probes a variety of qABPs have been generated, including 2,3,5,6-tetrafluoro phenoxymethyl ketone (PMK)-modified probes, with greatly improved in vivo stability. An example of such a PMK probe is the fluorescently quenched pan-cathepsin probe BMV109, reported by Verdoes et al.[13] Verdoes and co-workers additionally showed that upon modification of the peptide scaffold of BMV109, non-peptidic analogs could be developed with a high selectivity for individual cathepsins, such as cathepsin S-specific probes.[14, 15]

References

1. L. I. Willems, N. Li, B. I. Florea, M. Ruben, G. A. van der Marel and H. S. Overkleeft, *Angew Chem Int Ed Engl*, 2012, **51**, 4431-4434.
2. N. K. Devaraj, R. Weissleder and S. A. Hilderbrand, *Bioconjug Chem*, 2008, **19**, 2297-2299.
3. D. M. Patterson, L. A. Nazarova, B. Xie, D. N. Kamber and J. A. Prescher, *J Am Chem Soc*, 2012, **134**, 18638-18643.
4. B. G. Kopek, M. G. Paez-Segala, G. Shtengel, K. A. Sochacki, M. G. Sun, Y. Wang, C. S. Xu, S. B. van Engelenburg, J. W. Taraska, L. L. Looger and H. F. Hess, *Nat Protoc*, 2017, **12**, 916-946.
5. J. T. Ngo, S. R. Adams, T. J. Deerinck, D. Boassa, F. Rodriguez-Rivera, S. F. Palida, C. R. Bertozzi, M. H. Ellisman and R. Y. Tsien, *Nat Chem Biol*, 2016, **12**, 459-465.
6. D. M. van Elsland and S. I. van Kasteren, *Angew Chem Int Ed*, 2016, **55**, 9472-9473.
7. M. B. Ohlson, K. Fluhr, C. L. Birmingham, J. H. Brumell and S. I. Miller, *Infect Immun*, 2005, **73**, 6249-6259.
8. H. Ruan, Z. Zhang, L. Tian, S. Wang, S. Hu and J. J. Qiao, *Biochem Biophys Res Commun*, 2016, **478**, 618-623.
9. K. Miranda, W. Girard-Dias, M. Attias, W. de Souza and I. Ramos, *Mol Reprod Dev*, 2015, **82**, 530-547.
10. N. Jimenez, E. G. Van Donselaar, D. A. De Winter, K. Vocking, A. J. Verkleij and J. A. Post, *J microsc*, 2010, **237**, 208-220.
11. G. Blum, S. R. Mullins, K. Keren, M. Fonovic, C. Jedeszko, M. J. Rice, B. F. Sloane and M. Bogyo, *Nat Chem Biol*, 2005, **1**, 203-209.
12. L. E. Edgington, M. Verdoes and M. Bogyo, *Curr Opin Chem Biol*, 2011, **15**, 798-805.
13. M. Verdoes, K. Oresic Bender, E. Segal, W. A. van der Linden, S. Syed, N. P. Withana, L. E. Sanman and M. Bogyo, *J Am Chem Soc*, 2013, **135**, 14726-14730.
14. K. Oresic Bender, L. Ofori, W. A. van der Linden, E. D. Mock, G. K. Datta, S. Chowdhury, H. Li, E. Segal, M. Sanchez Lopez, J. A. Ellman, C. G. Figdor, M. Bogyo and M. Verdoes, *J Am Chem Soc*, 2015, **137**, 4771-4777.
15. M. Verdoes, L. E. Edgington, F. A. Scheeren, M. Leyva, G. Blum, K. Weiskopf, M. H. Bachmann, J. A. Ellman and M. Bogyo, *Chem Biol*, 2012, **19**, 619-628.

Nederlandse Samenvatting

Om inzicht te krijgen in hoe biomoleculen cellulaire processen coördineren zijn er verschillende methoden ontwikkeld die het mogelijk maken om biomoleculen te bestuderen. Eén van deze strategieën is bioorthogonale chemie, een chemische markeringstechniek waarbij met behulp van een kleine chemische aanpassing biomoleculen ontvankelijk gemaakt voor detecteerbare labels. Bioorthogonale chemie kan worden toegepast bij onderzoek naar een veelvoud aan biomoleculen waaronder DNA, RNA, eiwitten, lipiden en suikers en heeft veel informatie opgeleverd over de eigenschappen en interacties van deze biomoleculen. Echter is het tot dus ver niet mogelijk geweest om bioorthogonaal gelabelde biomoleculen te bestuderen in de context van de complete cellulaire omgeving. In dit proefschrift wordt de ontwikkeling en de toepassing van een methode beschreven waarbij, door het combineren van bioorthogonale chemie en elektronen microscopie, biomoleculen bestudeerd kunnen worden in de ultrastructurele context van hun cellulaire omgeving.

In **hoofdstuk 1** worden de algemene principes beschreven van electronen microscopie voor biochemisch onderzoek. Allereerst worden twee verschillende elektronen microscopen beschreven; de 'Scanning Electron Microscope' (SEM) en de 'Transmission Electron Microscope' (TEM). Vervolgens worden verschillende preparatie technieken besproken die nodig zijn om biologische monsters te bekijken met de TEM. Tot slot wordt er beschreven met welke reeds ontwikkelde strategieën biomoleculen gelokaliseerd kunnen worden in deze biologische TEM-monsters. Eén van deze strategieën correlatieve licht en elektronen microscopie (CLEM) wordt verder uitgelegd aan de hand van twee strategieën; CLEM op levende cellen en CLEM op dunne coupes van cellen.

In **hoofdstuk 2** wordt het belang en de potentie benadrukt van bioorthogonale labellingsstrategiën voor CLEM. In dit review wordt een overzicht gegeven van veel gebruikte bioorthogonale labellingsstrategiën, onder andere; de koper gekatalyseerde Huisgen cycloadditie reactie, de 'strain-promoted' cycloadditie, de 'inverse electron-demand' Diels-Alder cycloadditie en de 'photoclick' reactie. **Hoofdstuk 2** bediscussieerd tevens welk onderzoek reeds is uitgevoerd op het gebied van bioorthogonale labellingsstrategieën en CLEM. Hieronder vallen onder andere strategieën zoals azide-gemodificeerde goud partikels, bioorthogonaal gefunctionalizeerde seleen/zink sulphine 'core-shell quantum dots' en bioorthogonaal gefunctionalizeerde fluorophoren die in staat zijn om diaminobenzidine te foto oxideren.

In **hoofdstuk 3** worden twee methoden beschreven die zijn ontwikkeld om bioorthogonaal gelabelde biomoleculen te detecteren met de elektronen microscoop. In de eerste methode worden bioorthogonaal gelabelde biomoleculen direct in de elektronen microscoop gedetecteerd met behulp van colloïdale goud partikels. In het geval van de tweede strategie wordt er gebruik gemaakt van een CLEM methode waarbij allereerst bioorthogonale groepen fluorescent gelabeld worden en geïdentificeerd worden met een lichtmicroscoop. Vervolgens wordt er elektronen microscopie toegepast op dezelfde locaties waarna de informatie uit beiden microscopie strategieën aan elkaar wordt gekoppeld. Beide strategieën zijn toegepast om bioorthogonaal gelabelde bacteriën te identificeren in een mengsel van ongelabelde bacteriën.

In **hoofdstuk 4** wordt een grondige analyse beschreven van goud en fluorescentie labelling voor EM. Door het vergelijken van beide strategieën wordt aangetoond dat -indien epitopen aanwezig zijn in verschillende cellulaire structuren- er verschillen bestaan tussen de fluorescentiesignalen en de verdeling van goud partikels. Dit is aangetoond en gekarakteriseerd met behulp van de technieken die zijn beschreven in **hoofdstuk 3**; de labelling van bioorthogonale groepen met zowel goud als fluorescentie.

In **hoofdstuk 5** wordt de CLEM detectie van bioorthogonale labels toegepast om bacteriële afbraak in het fagolysosomale stelsel van fagocytische cellen te bestuderen. Onderzoek naar de afbraak van bacteriën in fagocytische cellen is problematisch aangezien de genetische modificatie van pathogenen gecompliceerd is en –indien succesvol- alleen gebruikt kan worden tot het punt waarop de genetisch geïntroduceerde markerings-eiwitten worden afgebroken. In **hoofdstuk 5** wordt aangetoond dat de CLEM-detectie van bioorthogonale groepen het mogelijk maakt om met zeer hoge resolutie de sub-cellulaire locatie van gedegradeerde bacteriën te bestuderen, zelfs nadat het signaal van de genetische reporter constructen verloren zijn gegaan.

In **hoofdstuk 6** wordt geïllustreerd hoe implementatie van ‘stochastic optical reconstruction microscopy’ microscopie -in de gerapporteerde strategie van de **hoofdstuk 5-** kan worden toegepast om de sub-cellulaire locatie van *Salmonella*-virulentiefactoren te bekijken. Deze strategie biedt de mogelijkheid om virulentiefactoren die afkomstig zijn van pathogenen te bestuderen in de context van de gastheercel. Met behulp van deze strategie is het mogelijk om te bestuderen op welke manier de injectie van virulentiefactoren gastheercellen beïnvloed en hoe deze interacties veranderingen veroorzaken in de gastheercel.

In **hoofdstuk 7** word beschreven hoe actieve enzym populaties kunnen worden bestudeerd met behulp van ‘activity based probes’ (ABPs) en CLEM. In dit hoofdstuk wordt beschreven dat zowel met twee-staps als directe ABPs actieve cysteïneproteasen populaties kunnen worden bestudeerd in de context van cellulaire ultrastructuren. Bij het gebruik van zowel twee-staps als directe ABPs kunnen actieve populaties van cysteïneproteasen gedetecteerd worden met hoge selectiviteit en efficiëntie. Bovendien laat **hoofdstuk 7** zien dat met behulp van directe ABP labelling meerdere enzym populaties kunnen worden bestudeerd met CLEM.

In het concluderende **hoofdstuk 8** worden alle bevindingen samengevat en worden er suggesties gegeven voor alternatieve technieken en toekomstige toepassingen, onder andere; labelling met behulp van diaminobenzidine precipitatie; het inbouwen van bioorthogonale aminozuren in *Salmonella* mutanten; 3D-CLEM van bioorthogonaal gelabelde bacteriën in fagocytische cellen en suggesties voor verbetering van de CLEM-ABP strategie.

List of publications

Correlative light and electron microscopy reveals discrepancy between gold and fluorescence labelling. **Daphne M. van Elsland**, Erik Bos, Joanna B. Pawlak, Herman S. Overkleeft, Abraham J. Koster and Sander I. van Kasteren. *J. Microsc.*, **2017,** 267(3), 309-317.

Negatively Charged Lipid Membranes Catalyze Supramolecular Hydrogel Formation. Frank Versluis, **Daphne M. van Elsland**, Serhii Mytnyk, Dayinta Perrier, Fanny Trausel, Jos Poolman, Chandan Maity, Sander I. van Kasteren, Jan H. van Esch and Rienk Eelkema. *J Am Chem Soc.,* **2016**, 138, 8670-8673.

Imaging Bioorthogonal Groups In Their Ultrastructural Context. **Daphne M. van Elsland**, and Sander I. van Kasteren. *Angew. Chem. Int. Ed.*, **2016**, 55, 9472-9473.

Detection of bioorthogonal groups by correlative light and electron microscopy allows imaging of degraded bacteria in phagocytes. **Daphne M. van Elsland**, Erik Bos, Wouter de Boer, Herman S. Overkleeft, Abraham J. Koster and Sander I. van Kasteren. *Chem. Sci.*, **2016**, 7, 752-758.

The potential of bioorthogonal chemistry for correlative light and electron microscopy: a call to arms. **Daphne M. van Elsland**, Erik Bos, Herman S. Overkleeft, Abraham J. Koster, Sander I. van Kasteren. *J Chem Biol.* **2015**, 8, 153–157.

Curriculum Vitae

English

Daphne van Elsland was born on March 5th 1989 in Zaandam. In 2007 she obtained her high school (Atheneum) diploma at the Bertrand Russell College in Krommenie. In the same year she started with the bachelor's programme Health and Life Sciences at the Vrije Universiteit (VU) in Amsterdam. As part of the bachelor's programme she performed a research internship on the development of bacterial protein expression systems under supervision of dr. W.S. Jong and prof.dr. J. Luirink in the department of Molecular Microbiology (VU, Amsterdam)

Following her bachelor's degree she started the master's program in Biomolecular Sciences at the VU in Amsterdam. As part of her master's program she performed two research internships. Her first research internship entitled 'Investigation of the type VII secretion system in Mycobacteria using a set of newly produced antibodies', and was performed at the departments of Medical Microbiology & Infection prevention (VU, Amsterdam) and Cell Biology II (NKI-AVL, Amsterdam) under supervision of dr. E.N.G. Houben, prof.dr. W. Bitter, dr. N.N. van der Wel and prof. dr. P.J. Peters. Her second internship entitled 'Investigation of rhamnose promoter based bacterial overexpression of secretory proteins' was performed at the departments of Biochemistry and Biophysics (SU, Stockholm) and Molecular Microbiology (VU, Amsterdam) under supervision of prof.dr. J.W. de Gier and prof.dr. J. Luirink. In October 2012 she obtained her Master of Science degree.

From November 2012 until November 2016 she conducted her doctoral studies at the department of Bio-Organic Synthesis under supervision of dr. S.I. van Kasteren and prof.dr. H.S. Overkleeft. A large part of the research described in this thesis was conducted at the Electron Microscopy section of the department of Molecular Cell biology (LUMC, Leiden) under supervision of prof.dr.ir. A.J. Koster. In addition parts of the described research were conducted at the Institute of Experimental Immunology (Universität Bonn, Bonn) under supervision of prof.dr. W. Kastenmüller and at the Nanoscopy for nanomedicine group (IBEC, Barcelona) under supervision of dr. L. Albertazzi. Parts of the Ph.D. research were presented with poster presentations at CHAINS (2014) and at the Bioorganic Chemistry Gordon Research Conference (Andover NH, United States 2016). Oral presentations were given at CHAINS (2016) and as invited speaker at an 'Advanced Imaging and Analysis Forum'-seminar (Londen, England 2017).

Currently the author of this thesis works as a post-doctoral researcher in the group of prof.dr. J.J.C. Neefjes, LUMC, Leiden.

Curriculum Vitae

Nederlands

Daphne van Elsland werd op 5 maart 1989 geboren te Zaandam. Zij behaalde in 2007 het Atheneum diploma (profiel Natuur & Gezondheid) aan het Bertrand Russell College te Krommenie en begon in dat jaar aan de bacheloropleiding Gezondheid en Leven aan de Vrije Universiteit (VU) Amsterdam. In het kader van deze bacheloropleiding deed zij in 2009 een korte onderzoeksstage naar de ontwikkeling van bacteriële eiwit productie systemen onder begeleiding van dr. W.S. Jong en prof.dr. J. Luirink in de vakgroep Molecular Microbiology (VU, Amsterdam).

Aansluitend begon ze aan de masteropleiding Biomolecular Sciences aan dezelfde universiteit. In het kader van deze masteropleiding deed zij twee onderzoekstages. Haar eerste stage met als onderwerp ‘Investigation of the type VII secretion system in Mycobacteria using a set of newly produced antibodies’, voerde zij uit in de vakgroepen Medical Microbiology & Infection prevention (VU, Amsterdam) en Cell Biology II (NKI-AVL, Amsterdam), onder begeleiding van Dr. E.N.G. Houben, prof.dr. W. Bitter, dr. N.N. van der Wel en prof.dr. P.J. Peters. Haar tweede onderzoekstage met als onderwerp ‘Investigation of rhamnose promoter based bacterial overexpression of secretory proteins’, voerde zij uit in de vakgroepen Biochemistry and Biophysics (SU, Stockholm) en Molecular Microbiology (VU, Amsterdam) onder begeleiding van prof.dr. J.W. de Gier en prof.dr. J. Luirink. In oktober 2012 behaalde zij haar Master of Science diploma.

Van november 2012 tot november 2016 werd als assistent in opleiding het onderzoek, beschreven in dit proefschrift, uitgevoerd in de vakgroep Bio-Organische Synthese onder leiding van dr. S.I. van Kasteren en prof.dr. H. S. Overkleeft. Tevens werd een groot gedeelte van het beschreven werk uitgevoerd bij de Electron Microscopy sectie van de afdeling Molecular Cell biology (LUMC, Leiden) onder leiding van prof.dr.ir. A.J. Koster. Een deel van het beschreven onderzoek werd bovendien uitgevoerd op het Institute of Experimental Immunology (Universität Bonn, Bonn) onder begeleiding van prof.dr. W. Kastenmüller en bij de Nanoscopy for nanomedicine groep (IBEC, Barcelona) onder begeleiding van dr. L. Albertazzi. Delen van dit onderzoek zijn gepresenteerd door middel van posters op CHAINS (2014) en op het Bioorganic Chemistry Gordon Research Conference (Andover NH, United States 2016). Daarnaast werd op CHAINS (2016) en als invited speaker voor de ‘Advanced

Imaging and Analysis Forum' (Londen, England 2017) een mondelinge presentatie gegeven.

Thans is de auteur van dit proefschrift werkzaam als postdoctoraal onderzoeker in de groep van prof.dr. J.J.C. Neefjes, LUMC, Leiden.